SHIP / MODEL CORRELATION STUDY

DWAYNE H. HOPKINS

SHIP / MODEL CORRELATION STUDY

by

© Dwayne H. Hopkins

A thesis submitted to the School of Graduate Studies

in partial fulfilment of the requirements for the degree of

Master of Engineering

Faculty of Engineering and Applied Science

Memorial University of Newfoundland

December 2003

St. John's Newfoundland

Your file Votre référence
ISBN: 0-612-99081-8
Our file Notre référence
ISBN: 0-612-99081-8

ABSTRACT

Information regarding a ship's performance in seakeeping, propulsion and manoeuvring cannot always be reliably predicted using existing numerical models. In addition, methodology deficiencies in scaling physical model data to full scale can significantly compromise the results. There is very little detailed full scale ship data available to the researcher in the open literature for validation of physical modeling methodology and/or numerical models. With this design ambiguity in mind, Memorial University of Newfoundland (MUN) in collaboration with the Institute for Marine Dynamics (IMD) of the National Research Council (NRC) of Canada and Marineering Ltd. designed and performed a ship / model correlation study on a 40 m long research vessel, M/V Louis M. Lauzier. Full scale sea trials were carried out on the 'Lauzier' in the Summer and Fall of 2001, while model scale research was performed on two different scale models (1:6 & 1:12) between August 2002 and June 2003. Numerical research was carried out concurrently using a computer generated replica of the 'Lauzier'.

The powering, or propulsion, trials were performed to obtain the performance and propulsive characteristics of the vessel. I am able to correlate the model scale results to the full scale results to within 10% using the ITTC '78 power prediction.

The manoeuvring trials provided information of the handling characteristics of the ship, for operational purposes. I am able to correlate certain parameters of each manoeuvre with a moderate level of accuracy: within 11% for the turning circle manoeuvres and within 15% for the zigzag manoeuvres. The analysis also showed that

the Nomoto coefficients could be accurately calculated for the vessel from the zigzag manoeuvre.

The seakeeping trials were carried out to define the seaworthiness characteristics of the ship by assessing the relationship between the motions of the ship and the related environmental conditions in which the ship was tested. With the correlation analysis, the model scale results compared relatively well to the full scale motions. In the particular cases where the peaks of the model scale motions were slightly shifted compared to the full scale motions, it can be attributed to the uncertainty of the wave direction from the analyzed full scale sea state.

By carrying out this study, I am able to validate the methodologies of the above research bodies for physical modeling and their numerical ship performance prediction models, by using quality full scale ship data. Validation of the testing procedure allows the consortium to be more competitive in the international research industry.

ACKNOWLEDGMENTS

The author would like to extend a huge thank you to Mr. David Cumming of IMD for his guidance and suggestions throughout my studies. His support and profound knowledge of the naval architecture field enabled me to complete my work with a higher degree of understanding and accuracy.

I would also like to thank Dr. Don Bass and Dr. Neil Bose for giving me this opportunity to broaden my expertise in the research field.

Finally, I extend a thank you to the staff of IMD. Without their knowledge and know-how, this project would never have happened or at least been as much fun!

TABLE OF CONTENTS

LIST OF TABLES

LIST OF FIGURES

LIST OF ABBREVIATIONS

3-D	Three dimensional
A_{VT}	Projected frontal area of the ship above the waterline
AP	Aft perpendicular
c	Propeller chord length @ 0.7 radius
cm	Centimetre(s)
C_A	Incremental resistance coefficient, Roughness allowance
C_{AA}	Air resistance coefficient
C_D	Drag coefficient
C_F	Frictional resistance coefficient
C_R	Residuary resistance coefficient
C_T	Total resistance coefficient
CCG	Canadian Coast Guard
CG	Centre of gravity
COG	Course over ground
c/w	Calm water
D	Size of the propeller (diameter)
DAS	Data acquisition system
DC	Direct current
deg.	Degree(s)
DFO	Department of Fisheries and Ocean

DGPS	Differential Global Positioning System
EAR	Expanded Area Ratio (propeller)
f	Coefficient of friction
FM	Frequency modulation
Fn	Froude Number
FP	Forward perpendicular
FS	Full scale
g	Acceleration due to gravity
GM	Metacentric height
GPS	Global Positioning System
$H_{1/3}$	Significant wave height
HF	High frequency
hr	Hour(s)
Hz	Hertz
in	Inch(es)
I	Ship mass properties (mass moment of inertia)
IMD	Institute for Marine Dynamics
ITTC	International Towing Tank Conference
J	Advance coefficient
k	Wave number, Form factor
k_p	Propeller blade roughness
k_s	Ship hull roughness

K	Nomoto coefficient for turning ability
K_{FD}	Skin-friction coefficient
K_Q	Torque coefficient
K_T	Thrust coefficient
kg	Kilogram(s)
kHz	Kilohertz
kN	KiloNewton(s)
kts	Knot(s)
kW	Kilowatt(s)
K&R	Kempf & Remmers
L	Ship size (length), Length
L_R	Rudder size (span length)
Lat.	Latitude
LBP	Length between perpendiculars
LCB	Longitudinal Centre of Buoyancy
LOA	Length overall
Long.	Longitude
LWL	Length of the waterline
$_m$	Model scale (subscript)
m	Metre(s)
M	Mass
MHz	Megahertz

min	Minute(s)
mm	Millimetre(s)
MS	Model scale
MUN	Memorial University of Newfoundland
m/s	Metre(s) per second
n	Speed of Rotation
nm	Nautical mile(s)
N	Newton, Total moment through the CG and parallel to z_o axis
Nm	Newton – metre(s)
NRC	National Research Council
$_o$	Open water (subscript)
OEB	Offshore Engineering Basin
$_P$	Self-propulsion (subscript)
p	Water static pressure
P	Propeller pitch @ 0.7 radius, Port
P_D	Delivered power
P_E	Effective power
P_T	Thrust power
PID	Proportional-Integral-Differential
PMM	Planar motions mechanism
Q	Propeller torque
r	Yaw rate

R	Resistance
R_F	Frictional resistance
R_R	Residuary resistance
R_T	Total resistance
RAO	Response amplitude operator
RF	Radio frequency
RMS	Root mean squared
Rn	Reynolds Number
Rn_{CO}	Propeller Reynolds Number @ 0.7 radius
RPM	Revolutions per minute
rps	Revolutions per second
s	Full scale (subscript)
s	Second(s)
S	Starboard, Total wetted hull surface
S_{BK}	Surface area of the bilge keels
S_ζ	Wave amplitude energy density spectrum
SOG	Speed over ground
t	Tonne(s), Thrust deduction fraction, Propeller thickness @ 0.7 radius, Temperature
T	Time, Nomoto coefficient for stability on course, Propeller thrust
T_o	Modal wave period
TRE	Time to reach execute

V	Ship speed, Volt(s)
V_A	Speed of advance
VCG	Vertical centre of gravity
w_T	Wake fraction
x_{OG}/y_{OG}	Position of the CG with respect to the origin of the fixed axis
x	Surge displacement
X_o	Total force in the x_o direction
y	Sway displacement
Y_o	Total force in the y_o direction
z	Heave displacement
Z	Number of propeller blades
$[x_B]$	Sufficient number of coordinates to define the shape of the hull
$[x_R]$	Sufficient number of coordinates to define the shape of the rudder
β	Drift angle, Appendage scale factor
δ	Rudder angle
Δ	Mass of the ship
ε	Bandwidth parameter of the wave spectrum
ϕ_x	Roll displacement
ϕ_y	Pitch displacement
ϕ_z	Yaw displacement
γ	Specific weight of the water
η_o	Propeller open water efficiency

η_B	Efficiency behind the hull
η_R	Relative rotative efficiency
η_H	Hull efficiency
η_D	Overall propulsive efficiency
λ	Scale ratio
μ	Dynamic viscosity of water
μstrain	Microstrain
ν	Kinematic viscosity of water
θ	Heading angle
ρ	Density of water
ω	Wave frequency
ω_e	Encountered wave frequency
ψ	Yaw angle, Heading angle
ζ_o	Wave amplitude
°	Degree(s)
°C	Degree(s) centigrade

Chapter 1 Introduction

In the early stages of the design process, the designer must establish the performance characteristics for the proposed vessel's propulsion, manoeuvring, and sea-keeping attributes. In order to achieve these attributes, the engineer must use a combination of numerical and physical modeling tests on the proposed design. Using empirical data of similar ship types, a preliminary design of the ship can be created. This process quantifies the hull form, the required appendages and their sizes, and the required propulsion system. However, the credibility of these theoretical and physical model experiments depends on the designer's ability to accurately and reliably correlate the test results to that of a full scale vessel. With this design ambiguity in mind, Memorial University of Newfoundland (MUN) in collaboration with the Institute for Marine Dynamics (IMD) of the National Research Council (NRC) of Canada and Marineering Ltd. designed and performed a ship / model correlation study on a 40 m long research vessel, M/V Louis M. Lauzier.

Information regarding a ship's performance in seakeeping, propulsion and manoeuvring cannot always be reliably predicted using existing numerical models. In addition, methodology deficiencies in scaling physical model data to full scale can significantly compromise the results. There is very little detailed full scale ship data available to the researcher in the open literature for validation of physical modeling methodology and/or numerical models. By carrying out this study, the above research bodies are validating their methodology for physical modeling and their numerical ship

performance prediction models, by using quality full scale ship data. Validation of the testing procedure enables these research bodies to interpolate full scale results based on model tests with a higher level of confidence and accuracy, allowing them to be more competitive in the international research industry.

This thesis describes the testing methodology that was used in the two-phase ship / model correlation study as well as an in-depth analysis and comparison of the experimental results. The first phase of this study involved full scale sea trials aboard the 'Lauzier'. There were three separate tests performed on the 'Lauzier': propulsion trials, manoeuvring trials, and seakeeping trials. The propulsion trials were performed to obtain the performance and propulsive characteristics of the vessel. The manoeuvring trials provided information of the handling characteristics of the ship, for operational purposes. Finally, the seakeeping trials were carried out to define the seaworthiness characteristics of the ship by assessing the relationship between the motions of the ship and the related environmental conditions in which the ship was tested.

The second phase of the study involved performing physical model tests on a model replica of the 'Lauzier'. The testing procedure was based on the testing procedures used during the first phase of the research. The model test plan was expanded in order to achieve more comprehensive results. For example, during the resistance testing, additional speeds were included to achieve a more defined resistance curve. Also, the wave data collected during the full scale seakeeping sea trials was used to generate a similar sea state to interact with the model during the model tests. There were

two scaled models built for this experiment: a 1:6 scale and a 1:12 scale, approximately 6 m and 3 m long respectively.

1.0 M/V Louis M. Lauzier

The 'Lauzier' is a 40 m long coastal research and survey vessel owned by MUN. The vessel is based in St. John's, Newfoundland and is primarily used by the Marine Institute as a training platform for sea-going personnel as well as a research platform by MUN's Physics & Physical Oceanography Department. The 'Lauzier' is a hard chine aluminium hulled, twin-screw vessel fitted with fixed pitch propellers, twin rudders, bow thruster, centerline skeg and a cylindrical shaped bulbous bow. During the time of the sea trials, the vessel was also fitted with a large faired sonar caisson situated slightly forward of midship on the starboard side. Each propeller is attached to a long length of exposed shafting, which is supported by a single 'A' bracket. The rudders are of simple balanced flat plate design under hung from the hull. They are controlled in tandem by a single control signal. Other appendages include a set of flat plate bilge keels fitted inboard of the chine.

The vessel is equipped with a modern navigation suite and can be steered using autopilot or manual control. The main engines can be controlled from the bridge using slip mode for better low speed control, ideal for docking and undocking manoeuvres, or conventional mode for normal operation. The electro-hydraulic steering system can be controlled by a single port or starboard steering motor or can be controlled by both motors simultaneously. The deck equipment fitted to the quarterdeck includes a

hydraulic boom crane, an A-frame over the stern and an electric motor driven capstan. The principal dimensions and a description of the outfit onboard the 'Lauzier' is presented in Table 1-1. Photographs of the 'Lauzier' are provided in Figure 1-1 to Figure 1-5.

Table 1-1: Principal Particulars and Description of Outfit

DESCRIPTION OF THE M/V LOUIS M. LAUZIER

Principal Particulars:

Length Overall	40 m
Length Between Perpendiculars	37.1 m
Breadth	8.2 m
Draft	2.44 m
Gross Displacement	332 t
Bare Hull Displacement	265.2 t
Cruising Speed	11.5 knots
Range	3500 nm
Day Trip Crew	4
Day Trip Personnel Accommodation (Incl. Crew)	37

Machinery Description:

Propulsion Type:	Geared Diesel
Main Engines:	2 * Cummins K2300
Propulsion Power:	2 * 600 kW
Electrical Generators:	2 * Caterpillar 3302
Electrical Power:	2 * 140 kW
Bow Thruster:	American™ Bow Thruster
Maximum Shaft RPM:	425 RPM (7.1 rps) (nominal)
Maximum Rudder Angle:	± 35 degrees (nominal)

Navigation/Communication Equipment:

Heading Gyro:	Sperry Mk 37 Mod 1 w/ 4 Repeaters
Radar (1):	JRC JMA-627-6-X Band
Radar (2):	Decca Racal 6520/CAD – X Band
GPS Position:	Trimble Navtrac XL
DGPS Position:	Furuno DPSS GP-36
VHF Direction Finder:	Taiyo TD-L1550
LORAN C:	Furuno LC 90
Depth Sounder:	1-Elac LAz 72, 1-Lowrange X-16
VHF AM:	Motorola PT 400
VHF AM:	Sailor RT 2047
Watch Receiver:	Skanti WR 6000
Transceiver:	Scansat – CG Transceiver C 9000
NavTex Receiver:	JRC NCR-300A
MF/HF SSB Radio System:	Skanti TRP 8000
MF/HF DSC Receiver:	Skanti DSC 9000

Magnetic Compass
Barometer
Barograph
Computer used to support Electronic Chart Data
Depth Sonar

Figure 1-1: M/V Louis M. Lauzier

Figure 1-2: Bulbous Bow

Figure 1-3: Sonar Caisson

Figure 1-4: Bilge Keel

Figure 1-5: Propeller Shaft, 'A' Bracket, & Propeller

The history of the 'Lauzier' is as follows:

- Built for the Federal Department of Fisheries & Ocean (DFO) in 1976 by Breton Industries Ltd, Port Hawkesbury, NS.
- Re-engined, new propellers fabricated and stern extended.
- Bulbous bow / bow thruster added.
- Leased to the Marine Institute by the CCG in 1998
- Bought by MUN in 2002.

Although the 'Lauzier' is not representative of any major commercial class of vessel, making it a less than ideal candidate for this study; its accessibility, relatively low operating / charter cost and internal layout brings about an attractive vessel for the ship /

model correlation project. It should be noted that the vessel proportions and hull form do conform to common designs for large luxury motor yachts.

2.0 Research Facilities

2.1 Memorial University of Newfoundland

Memorial University of Newfoundland is Atlantic Canada's premiere comprehensive university and one of the region's most important research facilities. It is located in a port city (St. John's, NL) where practical results and evidence of the work from ocean engineers and naval architects are easily accessible by both professors and students. With MUN's commitment to research and the surrounding community of marine studies, a comprehensive ship / model correlation study cements MUN as a research leader in this region.

2.1.1 Description of the MUN Towing Tank

The MUN Towing Tank, as seen in Figure 1-6, has a working area of 4.5 m by 60 m with a water depth that can vary up to 2 m. The tank is equipped with wave making machinery located at south end of the tank that is capable of generating regular and irregular waves up to 0.3 m significant wave height, which travel the length of the tank. The tank is fitted with passive wave absorbers on the three other sides of the tank: pool dividers along the length of the tank (fitted during calm water experiments only) and wire mesh at the north end of the tank. A carriage is installed on the tank to provide work over

capabilities as well as to be able to pull models through the water up to speeds of 5 m/s. This facility is used primarily by the Ocean & Naval Architectural Engineering Group.

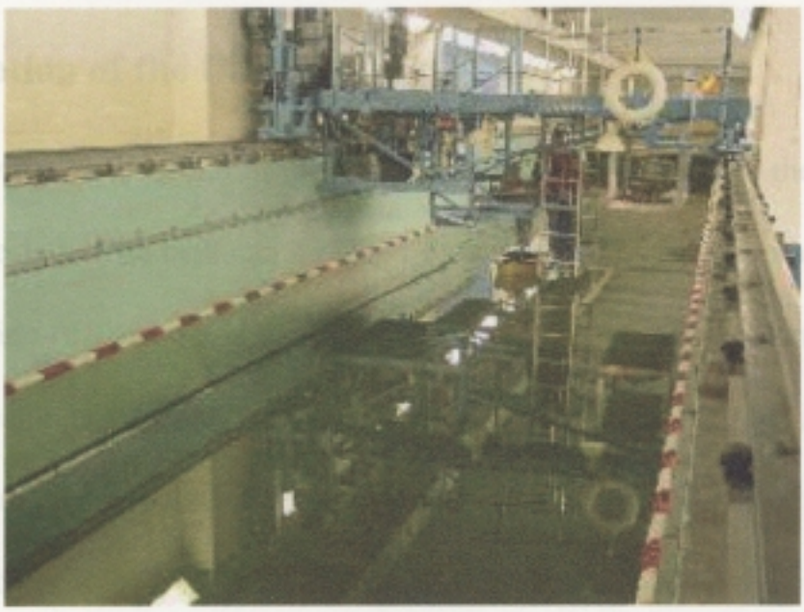

Figure 1-6: MUN Towing Tank

2.2 Institute for Marine Dynamics

The Institute for Marine Dynamics (IMD) was established in 1985 to provide innovative solutions and technical expertise in support of Canadian ocean technology industries. IMD's capability is unique to the nation; no other organization offers the combination of knowledge, experience and world-class facilities. IMD employs numerical, model and full-scale studies to predict or evaluate the performance of a range of systems in the ocean environment. It has established a worldwide reputation for the excellence of its work, building an impressive record of collaborative and contractual research, and a history of solid scientific achievement. Adding a comprehensive ship / model correlation study to the facility's achievements solidifies the facility as an

international research institution. IMD has three major testing facilities: a Towing Tank, an Ice Tank, and an Offshore Engineering Basin (OEB).

2.2.1 Description of the IMD Towing Tank

The Towing Tank is 200 m long, 12 m wide and 8 m high to the top of the wall, as seen in Figure 1-7. The tank can be filled with fresh water up to a constant depth of 7 m. The West side of the tank is equipped with a dual flap wavemaker. The East side contains a moveable beach that can be lowered in order for models to have access to the tank from the trim dock located behind the beach. The wavemaker is installed on a raised level with the lower and upper hinges located 4.0 m and 1.2 m below the water level, respectively. This computer controlled hydraulic dry-back wavemaker system can generate unidirectional regular and irregular waves up to wave heights of 1.0 m. Waves are absorbed at the opposite end of the tank by a parabolic beach constructed of a steel frame and covered with wooden slats.

The Towing Tank is equipped with a towing carriage. The towing carriage is an 80,000 kg steel structure with dimensions of 15 m long, 14.2 m wide, and 3.96 m high. The carriage is mounted on four sets of bogey wheels and two sets of rack drive wheels and has a speed range of 0.0002 m/s to 10 m/s. The carriage has a control room that is 14 m long, 2 m wide which houses the computer equipment for the drive control, data acquisition system, and the signal conditioning electronics for the model test transducers. The model test frame is capable of handling a 12 m long model with a displacement of 12000 kg.

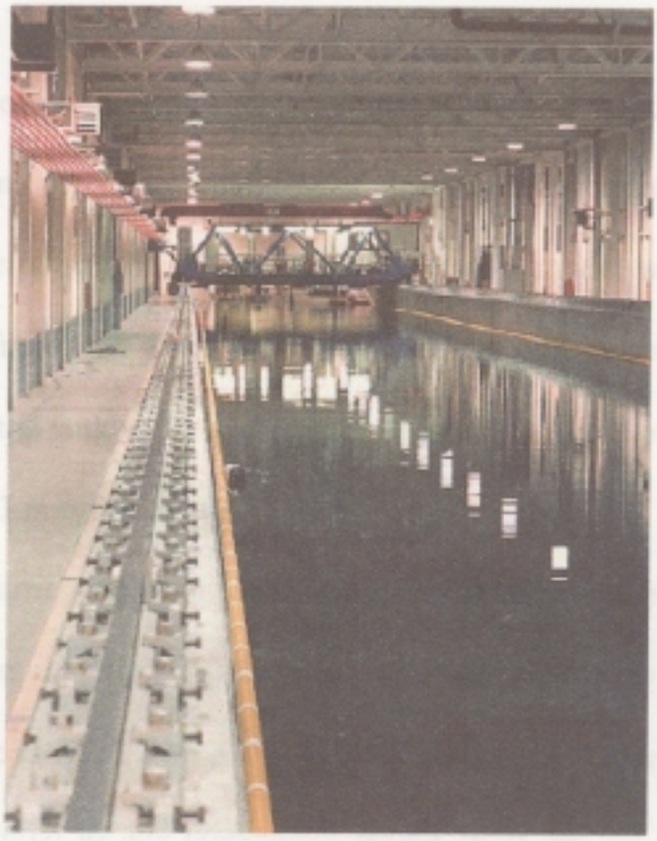

Figure 1-7: IMD Towing Tank

2.2.2 Description of the IMD Ice Tank

The Ice Tank is 91 m long, 12 m wide and a depth of 3 m, as seen in Figure 1-8. The Ice Tank is divided into 76 m of usable testing area for ice sheets and a 15 m long setting up area. A large thermal barrier door separates the two areas. At the opposite end of the tank is a melt pit with an isolated cover that allows an ice sheet to be grown while the remains of the previous one are melting.

The Ice Tank is equipped with 3 carriages: a towing carriage, a service carriage, and an underwater carriage. The Ice Tank towing carriage is an 80,000 kg steel structure with dimensions of 15 m long, 14.2 m wide, and 3.96 m high. This carriage is mounted on four sets of bogey wheels and two sets of rack drive wheels and has a speed range of

0.0002 m/s to 4 m/s. The carriage control room is 14 m long, 2 m wide and is thermally insulated. The control room houses the computer equipment for the drive control, data acquisition system, and the signal conditioning electronics for the model test transducers. The model test frame is capable of handling a 12 m long model with a displacement of 12000 kg. The test frame can position the model on the tank centre line, or on either of the quarter points of the tank width and is designed for ice forces of 60 kN on the centre line, or 30 kN on the 3 m offset points.

The service carriage is used for ice control and measurement work. It is a four wheel, 24 tonne, hydraulically driven carriage with manually controlled speeds of up to 0.5 m/s. The carriage is fitted with a working platform separated into three sections that can be raised or lowered to any convenient height from the ice. The sections can be operated individually or in unison. A three-section ice boom is installed in front of the carriage and these sections can also be raised or lowered together or separately. The boom can be tilted from horizontal to vertical for ice pushing and cleaning operations. The combined tilting and lifting effects are used to build pressure ridges, and the boom is capable of lifting 1800 kg. The boom can withstand thrust forces of 60 kN, though for such work the carriage is attached to the main towing carriage.

An underwater carriage can be readily attached and detached from the main tow carriage by a vertical mast. The underwater carriage is approximately 6 m wide and 8 m long and normally supports 2 underwater video cameras with underwater lights that supplement the 2 surface video cameras housed on the main carriage. The cameras are mounted on remote controlled pan and tilt heads and can be manually moved a limited

axial distance which permits a view of just about anywhere within the model test frame. The cameras are used to observe the ice interaction on structures and occasionally for flow visualization experiments of ship hulls in open water. Most model tests in ice are relatively slow so the underwater carriage was designed for use at speeds of up to about 1 m/s. Since the underwater carriage is directly below the model, hydrodynamic blockage effects may become noticeable at higher speeds. This carriage is generally disconnected during open water resistance and propulsion experiments

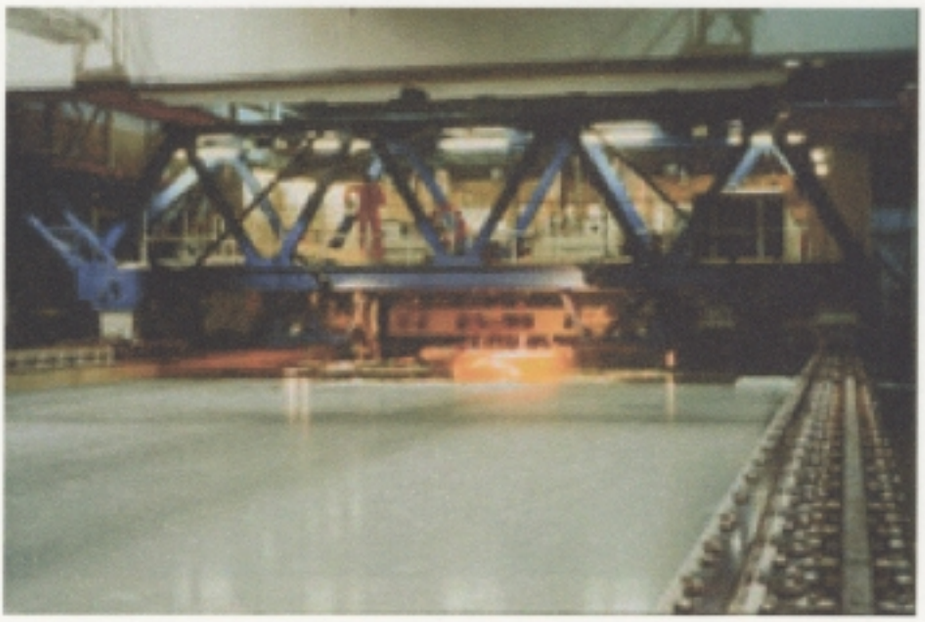

Figure 1-8: IMD Ice Tank

2.2.3 Description of the IMD Offshore Engineering Basin

The IMD Offshore Engineering Basin (OEB) has a working area of 26 m by 65.8 m with a depth that varies from 0.1 m to 3.2 m, as seen in Figure 1-9. The depth used for the experiments described in this report was 2.5 m. Waves are generated using 168 individual, computer controlled wet back wavemaker segments, hydraulically activated, fitted around the perimeter of the tank in an "L" configuration. Each segment can be

operated in one of three modes of articulation: flapper mode (± 15°), piston mode (± 400 mm) or a combination of both modes. The wavemakers are capable of generating both regular and irregular waves up to 0.5 m significant wave height. Passive wave absorbers are fitted around the other two sides of the tank. The facility has a recirculating water system based current generation capability with current speed dependent on water depth, extensive video coverage and is serviced over its entire working area by a 5 t lift capacity crane.

Figure 1-9: IMD Offshore Engineering Basin

Chapter 2 Background Research

1.0 Introduction

This chapter describes the basic theories involved in the set of tests in the ship / model correlation study: powering, manoeuvring, and seakeeping.

2.0 Powering

In the preliminary stages of ship design, there are two main design components the designer considers. They are the shape of the hull and how to propel the ship through the water. Care needs to be taken at this stage since the components are co-dependent. For optimal design efficiency, the design comprises of the following: the shape or form of the hull, the size and type of propulsion plant to provide motive power and the device to transform the power into effective thrust. The following sections detail the aspects of drag or resistance on the form of the ship and the required thrust or power required to move a particular hull. The type of propulsion plant is outside the scope of this project.

2.1 Resistance

When a ship is moving through the water at a given speed, the resistance of the ship is the fluid force acting on the ship in such a way as to oppose its motion. Resistance is the preferred term in ship hydrodynamics, while the term drag is preferred for aerodynamics and submerged bodies. For a designer, determining the form of the ship that provides the least amount of resistance, while simultaneously optimizing the hull in order to carry out its design function (e.g. carry oil from Kuwait to North

America), can be a tedious process. Once the ideal form is developed theoretically, model scale testing is performed to test the resistance of the hull before the full scale ship is built. This ensures that indeed the optimal design has been achieved.

The following subsections explore the various components involved in resistance of ships and various theories that are used to extrapolate model scale results to full-scale ship resistance.

2.1.1 Dimensional Analysis

In order to study the resistance acting upon a body moving through the water, the basic laws of resistance must be examined. Since it is difficult to explicitly define these laws or factors, dimensional analysis is used to characterize the relationship. First break up the function into its independent components. In this case, resistance can be expressed as a function of the characteristics of the water and of the ship:

$$R = f_1\{L, [x_B], V, \rho, \mu, g, p\} \qquad \textbf{(2-1)}$$

Where: R = Resistance; ρ = Density of water;

L = Ship size (length); μ = Dynamic viscosity of water;

V = Ship speed; g = Acceleration due to gravity;

p = Water static pressure; and

$[x_B]$ = Sufficient number of coordinates to define the shape of the hull.

Since these tests will involve ships that are geometrically similar, $[x_B]$ can be ignored.

To develop an expression that correlates the resistance to the factors mentioned above, it is necessary to develop non-dimensional terms that will apply to both model

scale and full scale ships. To perform this, the matrix method for dimensional analysis is employed. For this method, each identity is expressed in terms of their fundamental dimensions: mass (M), length (L), and time (T), as seen in the top portion of Table 2-1. The individual number represents the number of terms present. For example, the resistance term, *R*, can be equated to 'mass x length / time^2'. The terms are then divided by three common factors that can easily be distinguished from each other. In this case, these factors are: ship size (*L*), ship speed (*V*), and density of water (ρ). These terms were chosen because ρ is the only term with a mass component and *V* is the only term with a time component. The ship size term is then used to non-dimensionalize the term since it only contains the length component. Using the resistance term again, it contains 1 mass term, -2 time terms, and 1 length term. It can be replaced by 1 ρ term (only term with a mass component), 2 *V* terms (only term with a time component, and opposite sign since the time component is in the numerator) and 2 *L* terms. The ship size term not only replaces the length term in the resistance but any length terms associated with the ρ and *V* terms to make the entire term dimensionless (# of *L* terms = 1 (R) + -3 (ρ) + 2 (*V*)).

Table 2-1: Matrix Method – Resistance

	L	V	ρ	R	p	μ	g
L	1	1	-3	1	-1	-1	1
T	0	-1	0	-2	-2	-1	-2
M	0	0	1	1	1	1	0
L	1	0	0	2	0	1	-1
V	0	1	0	2	2	1	2
ρ	0	0	1	1	1	1	0

The various non-dimensional 'π' terms formulated from the above matrix are as follows:

$$\pi_1 = \frac{R}{\rho V^2 L^2}\ ;\ \pi_2 = \frac{p}{\rho V^2}\ ;\ \pi_3 = \frac{\mu}{\rho VL}\ ;\ \pi_4 = \frac{gL}{V^2} \qquad (2\text{-}2)$$

By compounding, the non-dimensional resistance can be expressed as follows:

$$\frac{R}{\rho V^2 L^2} = f_2\left\{\left(\frac{p}{\rho V^2}\right),\left(\frac{\mu}{\rho VL}\right),\left(\frac{gL}{V^2}\right)\right\} \qquad (2\text{-}3)$$

Equation 2-3 states that the non-dimensional resistance will be the same for any ship as long as they are geometrically similar, provided that the non-dimensional terms inside the function have the same numerical values. It is irrelevant what the relationship of f_2 has with its terms since it will be the same for the geometrically similar ships.

The π_2 term is the ratio of static pressure to dynamic pressure. Although there are particular circumstances, such as with cavitation on propellers, where this term may be of great importance, in the instance of ship resistance, the π_2 term may be ignored. The π_3 term contains the viscosity of water that is related to frictional resistance. The π_4 term contains the gravitational factor that is connected to wave-making resistance; the energy expended to generate gravity waves.

2.1.2 Resistance Equation

A major assumption made when dealing with ship resistance is that the frictional and wave-making resistances are independent of each other [1]. For this reason, the resistance equation can be rewritten as follows:

$$\frac{R}{\rho V^2 L^2} = f_3\left\{\left(\frac{\mu}{\rho VL}\right) + \left(\frac{gL}{V^2}\right)\right\} \qquad (2\text{-}4)$$

For geometrically similar models, the wave-making resistance for one model (or ship) could be deduced from the wave-making resistance of a second model as long as their speeds are in the ratio of the square roots of their lengths. This is known as Froude's law of comparison.

$$\frac{V_1}{V_2} = \sqrt{\frac{L_1}{L_2}} \qquad \textbf{(2-5)}$$

Since the frictional resistance deals with both geometrical and dynamical similarity (similar water density), in order to relate the resistances for the two different models, $V_1L_1 = V_2L_2$. This is known as Rayleigh's law [1].

In order to satisfy both laws, the two models must be the same size. If the first model is half the length of the second model, using Froude's law, the speed of the smaller model is less by 0.707 times. On the other hand, if Rayleigh's law is used, the speed of the smaller model is faster by 2 times. So, reason suggests that when attempting to estimate ship resistance from geometrically similar models, satisfying Froude's law would be the most practical design approach.

The designer must also be aware of the region of laminar and turbulent flow on the model. In the case of the larger model (or ship), the vessel mainly travels through a turbulent flow due to the higher speeds, whereas the smaller model may experience laminar flow with its decreased model speed, especially in the bow of the ship. Since turbulent flow creates a higher frictional resistance than does laminar flow, it is important to create turbulent flow on the smaller model. To achieve this, turbulence stimulators are

attached to the bow of the ship to prevent laminar flow. One such device that is commonly used is 3 mm diameter studs or pins fitted on the forward end of the bow.

2.1.3 Full Scale Prediction

To solve the correlation resistance problem, William Froude, a pioneer in model scale testing, developed the first scientific way to relate model scale resistance to ship resistance. It has since been called Froude's Method [1]. The total model resistance, R_{TM}, is measured at various speeds and broken up into two parts: the frictional resistance (R_{FM}) plus the residuary resistance (R_{RM}). If the residual resistance is to be assumed independent of the frictional resistance, Froude's law must be obeyed. As such, the following equation applies:

$$V_M = \frac{V_S}{\sqrt{\lambda}} \qquad \textbf{(2-6)}$$

where V_M and V_S are the speed of the model and ship, respectively, and λ is the scale ratio based on geometric similar models.

The accuracy of this procedure depends largely on the accuracy of the frictional resistance calculation. Froude calculated the frictional resistance using the formula,

$$R_F = fSV^n \qquad \textbf{(2-7)}$$

where S is the total wetted surface area of the ship/model, f is its coefficient of friction, V is its speed, and n is an index giving the power of V according to which R_F is increasing. Froude assumed that a ship form has a frictional resistance equal to that of a flat

rectangular plate having the same wetted area and length as the ship. However over time, the formula for frictional resistance has changed:

$$R_F = \frac{\gamma\lambda}{1000} SV^{1.825}$$
$$\lambda = \left(0.1392 + \frac{0.258}{2.68 + L}\right)\left[1 + 0.0043(15 - t)\right] \quad \textbf{(2-8)}$$

where: L = Length of the ship/model;

t = Temperature of the water;

S = Wetted surface area;

V = Ship speed in m/s^2; and

γ = Specific weight of the water.

Since the value of R_{FM} is calculated, R_{RM} can be deduced by subtracting R_{FM} from the total model resistance. R_{RM} is considered to be made up of almost entirely wave-making resistance. The residuary resistance of the model is then scaled up to find the residuary resistance of the ship using

$$R_{RS} = \lambda^3 R_{RM} \quad \textbf{(2-9)}$$

Using the same principles for calculating R_{FM} to calculate the frictional resistance for the ship, R_{FS}, the total ship resistance can be calculated by

$$R_{TS} = R_{FS} + \lambda^3 R_{RM} = R_{FS} + \lambda^3 \left(R_{TM} - R_{FM}\right) \quad \textbf{(2-10)}$$

However, using Froude's Method to calculate the ship resistance, the following factors have been ignored:

1. the fluid particle moves in complicated paths due to the waves formed by the ship;

2. the speed of the fluid along the hull does not always equal that of the ship;
3. that water separation from the hull can occur; and
4. the boundary layer on the hull surface can be different from that on a corresponding flat plate.

In spite of these drawbacks, Froude's idea of splitting the resistance into two components is still used in other resistance methods.

In 1957, using Froude's basic principal of splitting up the resistance components, the International Towing Tank Conferences (ITTC) worked out their own method to transform model test results from model scale to full scale. This method, called ITTC 1957 Method [2], is built on Froude's method in three ways.

The first difference is that ITTC '57 deals with the non-dimensional resistance coefficient instead of the resistance terms alone. The total model resistance coefficient is stated as:

$$C_{TM} = \frac{R_{TM}}{\frac{1}{2}\rho_M V_M^2 S_M} \qquad \textbf{(2-11)}$$

where: R_{TM} = Total model resistance;

ρ_M = Density of testing water;

V_M = Speed of the model; and

S_M = Wetted surface area of the model.

The second difference is the implementation of the 'ITTC 1957 Model-Ship Correlation Line'. This line replaces the frictional resistance calculation in the previous method. The line formulation for the frictional resistance coefficient (C_F) was regarded

as an interim solution to the frictional problem for practical engineering purposes. The friction coefficient is found by

$$C_F = \frac{0.075}{(\log_{10} R_n - 2)^2} \quad \textbf{(2-12)}$$

where R_n is the local Reynolds Number expressed as:

$$R_n = \frac{VL}{\nu} \quad \textbf{(2-13)}$$

ν is the kinematic viscosity of the fluid that is equal to the dynamic viscosity divided by the density of the fluid (μ/ρ).

The third difference is the addition of the incremental resistance coefficient (C_A) that takes into account the effect of roughness on the surface of the ship. Most model tests organizations use a standard C_A coefficient of 0.0004 for all types of ships.

As a result, to obtain the total resistance of the ship, the following calculations are performed: (the subscripts S and M stand for ship and model, respectively).

$$R_S = C_{TS}\left(\tfrac{1}{2}\rho_s V_S^2 S_S\right) \quad \textbf{(2-14)}$$

where

$$C_{TS} = C_{FS} + C_{RS} + C_A \quad \textbf{(2-15)}$$

Since it is assumed that the residual resistance is the same for both the model and the ship at the same Froude Number;

$$C_{TS} = C_{FS} + C_{RM} + C_A = C_{FS} + (C_{TM} - C_{FM}) + C_A \quad \textbf{(2-16)}$$

where C_F is calculated using Equation 2-12.

In 1978, ITTC introduced the '1978 ITTC Performance Prediction Method' [3]. This method introduced the form factor philosophy developed by Prohaska in 1966 [4], by determining a three-dimensional form factor (k) on flat plate friction. To obtain the form factor, Prohaska proposed to run the model at ten low speed tests corresponding to $0.1 < Fn < 0.22$ to determine the total resistance coefficient, C_T, where Fn is the local Froude Number expressed as

$$Fn = \frac{V}{\sqrt{gL}} \tag{2-17}$$

Owing to the uncertainty involved in measuring resistance at very low speeds, ITTC recommended a speed interval of $0.12 < Fn < 0.2$. The form factor is determined by plotting C_T / C_F versus Fn^4 / C_F. A straight line is plotted through the points with a slope of c and an intercept of $(1+k)$. Therefore, the equation of the line is

$$\frac{C_T}{C_F} = (1+k) + c\frac{Fn^n}{C_F} \tag{2-18}$$

where the exponent n for Fn has to be evaluated in order to obtain the best approximation of the measured data points. Prohaska proposed a power between 4 and 6 for full scale ships.

ITTC '78 Method states the total resistance coefficient of a ship without bilge keels is

$$C_{TS} = (1+k)C_{FS} + C_R + C_A + C_{AA} \tag{2-19}$$

$$C_R = C_{TM} - (1+k)C_{FM} \tag{2-20}$$

$$C_A = \left[105 \left(\frac{k_s}{LWL} \right)^{1/3} - 0.64 \right] \times 10^{-3} \quad \text{(2-21)}$$

$$C_{AA} = 0.001 \left(\frac{A_{VT}}{S} \right) \quad \text{(2-22)}$$

where: C_{FS} = Frictional resistance coefficient based on the ITTC '57 ship-model correlation line;

C_R = Residual resistance coefficient;

C_A = Roughness allowance;

C_{AA} = Air resistance coefficient;

k_s = Mean amplitude of the surface roughness over a 50mm span of hull (if a value is not available, the designer can use a standard amplitude of 150 x 10^{-6} meters);

LWL = Length of the waterline of the ship; and

A_{VT} = Projected frontal area of the ship above the waterline.

However, Equation 2-19 can be altered to accommodate a ship with fitted bilge keels:

$$C_{TS} = \frac{S + S_{BK}}{S} [(1+k)C_{FS} + C_A] + C_R + C_{AA} \quad \text{(2-23)}$$

where: S_{BK} = Surface area of the bilge keels.

Figure 2-1 displays the transformation of the resistance coefficient from model scale values to the full scale values. The figure displays the effect form factor has on the results as well as the addition of the roughness coefficient on the full scale values.

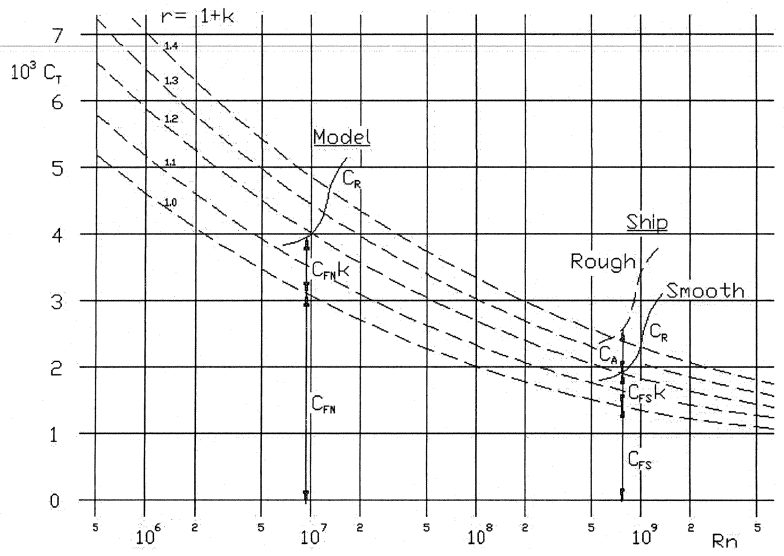

Figure 2-1: ITTC '78 Resistance Prediction Method

2.2 Propulsion

Over the decades, there have been many innovative ways to propel a vessel through the water; from the beginning of the oar and the evolution of the sail, to the paddlewheel, water jets and screw propellers. Of the aforementioned, the screw propeller has become the most popular choice to propel the designed vessel due to several key advantages: they are well protected underneath the hull away from damages caused by the sea and collisions; they can be driven using small, light weight and fast-running engines; and their design is quite flexible so they can be changed for either high thrust or high torque, or both. With that in mind, the designer must develop the propeller that meets the vessel's needs while at the same time optimizing the efficiency of the propeller. Although the propeller can be designed theoretically, model tests are performed with the propeller in open water to ensure that the ideal design of the propeller is achieved and

with the propeller connected to a model replica of the vessel to see the effect that the propeller interaction with the hull has on the propeller thrust and efficiency.

The following subsections explore the various components involved in designing an optimal propeller and the theory involved in extrapolating the model scale results to full scale thrust/torque requirements.

2.2.1 Dimensional Analysis

As in the case of resistance, the basic laws governing the thrust and torque values of the propeller with the associated water traveling through the propeller blade area must be examined by applying dimensional analysis. The thrust / torque can be expressed as a function of the characteristics of the propeller and the fluid:

$$T/Q = f_4\{\rho, D, V_A, g, n, P, \mu\} \quad \textbf{(2-24)}$$

Where: T = Propeller thrust; g = Acceleration due to gravity;

Q = Propeller torque; n = Speed of rotation;

ρ = Density of water; p = Water static pressure;

V_A = Speed of advance; μ = Dynamic viscosity of water; and

D = Size of the propeller, represented by its diameter.

Similar to the dimensional analysis performed for resistance, the matrix method, as seen in Table 2-2 and Table 2-3, is employed to develop an expression that relates the thrust / torque to the above factors in a non-dimensional form, enabling the designer to relate model scale values to full scale values. The common factors used in this method are ρ, D, and V_A.

Table 2-2: Matrix Method – Thrust

	L	Va	ρ	T	g	n	P	μ
L	1	1	-3	1	1	0	-1	-1
T	0	-1	0	-2	-2	-1	-2	-1
M	0	0	1	1	0	0	1	1
L	1	0	0	2	-1	-1	0	1
Va	0	1	0	2	2	1	2	1
ρ	0	0	1	1	0	0	1	1

Table 2-3: Matrix Method – Torque

	L	Va	ρ	Q	g	n	P	μ
L	1	1	-3	2	1	0	-1	-1
T	0	-1	0	-2	-2	-1	-2	-1
M	0	0	1	1	0	0	1	1
L	1	0	0	3	-1	-1	0	1
Va	0	1	0	2	2	1	2	1
ρ	0	0	1	1	0	0	1	1

By compounding, the non-dimensional thrust / torque can be expressed as follows:

$$\frac{T}{\rho D^2 V_A^2} = f_5\left\{\frac{gD}{V_A^2}, \frac{nD}{V_A}, \frac{P}{\rho V_A^2}, \frac{\mu}{\rho D V_A}\right\} \quad \textbf{(2-25)}$$

$$\frac{Q}{\rho D^3 V_A^2} = f_6\left\{\frac{gD}{V_A^2}, \frac{nD}{V_A}, \frac{P}{\rho V_A^2}, \frac{\mu}{\rho D V_A}\right\} \quad \textbf{(2-26)}$$

The above equations state that for any propeller that is geometrically similar, if the non-dimensional terms inside the function have the same numerical values, the non-dimensional thrust / torque will be the same regardless of the relationship of f_5 and f_6.

The first term inside the expressions is a form of the Froude Number. The second term is referred to as the advance coefficient, *J*. The third term deals with the atmospheric pressure acting on the propeller. This pressure is difficult to correlate

between model and full scale, since the forces on the propeller blades are caused by differences in pressure, this term can be ignored in this equation. In the instance that cavitation occurs, a set of specific tests can be carried out on the propeller. Finally, the fourth term is a form of the Reynolds Number.

2.2.2 Propeller Coefficients

The propeller thrust and torque characteristics are plotted in the non-dimensional terms stated in Equations 2-25 & 2-26 to the base of the advance coefficient. The disadvantage that those particular coefficients create is that they become infinite for zero speed of advance. However, since J is the same for both the model and the ship, V_A can be replaced by nD in the thrust and torque coefficients which would not have the above disadvantage. As a result, the typical propeller coefficients are:

Advance Coefficient: $$J_O = \frac{V_A}{nD} \quad \textbf{(2-27)}$$

Thrust Coefficient: $$K_{TO} = \frac{T_O}{\rho n^2 D^4} \quad \textbf{(2-28)}$$

Torque Coefficient: $$K_{QO} = \frac{Q_O}{\rho n^2 D^5} \quad \textbf{(2-29)}$$

To determine these coefficients, a set of open water experiments are carried out. These tests are performed with the propeller extruding in front of a specialized testing apparatus so that the propeller blade area will experience homogenous velocity fluid flow, undisturbed by the flow of the apparatus. An example of this specialized apparatus can be seen in Figure 2-2.

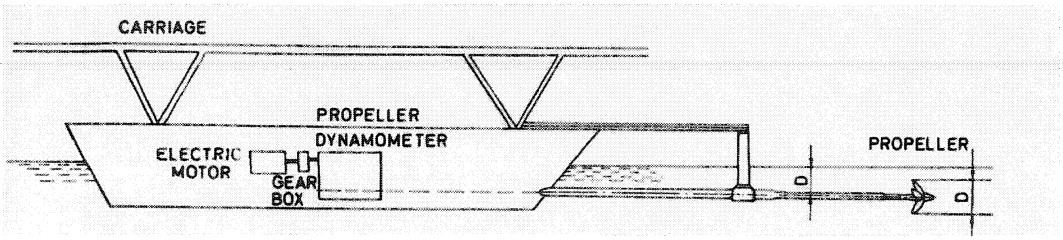

Figure 2-2: Propeller Open Water Testing Apparatus

The propeller open water efficiency is then expressed as follows:

$$\eta_O = \frac{J}{2\pi} \cdot \frac{K_{TO}}{K_{QO}} \qquad \textbf{(2-30)}$$

Typical propeller curves generated from propeller open water experiments can be seen in Figure 2-3.

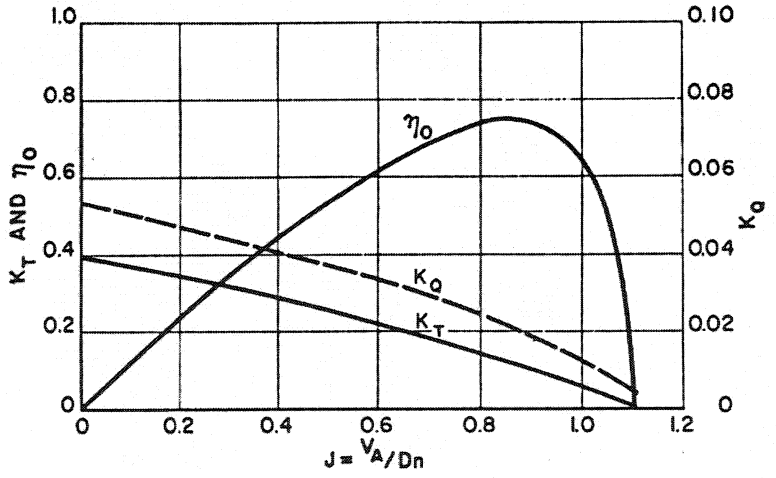

Figure 2-3: Typical Propeller Curves in Open Water

In dealing with geometrically similar propellers, the first condition for similarity of flow is that the speed of advance of the model and the ship propellers should be in accordance with Froude's Law of Comparison. As in the case of resistance, one cannot meet Froude's law and at the same time have the same Reynolds Number. Since the

frictional resistance is only a very small component of the total force, this inconsistency can be neglected. In spite of this, the propellers should be made as large as possible within the limitations of the hull model scale, measuring apparatus, etc. to avoid any laminar flow over the blades [5]. In practice, the open water experiments are carried out at constant propeller revolutions with different speeds of advance. This is done to obtain as high a value of Reynolds Number as possible provided the propeller is run with adequate immersion, approximately at a depth of 1.5x the diameter of the propeller, so that there is no wave-making on the surface. Meeting this condition, the lack of Froude Number identity will not have any important effects.

2.2.3 Hull / Propeller Interaction

When the propeller is in its correct location behind the model or ship, the propeller is no longer operating in a uniform flow field. The flow field is disturbed by the passage of the hull. This disturbance is called the wake which results in the propeller experiencing a fluid flow at a lower speed, V_A, than the relative speed of the model / ship, V. Since the wake produces a non-uniform flow field, there is a possibility of experiencing different propeller efficiencies behind the hull than in open water.

A wake factor represents the effective wake felt by the propeller. This factor can be deduced by comparing the propeller performance from behind the hull and in open water. For example, at a model speed, V, the propeller develops a thrust, T at n revolutions per second. Referring to the open water curves at that particular shaft speed and thrust, one produces a lower speed, V_A. Thus, the effective wake fraction, w_T is:

$$w_T = \frac{V - V_A}{V} \qquad (2\text{-}31)$$

The effective wake fraction can be also be derived by using the torque values; however, the fractions will be slightly different. When using the tests for model experiments only, deriving the fraction using the thrust values is the preferred method because the thrust can be measured more accurately than the torque. On the other hand, if the experiments are used in a ship / model correlation study, it might be necessary to use torque value to calculate the fraction since it is usually quite difficult to measure thrust on a full scale ship.

Due to the wake, the open water efficiency is different at the same V_A, T and n due to the Q value experienced behind the hull. This new efficiency is known as the efficiency behind the hull, η_B and the ratio of the two efficiencies is known as the relative rotative efficiency, η_R.

$$\eta_B = \frac{TV_A}{2\pi nQ} \qquad (2\text{-}32)$$

$$\eta_R = \frac{\eta_B}{\eta_O} = \frac{Q_O}{Q} \qquad (2\text{-}33)$$

Besides the hull having an effect on the propeller, the opposite is true as well. Through the actions of the propeller, the water passing along the stern of the model / ship is at a much faster rate than during the resistance experiments. This enhanced rate decreases the pressure aft, which in turn increases the necessary thrust needed to propel the vessel. For example, at model speed, V, the measured propeller thrust, T is greater

than the measured resistance, R_T. This can be expressed as a thrust deduction fraction, t where *(1-t)* is known as the thrust deduction factor.

$$t = \frac{T - R_T}{T}$$

or

$$R_T = (1-t)T \qquad \textbf{(2-34)}$$

Hence, the interaction between the hull and the propeller can be summed up as the hull efficiency, η_H which is the ratio of the effective power, P_E, (calculated from the resistance) and the thrust power, P_T. The efficiency can also be expressed as the ratio of the thrust deduction factor and the wake factor.

$$\eta_H = \frac{P_E}{P_T} = \frac{R_T V}{T V_A}$$

or

$$\eta_H = \frac{(1-t)}{(1-w)} \qquad \textbf{(2-35)}$$

To optimize the propeller design, the designer must look at the overall propulsive efficiency, η_D.

$$\eta_D = \frac{P_E}{P_D} = \frac{P_E}{P_T} \cdot \eta_B$$

or

$$\eta_D = \frac{(1-t)}{(1-w)} \cdot \eta_B = \eta_H \cdot \frac{\eta_B}{\eta_O} \cdot \eta_O = \eta_H \cdot \eta_R \cdot \eta_O \qquad \textbf{(2-36)}$$

In the above equation, P_D is the delivered power.

2.2.4 Full Scale Prediction

To relate the propulsive efficiency from model scale to full scale, three sets of model experiments have to be preformed: resistance tests, propeller open water tests, and self-propulsion tests. The resistance and propeller open water experiments have been discussed earlier. The self-propulsion experiments are tests run with the propeller attached to the model so that when the model is towed down the testing tank, the propeller revolutions are varied above and below the self-propulsion point. The self-propulsion point is the revolution rate at which the propeller produces enough thrust to mitigate any tow force.

The following calculations are based on ITTC '78 Power Prediction Method [5].

From the self-propulsion experiments, the advance, thrust and torque coefficients are calculated as per Equations 2-27, 2-28, & 2-29 and are denoted by J_P, K_{TP}, and K_{QP}, respectively. Using the thrust identity where $K_{TP} = K_{TO}$, J_O and K_{QO} are interpolated from the propeller open water experiments. From these values, the model wake fraction, relative rotative efficiency and thrust deduction fraction are calculated where S_S and D_S is the full scale wetted surface area and ship propeller diameter, respectively.

$$w_T = 1 - \frac{J_O}{J_P} \qquad \textbf{(2-37)}$$

$$\eta_R = \frac{K_{QO}}{K_{QP}} \qquad \textbf{(2-38)}$$

$$t = 1 - \frac{S_S}{2D_S} \cdot \frac{C_{TS} J_P^2}{K_{TP}} \qquad \textbf{(2-39)}$$

The thrust deduction fraction is independent of scale whereas the approximate full scale wake fraction needs to be expressed as:

$$w_{TS} = (t + 0.04) + (w_T - t - 0.04) \cdot \frac{(1+k)C_{FS} + C_A}{(1+k)C_{FM}} \quad \textbf{(2-40)}$$

The full scale propeller open water characteristics are then estimated by:

$$K_{TOS} = K_{TO} + 0.3(C_{DM} - C_{DS})\frac{P}{D}\frac{cZ}{D} \quad \textbf{(2-41)}$$

$$K_{QOS} = K_{QO} - 0.25(C_{DM} - C_{DS})\frac{cZ}{D} \quad \textbf{(2-42)}$$

$$C_{DM} = 2\left(1 + 2\frac{t}{c}\right)\left(\frac{0.044}{R_{nco}^{1/6}} - \frac{5}{R_{nco}^{2/3}}\right) \quad \textbf{(2-43)}$$

$$C_{DS} = 2\left(1 + 2\frac{t}{c}\right)\left(1.89 + 1.62\log\frac{c}{k_p}\right)^{-2.5} \quad \textbf{(2-44)}$$

where:

D = Full scale diameter;

P = Propeller pitch at 0.7 radius;

c = Propeller chord length at 0.7 radius;

Z = Number of propeller blades;

C_D = Drag coefficient;

t = Propeller thickness at 0.7 radius;

R_{nco} = Local Reynolds Number at 0.7 radius; and

k_p = Blade roughness, taken as 30×10^{-6} m.

The load on the full scale propeller behind the ship is estimated from:

$$\frac{K_{TS}}{J^2} = \frac{S}{2D^2} \frac{C_{TS}}{(1-t)(1-w_{TS})^2} \quad \textbf{(2-45)}$$

With $K_{TS} = K_{TOS}$, the full scale J_S and K_{QS} are obtained from the above equation and the full scale propeller open water curves. As a result, the following calculations can be made to predict the full scale delivered power, effective power, hull efficiency and propulsive efficiency.

$$n_S = \frac{(1-w_{TS})V_S}{J_S D} \quad \textbf{(2-46)}$$

$$P_{DS} = 2\pi\rho n_S^3 D^5 \frac{K_{QS}}{\eta_R} \quad \textbf{(2-47)}$$

$$P_{ES} = \tfrac{1}{2}\rho S V_S^2 C_{TS} \quad \textbf{(2-48)}$$

$$\eta_{HS} = \frac{(1-t)}{(1-w_{TS})} \quad \textbf{(2-49)}$$

$$\eta_{DS} = \frac{P_{ES}}{P_{DS}} \quad \textbf{(2-50)}$$

With the above experiments and prediction calculations, the designer can perform an iterative process to conceive either the optimal hull design for a particular propulsive system or the optimal propulsive system for a given hull or both.

3.0 Manoeuvring

Manoeuvrability is a very important design aspect when designing a ship. In considering the operations of the vessel in open water, in channels, and harbours, it is important to know the handling characteristics of the ship. To understand these characteristics, tests need to be carried out in order to determine the course keeping as

well as the course changing qualities of the ship. In the early stages of the design, numerical models are available to predict such qualities before the experimental stage is required. Once predictions are made, various model tests are performed to quantify these manoeuvring qualities.

The following subsections will examine the various theories employed to extrapolate model scale results to full scale results as well as experiments that are performed to establish the manoeuvrability of a ship.

3.1 Dimensional Analysis

To extrapolate the model test results to a full size ship, one must be able to correlate the data of the two identities. Correlation is simply performed by expressing the responses in such a way that the equation will be the same for both the model and the ship. To achieve this, dimensional analysis is employed to express relevant terms in non-dimensional functions equivalent to both model and full scale tests.

For example, the yaw rate of the vessel is extremely important in manoeuvring experiments. The yaw rate can be expressed as a function of the characteristics of the ship and the water, which can be written as follows:

$$\dot{\psi} = f_7\{V, L_S, I, \psi, [x_B], \delta, L_R, [x_R], \rho, \mu, g\} \qquad \textbf{(2-51)}$$

where: V = Ship Speed; L_S = Ship size (length);

I = Ship mass properties; ψ = Yaw angle;

δ = Rudder angle; L_R = Rudder size (length);

ρ = Density of water; μ = Dynamic viscosity of water;

g = Acceleration due to gravity; and

$[x_{B/R}]$ = Sufficient number of coordinates to define the shape of the hull / rudder.

In the above equation, the mass properties of the ship are represented by the mass moment of inertia of the ship about the z axis, assuming that the axis acts through the CG of the vessel. Since the experiments involve a ship and a geometrically similar model, $[x_{B/R}]$ can be removed since it will be the same for both objects. Also, the scale used for the rudder will be the same as the scale used for the ship; therefore, L_S and L_R can be combined as L.

The matrix method is utilized to develop the non-dimensional terms. First, each term is expressed by their basic quantities of length, time, and mass. Then the terms are characterized by three common factors: ship size, ship speed and the density of water. This is denoted in Table 2-4.

Table 2-4: Matrix Method - Yaw Rate

	L	V	ρ	ψ'	I	ψ	δ	μ	g
L	1	1	-3	0	5	0	0	-1	1
T	0	-1	0	1	0	0	0	-1	-2
M	0	0	1	0	0	0	0	1	0
L	1	0	0	1	5	0	0	1	-1
V	0	1	0	-1	0	0	0	1	2
ρ	0	0	1	0	0	0	0	1	0

By compounding, the non-dimensional yaw rate can be expressed as follows:

$$\frac{\dot{\psi}V}{L} = f_8\left\{\frac{I}{L^5}, \frac{\mu}{\rho VL}, \frac{gL}{V^2}, \delta, \psi\right\} \quad \textbf{(2-52)}$$

Equation 2-52 denoted that for geometrically similar models, if the non-dimensional terms inside the function have the same values, then the non-dimensional yaw rate will be the same regardless of the function f_8. On the other hand, as in the previous dimensional analysis performed in the powering section, the above equation is a function of both the Froude Number and Reynolds Number. Following Froude scaling to achieve model scale test speed, the effects of viscosity, or lack of Reynolds Number identity, can be ignored.

3.2 Linear Theory of Manoeuvring

One mathematical model used to predict the handling characteristics of a vessel is linear theory. Although most math models are non-linear, linear models actually allow analytic analysis. Linear theory [6] is based on linear equations that describe the motion of the ship in a horizontal plane. With respect to arbitrary axes fixed to the earth, the basic equation of motions for a ship traveling along a path can be expressed as:

Surge: $$X_0 = \Delta \ddot{x}_{0G}$$

Sway: $$Y_0 = \Delta \ddot{y}_{0G} \qquad \textbf{(2-53)}$$

Yaw: $$N = I_z \ddot{\psi}$$

Where: X_0 / Y_0 = Total forces in x_0 / y_0 direction;

Δ = Mass of the ship;

x_{0G} / y_{0G} = Position of the center of gravity of the ship (CG) with respect to the origin of the fixed axis;

N = Total moment about the axis through the CG and parallel to the z_0-axis;

I_z = Mass moment of inertia of the ship about the vertical axis through the CG; and

ψ = Yaw angle of the ship or the heading of the ship (positive clockwise).

Although Equations 2-53 is quite simple, it is customary to express the Equations of Motions in terms of the axes of the ship. The origin of the axes is located at the center of gravity of the ship with the x-axis positioned along the centerline of the ship (positive forward) and the y-axis being perpendicular to the x-axis (positive in the starboard direction). The z-axis is perpendicular to both y and x axes and is positive in the downward direction. The instantaneous linear velocity, V, shows the movement of the ship in the horizontal plane and is taken along the tangent path of the ship. Therefore, u is the x-axis velocity component of V, while v is the y-axis component. These variables can be seen in Figure 2-4, where ψ is the heading of the ship and β is the drift angle of the ship. The drift angle is the angle between the x-axis and the tangent path of the CG.

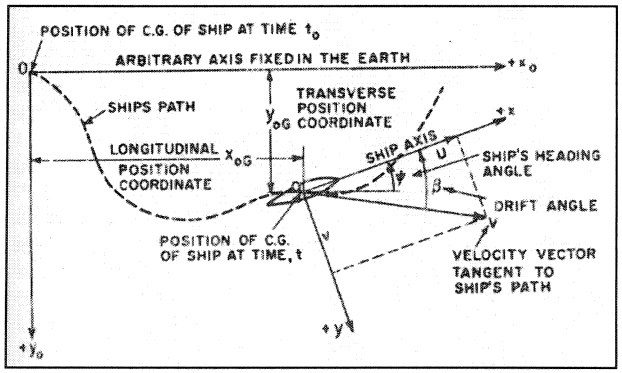

Figure 2-4: Axes used by the Equations of Motion [6]

In order to convert the Equations in 2-52 from the axes fixed to the earth to that of the ship, the following conversions need to take place:

$$\begin{aligned} X &= X_0 \cos\psi + Y_0 \sin\psi \\ Y &= Y_0 \cos\psi - X_0 \sin\psi \\ \dot{x}_{0G} &= u\cos\psi - v\sin\psi \\ \dot{y}_{0G} &= u\sin\psi + v\cos\psi \\ \ddot{x}_{0G} &= \dot{u}\cos\psi - \dot{v}\sin\psi - (u\sin\psi + v\cos\psi)\dot{\psi} \\ \ddot{y}_{0G} &= \dot{u}\sin\psi + \dot{v}\cos\psi + (u\cos\psi - v\sin\psi)\dot{\psi} \end{aligned} \qquad \textbf{(2-54)}$$

The Equations of Motion can now be expressed as follows:

$$\begin{aligned} X &= \Delta(\dot{u} - v\dot{\psi}) \\ Y &= \Delta(\dot{v} + u\dot{\psi}) \\ N &= I_z\ddot{\psi} \end{aligned} \qquad \textbf{(2-55)}$$

To completely understand Equations 2-55, X, Y, and N need to be expressed in terms of the forces and moments of the ship that are caused by disturbances. Using the linear portion of the Taylor expansion, which is valid for small perturbations from equilibrium, the *Y* force, for example, can be expressed as:

$$Y = F_y(u_1, v_1, \dot{u}_1, \dot{v}_1, \dot{\psi}_1, \ddot{\psi}_1) + (u - u_1)\frac{\partial Y}{\partial u} + (v - v_1)\frac{\partial Y}{\partial v} + \ldots + (\ddot{\psi} - \ddot{\psi}_1)\frac{\partial Y}{\partial \ddot{\psi}} \qquad \textbf{(2-56)}$$

The subscript 1 refers to the initial equilibrium conditions.

The assumption of linearity is that the Taylor series becomes more accurate as ∂; ∂u for example, becomes smaller in magnitude. So the higher order terms of the Taylor series as well as the product of two or more ∂'s can be neglected. This is consistent with the physical reality of the motion stability, as it is characterized on the basis of whether a very small disturbance from an initial condition is going to increase or decay with time.

Equation 2-56 can be simplified due to the initial equilibrium condition and the symmetry of the ship about the xz-plane. The initial equilibrium condition in investigating ship stability is usually taken as a straight-line motion at constant speed. With this condition set, there should be no Y-force component acting on the ship ($F_y = 0$), all accelerations and the angular velocity are zero ($\dot{u}_1 = \dot{v}_1 = \dot{\psi}_1 = \ddot{\psi}_1 = 0$), and v_1 is also zero. Only u_1 is not zero but it is equal to the resultant velocity, V. Due to symmetry, a change in forward velocity or forward acceleration will produce no transverse force. As a result, Equation 2-56 can be reduced to:

$$Y = \frac{\partial Y}{\partial v}v + \frac{\partial Y}{\partial \dot{v}}\dot{v} + \frac{\partial Y}{\partial \dot{\psi}}\dot{\psi} + \frac{\partial Y}{\partial \ddot{\psi}}\ddot{\psi} \qquad \textbf{(2-57)}$$

Similar reductions can be made to the Taylor series' for X and N.

$$\begin{aligned} X &= \frac{\partial X}{\partial \dot{u}}\dot{u} + \frac{\partial X}{\partial u}(u - u_1) \\ N &= \frac{\partial N}{\partial v}v + \frac{\partial N}{\partial \dot{v}}\dot{v} + \frac{\partial N}{\partial \dot{\psi}}\dot{\psi} + \frac{\partial N}{\partial \ddot{\psi}}\ddot{\psi} \end{aligned} \qquad \textbf{(2-58)}$$

Substituting Equations 2-57 & 2-58 into Equations 2-55, and using simplified derivative notation ($\partial Y/\partial v = Y_v$) the Equations of Motion can be expressed as follows:

$$\begin{aligned} &-X_u(u - u_1) + (\Delta - X_{\dot{u}})\ddot{u} = 0 \\ &-Y_v v + (\Delta - Y_{\dot{v}})\dot{v} - (Y_r - \Delta u_1)r - Y_{\dot{r}}\dot{r} = 0 \\ &-N_v v - N_{\dot{v}}\dot{v} - N_r r + (I_z - N_{\dot{r}})\dot{r} = 0 \end{aligned} \qquad \textbf{(2-59)}$$

In the above equation, $r = \dot{\psi}$ and $\dot{r} = \ddot{\psi}$ since the motions of the ship are restricted to the horizontal plane. For a more convenient expression that is used in modeling, the surge equation (X) in Equation 2-59 is neglected while the remaining terms are non-

dimensionalized, eg. $v' = v/V$. Furthermore, for usual ship configurations, $Y'_{\dot{r}} \approx 0$ and $N'_{\dot{v}} \approx 0$. This can be seen in Equation 2-61.

The effects of rudder deflection on controlling the path of the ship must also be considered. The linearized y-component of the rudder angle is $Y_\delta \delta_R$ and the linearized moment component is $N_\delta \delta_R$. They are expressed on the right-hand side in Equation 2-60. They represent the controlling forces and moments acting on the ship (see Figure 2-5). The only difference between Equations 2-59 and 2-60 is the absence of u_1 since $u_1/V \approx 1$ for small disturbances.

$$\begin{aligned} -Y'_v v' + (\Delta' - Y'_{\dot{v}})\dot{v}' - (Y'_r - \Delta')r' &= Y'_\delta \delta'_R \\ -N'_v v' - N'_r r' + (I'_z - N'_{\dot{r}})\dot{r}' &= N'_\delta \delta'_R \end{aligned} \qquad \textbf{(2-60)}$$

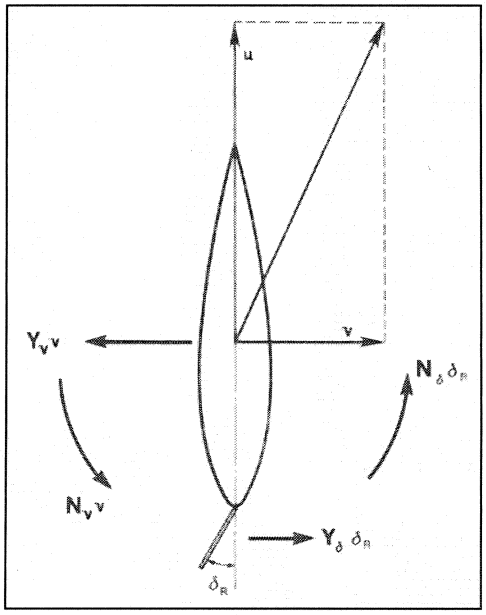

Figure 2-5: Rudder Induced Forces and Moments

3.3 Nomoto Coefficients

In order to get a measure of the ship's course stability and turning ability, Nomoto [7] developed an analysis of K and T indices that can be utilized to measure a ship's manoeuvrability. The non-dimensional K' index represents the ratio of the turning moment coefficient over the yaw damping coefficient, while T' index represents the ratio of yaw inertia coefficient over the yaw damping coefficient. In order to get the indices, a few simplifications are made. Since the force equation and the moment equation in 2-60 are coupled only through the terms $N_v'v$ and $Y_r'r$, which are typically small, they can be neglected. Also, the sway velocity can be eliminated since the turning primarily depends on the yaw rate. Therefore, the yaw equation in 2-60 can be rewritten as follows:

$$T'\dot{r} + r' = K'\delta_R \qquad \textbf{(2-61)}$$

Where:

$$T' = (I_z' - N_{\dot{r}}')/N_r'$$
$$K' = N_\delta'/N_r' \qquad \textbf{(2-62)}$$

From the above equations, the solution for r, in terms of T and K for a constant δ is given by:

$$r = K\delta_0(1 - e^{-t/T}) \qquad \textbf{(2-63)}$$

The proposed steering indices, or Nomoto coefficients, K and T together constitute a measure of manoeuvrability where K represents the turning ability and T represents the stability on course and quick response in steering. The importance of the

coefficients can be seen when the rudder angle δ_O is put over suddenly. The turning angular rate of a ship increases gradually and terminally approaches $K\delta_O$.

By analyzing Equation 2-63, it is noted that the larger the K value, the greater the turning angular rate and the smaller steady turning circle. As well, the smaller the T value, the quicker the build up of the ship's angular motion. In this way, the designer can use the Nomoto coefficients to analyze model and full scale manoeuvring trials to characterize the vessel's manoeuvrability.

Three different manoeuvring trials normally performed are: pullout manoeuvre, turning circle manoeuvre, and the zigzag manoeuvre. The pullout manoeuvre is used to quantify the straight course stability while the other two manoeuvres judge the course changing qualities of the vessel.

3.4 Straight Course Stability

Straight course stability of a ship relates to the ships behaviour after a small disturbance by an external force, like a rudder movement, that swerves the ship from a straight running course. After the disturbance is removed, the ship should settle into a straight running path along a new direction different from the original path. If this occurs, the ship is considered stable. If not and the heading rate does not decay to zero after the disturbance is removed, then the ship is classified as unstable. These examples can be seen in Figure 2-6.

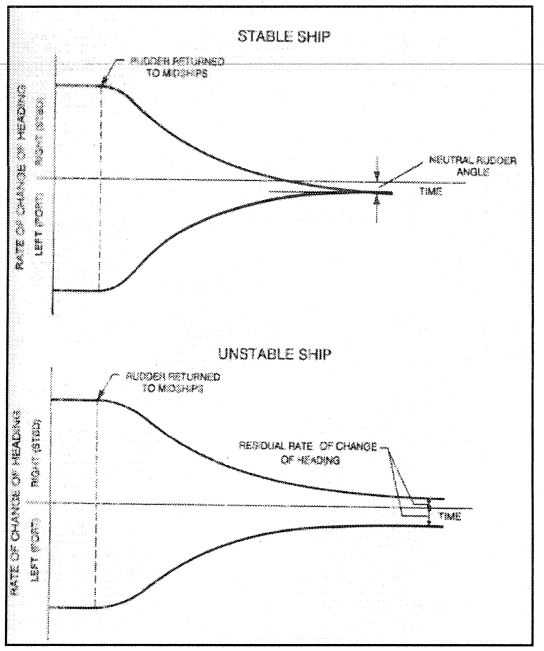

Figure 2-6: Pull-Out Test

The degree of stability can be expressed by the rapidity of the decay of the heading rate after the removal of the disturbance. This can be quantified using the Nomoto coefficients. If $\dot{\theta}_o$ is the heading rate caused by the disturbance, then Nomoto equation of motion is solved as:

$$\dot{\theta}(t) = \dot{\theta}_o e^{-t/T} \qquad \textbf{(2-64)}$$

As noted in the above equation, the smaller the T value, the quicker the decay of the heading rate and the more stable the ship is on course.

3.4.1 Stability Indices

The standard solution for the homogenous form of Equations 2-60 to solve the problem of course stability is given as:

$$v' = G_1 e^{\sigma_1 t} + G_2 e^{\sigma_2 t}$$
$$r' = H_1 e^{\sigma_1 t} + H_2 e^{\sigma_2 t} \quad \textbf{(2-65)}$$

Where G_1, G_2, H_1, and H_2 are constants of integration and σ_1 and σ_2 are the stability indices. If both values are negative, then v' and r' will approach zero with increasing time. From a practical stand point, σ_1 is taken as larger of the roots. This can be seen with substitution of the solutions in Equation 2-65 into Equations 2-60. The result is in the form of a quadratic equation of σ.

$$A\sigma^2 + B\sigma + C = 0 \quad \textbf{(2-66)}$$

Where:

$$A = (I_z' - N_{\dot{r}}')(\Delta' - Y_{\dot{v}}')$$
$$B = -(I_z' - N_{\dot{r}}')Y_v' - (\Delta' - Y_{\dot{v}}')N_r' \quad \textbf{(2-67)}$$
$$C = Y_v' N_r' - (Y_r' - \Delta')N_v'$$

The roots of Equation (2-64) need to be both negative for stability. Upon inspection of A and B, it is found that they are always large positive quantities. The term, $(\Delta' - Y_{\dot{v}}')$, which is found in both A and B, is almost equal to $+2\Delta$ because for ship shaped bodies with large length over breadth ratios, the magnitude of $Y_{\dot{v}}$ is approximately $-\Delta$. Similarly, the magnitude of $N_{\dot{r}}$ is almost as large as $-I_z$. Therefore, A is always a large positive quantity. Investigation into Y_v and N_r is needed in order to quantify B. In Figure 2-7, it is shown that due to the negative angle of attack produced by a positive v, a negative force is experienced at the bow and the stern. The opposite can be said for a negative v. Therefore, Y_v is always negative.

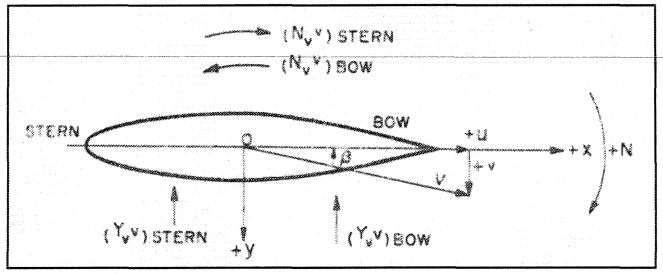

Figure 2-7: Investigation into Y_v [6]

To determine N_r, investigation similar to the one done for Y_v is carried out. It can be shown that N_r will always be negative for any *r*, since the moment that acts on the ship is the opposite sign to *r* that is applied to the ship, as seen in Figure 2-8. Therefore, with Y_v and N_r being negative quantities, B in the above quadratic equation will be a large positive quantity.

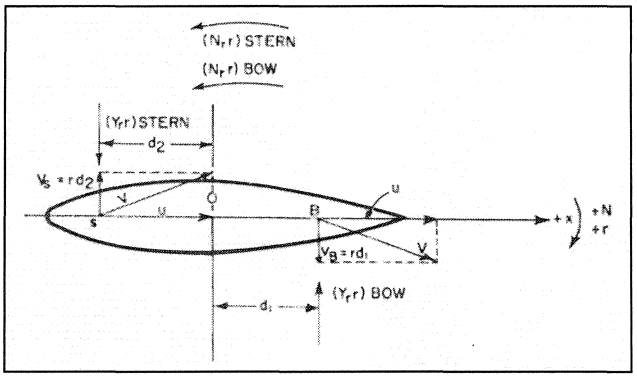

Figure 2-8: Investigation into N_r [6]

With B and A always being positive, the condition for stability reduces to C > 0. C is considered the discriminant of dynamic stability and the condition for stability is simply:

$$Y_v' N_r' - (Y_r' - \Delta')N_v' > 0 \qquad \textbf{(2-68)}$$

The above solution can be viewed as a relationship between sway and yaw with the lever arm of forces. It will signify if the ship is stable, but it will not give a quantitative measure. Further investigation into the development of the roots is needed.

3.5 Turning Circle Manoeuvre

The turning circle manoeuvre looks at the ship's manoeuvrability from the ship's performance in a steady turning circle with the rudder kept at a constant angle. The items of interest from the breakdown of the results are: (a) the advance of the ship from the point where the rudder angle was activated to the point in which the change of heading has reached 90 degrees; (b) the transfer of the ship in the lateral direction at the point where the advance is taken; (c) the tactical diameter, which measures the lateral distance to the point where the heading has changed by 180 degrees; and (d) the steady turning diameter of the vessel. This manoeuvre is a very important test since this is a type of manoeuvre ships frequently execute. A typical turning circle can be seen in Figure 2-9.

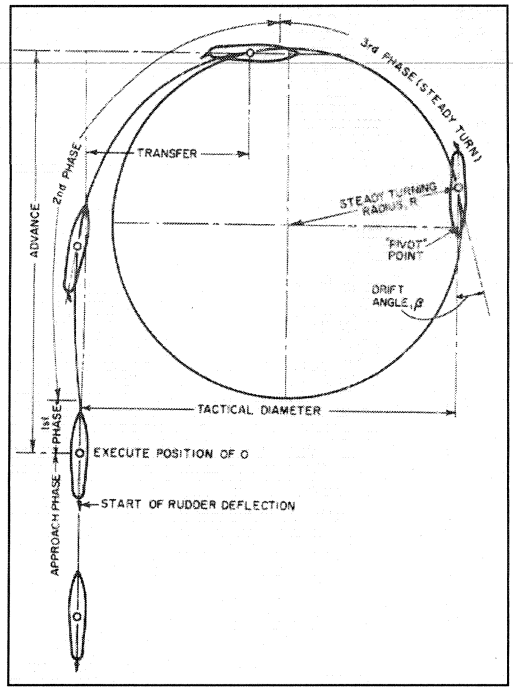

Figure 2-9: Typical Turning Circle Manoeuvre

It should be emphasized that manoeuvrability is expressed by the smallness of the steady turning circle (greatness of K) and the quick response of the steering (smallness of T). Using Nomoto coefficients, the radius and the advance can be evaluated, where V is the ship speed.

$$Radius = \frac{V}{K\delta_O} \tag{2-69}$$

$$Advance = VT + \frac{V}{K\delta_O} \tag{2-70}$$

3.6 Zigzag Manoeuvre

While the turning circle simply looks at the ships performance with a single rudder movement, the zigzag manoeuvre, developed by Nomoto, looks at the actual process of manoeuvring by a succession of transient phases of turning manoeuvres with

rudder angle put to starboard and port. The results of the manoeuvre that needs to be analyzed to illustrate the controllability of the ship are: (a) the time to reach the second executed yaw angle; (b) the overshoot yaw angle; and (c) the overshoot width of path. Part (a) is a direct measure of the ability of the ship to rapidly change course while parts (b) and (c) are measures of the counter manoeuvrability of the ship. These results are speed dependant since an increase in speed will decrease (a) and increase (b) and (c). A typical zigzag manoeuvre can be seen in Figure 2-10.

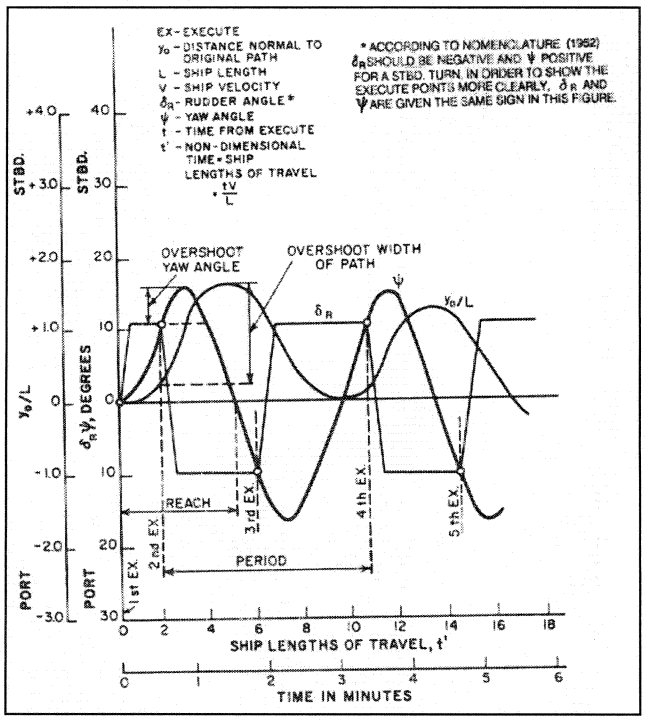

Figure 2-10: Typical Zigzag Manoeuvre [6]

By analyzing the manoeuvre [7], the Nomoto coefficients for the test run can be determined. The reliability of these coefficients are examined by inputting the calculated values back into Nomoto's equation of motion (Equation 2-61) and plotting the resulting heading against the observed heading. If the calculated heading simulates the observed

heading quite closely, then the K and T values are considered those for that particular vessel. As noted previously, the greater the K value and the smaller the T value, the greater the ships manoeuvrability. An example of a heading comparison is seen in Figure 2-11.

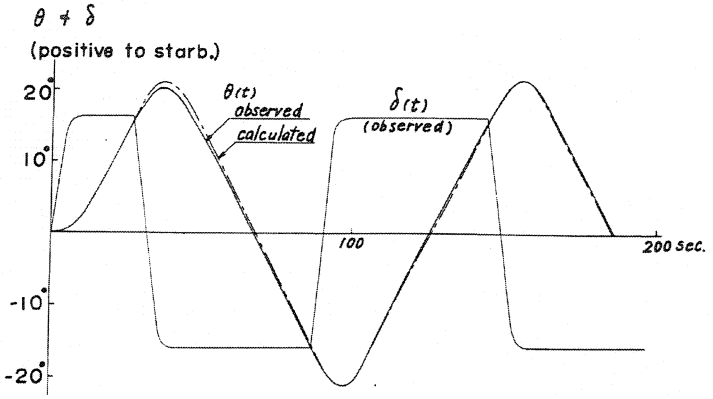

Figure 2-11: Typical Zigzag Comparison Plot

4.0 Seakeeping

Seakeeping trials are one of the important experimental components to be carried out in the design stage. Seakeeping experiments establish the seaworthiness characteristics of a ship. This is accomplished by assessing the relationship between the ship motions and the related weather environment acting upon it. Yet, a full-scale ship needs to be built in order to perform this test at the design stage. To overcome this obstacle, designers perform seakeeping experiments on a model of the ship. Although one cannot completely model the chaotic nature of the ocean, by performing the tests in a controlled artificial environment in a laboratory, one is able to achieve a good estimate on the ships motions with a high level of accuracy.

The following subsections will establish proper model scale testing procedures and accurate techniques to correlate the responses experienced by the model to full scale ship responses.

4.1 Dimensional Analysis

To extrapolate the model test results to that of a full size ship, one must be able to correlate the data of the two identities. Correlation is simply performed by expressing the responses in such a way that the equation will be the same for both the model and the ship. To achieve this, dimensional analysis is employed.

4.1.1 Heave Response

The first step in dimensional analysis is to correctly identify all the parameters that affect a particular response. Heave displacement is a function of the water and the ship's characteristics, which can be written as:

$$z = f_9\{\zeta_0, \omega, V, \theta, L, [x_B], \rho, \mu, g\} \quad \textbf{(2-71)}$$

Where: ζ_0 = Wave amplitude; ω = Wave frequency;

V = Ship speed; θ = Ship heading;

L = Ship size (length); g = Acceleration due to gravity;

ρ = Density of water; μ = Dynamic viscosity of water; and

$[x_B]$ = Sufficient number of coordinates to define the shape of the hull.

Given that the test involves a ship and a geometrically similar model, $[x_B]$ can be removed as it will be the same for both objects.

The second step in dimensional analysis is to use the matrix method to relate the above function in non-dimensional form so it will be the same for both the model and the ship. The common factors used in this analysis are: L, V, and ρ.

Table 2-5: Matrix Method - Heave Response

	L	V	ρ	z	ζ_o	ω	μ	g	θ
L	1	1	-3	1	1	0	-1	1	0
T	0	-1	0	0	0	-1	-1	-2	0
M	0	0	1	0	0	0	1	0	0
L	1	0	0	1	1	-1	1	-1	0
V	0	1	0	0	0	1	1	2	0
ρ	0	0	1	0	0	0	1	0	0

The various non-dimensional π terms formulated from the above matrix are:

$$\pi_1 = \frac{z}{L}; \pi_2 = \frac{\zeta_o}{L}; \pi_3 = \frac{\omega L}{V}; \pi_4 = \frac{\mu}{\rho V L}; \pi_5 = \frac{gL}{V^2}; \pi_6 = \theta \qquad \textbf{(2-72)}$$

By compounding, the non-dimensional heave amplitude can be expressed as:

$$\frac{z}{\zeta_o} = f_{10}\left\{\frac{\zeta_o}{L}, \omega\sqrt{\frac{L}{g}}, \frac{\mu}{\rho V L}, \frac{V}{\sqrt{gL}}, \theta\right\} \qquad \textbf{(2-73)}$$

Equation 2-73 states that the non-dimensional heave amplitude will be the same for both the model and the ship, provided that the terms inside the function have the same numerical values. Therefore, it is irrelevant what the relationship the function f_{10} has with its terms since it will be the same for both the model and the ship.

Although Equation 2-73 is fundamentally sound when it comes to dimensional analysis, this is not the final form it takes when correctly performing experiments on model tests. The third term inside the function is commonly recognized as the Reynolds Number while the fourth term is commonly known as the Froude Number. As in the case

in the powering analysis, achieving the proper model scale speed that would satisfy both the Reynolds Number and the Froude Number is impossible.

However, to the benefit of the designer, viscous forces do not play a significant role in seakeeping dynamics, except in roll motions. For that reason, it is not necessary to match the model and ship Reynolds Numbers.

Also, it is found that the non-dimensional heave amplitude is often independent of the non-dimensional wave amplitude and can be neglected in the formula. Thus, the non-dimensional heave response can be reduced to:

$$\frac{z}{\zeta_o} = f_{11}\left\{\omega\sqrt{\frac{L}{g}}, \frac{V}{\sqrt{gL}}, \theta\right\} \qquad \textbf{(2-74)}$$

The main problem with Reynolds Number is not the frictional drag as discussed above, but drag due to separation which may occur at different roll amplitudes, frequencies, and different positions on the hull.

4.1.2 Roll Response

The mass distribution properties of the vessel play a significant role in the way the ship behaves in waves, especially in roll and pitch. As a result, a separate dimensional analysis is needed that includes the mass properties in the function. The mass properties of the ship are represented by the mass moment of inertia of the ship, I, and the vertical centre of gravity, VCG.

$$\phi_x = f_{12}\{\zeta_o, \omega, V, \theta, L, [x_B], I, VCG, \rho, \mu, g\} \qquad \textbf{(2-75)}$$

Similar to the heave response, the matrix method is employed with the same common factors: L, V, & ρ.

Table 2-6: Matrix Method - Roll Response

	L	V	ρ	ϕ_x	ζ_o	ω	θ	I	VCG	μ	g
L	1	1	-3	0	1	0	0	5	1	-1	1
T	0	-1	0	0	0	-1	0	0	0	-1	-2
M	0	0	1	0	0	0	0	0	0	1	0
L	1	0	0	0	1	-1	0	5	1	1	-1
V	0	1	0	0	0	1	0	0	0	1	2
ρ	0	0	1	0	0	0	0	0	0	1	0

Through compounding, the following function is created to define the non-dimensional roll displacement:

$$\frac{\phi_x}{k\zeta_o} = f_{13}\left\{\frac{\zeta_o}{L}, \omega\sqrt{\frac{L}{g}}, \theta, \frac{I}{L^5}, \frac{VCG}{L}, \frac{\mu}{\rho VL}, \frac{gL}{V^2}\right\} \quad \textbf{(2-76)}$$

where k is the wave number that equates to 2π divided by the wave length.

Although during the matrix method, the roll displacement was not equated to any of the common factors; it is dependent on the amplitude of the wave slope, $k\zeta_o$ [6]. Equation 2-76 states that the non-dimensional roll displacement will be the same for both the model and the ship, provided that the terms inside the function have the same numerical values. Therefore, it is irrelevant what the relationship the function f_{13} has with its terms since it will be the same for both the model and the ship.

Although the Reynolds Number is an important parameter to consider in terms of fluid separation during a roll, it is assumed that it has little overall effect on the results in order for the model scaling to be based upon Froude scaling. So if there are any

differences between model scale and full scale roll measurements, the difference could be due to the lack of Reynolds Number scaling and the fluid separation issue.

4.1.3 Presentation of Results

Perhaps the most efficient way to present the results from Equation 2-74 is in a series of plots. Each plot will hold θ constant and have the non-dimensional heave response on the y-axis with the non-dimensional wave frequency on the x-axis. Each line on the graph will represent a Froude number. The set of diagrams will consist of the data set: $\theta = \{0°, 30°, 45°, 60°, 90°, 120°, 135°, 150°, 180°\}$, where 180° represent head seas. By representing the data in this fashion, one is able to predict the heave response due to a change in one of the wave parameters (wave amplitude or frequency) or a change in the ship's speed or heading.

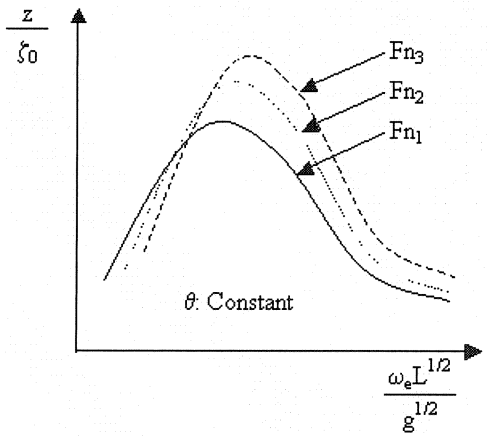

Figure 2-12: Seakeeping Model Results

4.1.4 Application to Other Seakeeping Responses

This method can be applied to all of the ships motions (linear and angular displacements, velocities, and accelerations) [8]. Since all the response amplitudes are generally proportional to wave amplitude, they will all develop the same general functions with minor differences in the non-dimensional response term. For all the motions, they are created with the wave amplitude in the denominator with additional quantities added to make it non-dimensional. The general forms are seen below:

Linear displacements: $$\frac{x}{\zeta_o}, \frac{y}{\zeta_o}, \frac{z}{\zeta_o} \quad \textbf{(2-77)}$$

Angular displacements: $$\frac{\phi_x}{k\zeta_o}, \frac{\phi_y}{k\zeta_o}, \frac{\phi_z}{k\zeta_o} \quad \textbf{(2-78)}$$

Linear velocity amplitudes: $$\frac{\dot{x}}{\varpi\zeta_o}, \frac{\dot{y}}{\varpi\zeta_o}, \frac{\dot{z}}{\varpi\zeta_o} \quad \textbf{(2-79)}$$

Linear Acceleration amplitudes: $$\frac{\ddot{x}L}{g\zeta_o}, \frac{\ddot{y}L}{g\zeta_o}, \frac{\ddot{z}L}{g\zeta_o} \quad \textbf{(2-80)}$$

where: $x / y / z$ = Surge / Sway / Heave displacement; and

$\phi_x / \phi_y / \phi_z$ = Roll / Pitch / Yaw displacement.

4.2 Motions in Irregular Seaway

During full scale seakeeping trials, the ship will be traveling in a sea state that will have an irregular wave pattern. An irregular wave spectrum is the designer's terminology for naturally occurring ocean waves. An individual wave is formed by wind continuing to blow for a long enough time and over sufficient length of water for ripples to grow in

length and height. As these waves progress, the wind energy generates new ripples and waves. Consequently, the sea state is made up of combinations of 'regular' waves. A regular wave is a single wind generated wave that can be classified by a sinusoidal function and behaves the same way as in ideal conditions, uncontaminated by waves of different wave lengths.

The full scale irregular time history of the sea state can be quantified in terms of a wave amplitude energy density spectrum, or simply 'wave spectrum' [8].

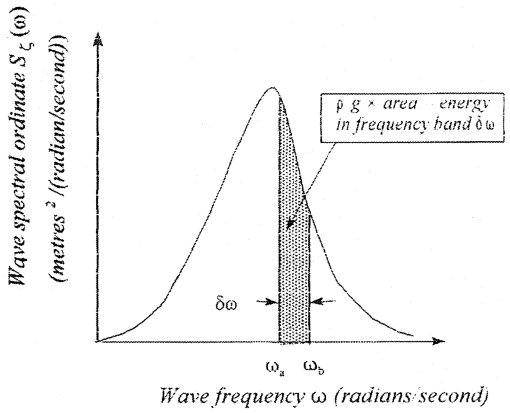

Figure 2-13: Wave Spectrum

The energy per square metre of sea surface of the n^{th} wave component is $\rho g \zeta_{nO}^2 / 2$. The wave spectrum is defined so that the area bound by a frequency range (ω_a to ω_b) is proportional to the total energy of the wave components with that range of frequencies. Therefore, the spectrum can be defined as:

$$S_\zeta(\omega_n) = \frac{\zeta_{nO}^2}{2\partial\omega} \qquad \textbf{(2-81)}$$

The simplest wave spectrum can be classified by two parameters: the significant wave height, $\overline{H}_{1/3}$ and the modal period, T_O. The significant wave height is the mean value of the highest 1/3 of all the wave heights in the time series, while the modal period corresponds to the frequency of the peak of the wave spectrum.

$$\overline{H}_{1/3} = 4\sqrt{m_0}\sqrt{1-\frac{\varepsilon^2}{2}} \quad \textbf{(2-82)}$$

$$\varepsilon = \sqrt{1-\frac{m_2^2}{m_0 m_4}} \quad \textbf{(2-83)}$$

$$m_n = \int_0^\infty \omega^n S_\zeta(\omega) d\omega \quad \textbf{(2-84)}$$

ε is the bandwidth correction parameter of the spectrum, where ε = 0 for a narrow bandwidth and ε = 1 for a wide bandwidth spectrum. The differences of the two spectra can be seen in Figure 2-14. m_0 is variance of the irregular wave time history that is equal to the area under the wave spectrum, while m_2 (second moment of area under the wave spectrum) and m_4 (fourth moment) is the variance for the velocity and the acceleration, respectively.

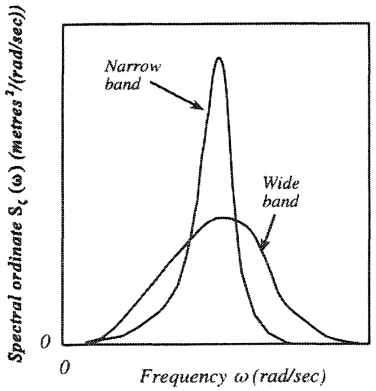

Figure 2-14: Narrow and Wide Band Spectra

This wave spectrum is generated at a fixed point, most likely from a wave buoy. The wave spectrum needs to be transformed from this reference point to a moving ship. For example, the frequency the waves encounter increases for a ship travelling in head seas compared to the fixed location and decreases for a ship travelling in following seas. Transforming the spectrum to the moving reference frame does not change the energy of the spectrum. Hence, the areas under the two spectra are identical. This can be seen in Figure 2-15 where:

$$S_\zeta(\omega_e) = S_\zeta(\omega)\frac{g}{g - 2\omega V\cos\theta} \qquad \textbf{(2-85)}$$

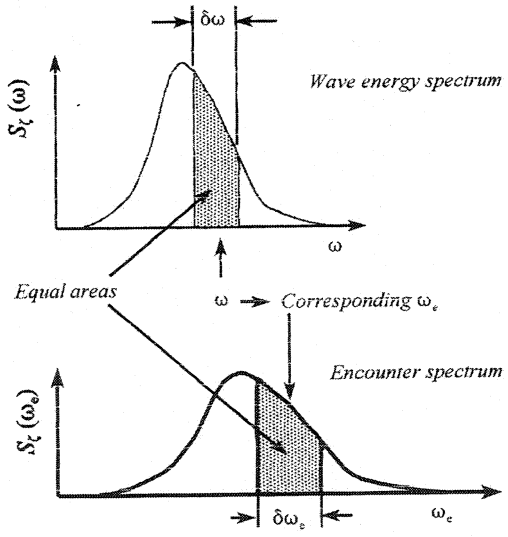

Figure 2-15: Transforming the Wave Spectrum into the Encounter Spectrum

Once the encounter frequency is determined, the designer can create the linear motion spectrum. This is done by filtering the wave spectrum with the appropriate transfer function, response amplitude operator (RAO). The RAO is the square of the non-dimensional linear displacement. For example:

Heave motion: $$S_z(\omega_e) = S_\zeta(\omega_e)\left(\frac{z}{\zeta_o}\right)^2 \quad \textbf{(2-86)}$$

Variance of heave motion: $$m_{0z} = \int_0^\infty S_Z(\omega_e)d\omega_e \quad \textbf{(2-87)}$$

RMS heave motion: $$\sigma_{0z} = \sqrt{m_{0z}} \quad \textbf{(2-88)}$$

Where the RMS of the heave velocities and accelerations are:

$$\sigma_{2z} = \sqrt{m_{2z}}; \sigma_{4z} = \sqrt{m_{4z}}$$
$$m_{nz} = \int_0^\infty \omega^n S_z(\omega)d\omega \quad \textbf{(2-89)}$$

The same calculations can be done for the linear surge and sway displacements.

For the angular motions, the wave amplitude energy density spectrum requires alteration to become the wave slope energy density spectrum [8].

$$S_\alpha(\omega_n) = \frac{\omega_n^4}{g^2} S_\zeta(\omega_n) \quad \textbf{(2-90)}$$

To obtain the angular motions, a slightly different procedure is required where the angular motion spectrum is only a pseudo spectrum. It does not deal with the encountered frequency; therefore, it does not have any significant physical importance. Nevertheless, the variance and RMS value of the motion can still be obtained because the area under the pseudo spectrum is the same as if under the 'true' spectrum in the encountered frequency domain. An example of the roll:

Pseudo spectrum: $$S_{\phi_x}(\omega) = S_\alpha(\omega)\left(\frac{\phi_x}{k\zeta_o}\right)^2 \quad \textbf{(2-91)}$$

Variance: $$m_{0\phi_x} = \int_0^\infty S_{\phi_x}(\omega)d\omega \quad \textbf{(2-92)}$$

RMS: $$\sigma_{0\phi_x} = \sqrt{m_{0\phi_x}} \quad (2\text{-}93)$$

4.3 Ship / Model Correlation

The dimensional analysis conceived earlier is ideal if the vessel is dealing with regular waves. In testing of irregular waves, the designer must deal in statistical rather than deterministic quantities, denoted using heave motion as an example. The RMS heave motion is a function of the water, the characteristics of the ship, as well as the given wave spectrum.

$$\sigma_{0z} = f_{14}\left\{\overline{H}_{1/3}, T_0, V, \theta, L, [x_B], \rho, \mu, g\right\} \quad (2\text{-}94)$$

Performing the same approach as before and dealing with Froude scaling, the non-dimensional RMS heave motion for a geometrically similar model can be expressed as follows:

$$\frac{\sigma_{0z}}{\overline{H}_{1/3}} = f_{15}\left\{\frac{\overline{H}_{1/3}}{L}, T_0\sqrt{\frac{g}{L}}, \frac{V}{\sqrt{gL}}, \theta\right\} \quad (2\text{-}95)$$

The non-dimensional RMS heave motion will be the same for the model and the ship as along as they are geometrically similar, provided that the non-dimensional terms inside the function have the same numerical values. In terms of the two parameter wave spectrum produced by a time history series, as long as the significant wave height and modal period abide by the appropriate scaling laws, then the relationship holds true.

The above analysis can also be performed for all linear and angular displacements. This assumes that responses to irregular seas are linear. Since large roll motions are not linear, the above analysis only holds true for moderate motions.

Chapter 3 Phase I: Full Scale Experiments

1.0 Introduction

This chapter describes the powering, manoeuvring, and seakeeping trials carried out on the 40 m long M/V Louis M. Lauzier off St. John's, NL and in Conception Bay, NL between July and November 2001. These sea trials were considered Phase I of the ship / model correlation study being carried out through the partnership of MUN and IMD. The following sections describe the trials instrumentation, the sea trials that were performed, and the online and offline analysis performed for each manoeuvre. The online analysis was carried out in the Biology Wet Lab onboard the 'Lauzier' at the end of each sea trial to verify the integrity of the collected data, while the offline analysis was performed on the data at IMD after the sea trials were complete.

2.0 Instrumentation

Before the sea trials commenced, the vessel was instrumented while it was stationed in the St. John's harbour in order to measure the parameters needed to analyze each sea trial.

2.1 Propeller Shaft Torque/Thrust

Although most parameters were simple to measure, the shaft thrust and torque had to be predicted in order to accurately install proper instrumentation for measurement of

these parameters. NavCAD™ software was used to provide an estimate of the torque and thrust range for calibration.

2.1.1 NavCAD™ Estimate of Shaft Torque/Thrust Range

When a vessel is propelled through the water, the propeller exerts both a torsion (twist) and thrust (longitudinal) strain on its propeller shaft. Thrust and torque were measured using strain gages bonded to the propeller shafts using the general procedure outlined by IMD [9]. From the torque and shaft RPM data, one can deduce the amount of shaft power needed to propel the vessel through the water. NavCAD™ version 3.6[1] developed by HydroComp, Inc was used to generate a speed/power prediction to estimate the values of thrust and torque that the 'Lauzier' would experience through a range of speeds. In order to predict the necessary thrust and torque levels for the 'Lauzier', a hull resistance calculation is first required to estimate the effective power before carrying out the shaft power prediction step of the analysis procedure.

To calculate the hull resistance, one must enter the appropriate hull and appendage data into the NavCAD™ program. Table 3-1 and Table 3-2 describe the input hull and appendage information, respectively, that was required for the software.

[1] NavCAD is a trademark of HydroComp, Inc. of Durham, NH, USA.

Table 3-1: NavCAD™ Hull Data

Hull Data

Primary

Description	Value	Comment
Length between perpendiculars (PP):	33.990 m	See Note 1
Length on WL	36.730 m	See Note 3
Maximum beam on WL:	7.700 m	See Note 3
Draft at mid WL:	2.590 m	See Note 1
Displacement bare:	265.2 t	See Note 1
Maximum area coefficient (Cx):	0.600	See Note 3
Waterplane coefficient:	0.830	See Note 3
Wetted surface area:	284.5 m^2	See Note 4

Secondary

Description	Value	Comment
Trim by stern:	0.58 m	See Note 1
Longitudinal Centre of Buoyancy (LCB) aft of FP:	18.98 m	See Note 1
Bulb extented forward of FP:	1.83 m	See Note 3
Bulb area at FP:	7.3 m^2	See Note 3
Bulb centre above Baseline (FP):	1.52 m	See Note 3
Transom Area:	5.53 m^2	See Note 3
Half entrance angle:	20 Deg	Estimated

Notes:
1 Taken from the Trim and Stability Booklet.
2 Values from Trim and Stability Booklet based on 80% Consumables.
3 Measured from the 'Docking Plan' Drawing.
4 Estimated using NavCad™ (Holtrop method).

Table 3-2: NavCAD™ Appendage Data

Appendages Data

(Total wetted surface)

Description	Value	Drag Coeff.
Rudders:	4.390 m^2	3.000
Shaft brackets:	2.580 m^2	4.000
Skeg:	41.000 m^2	1.750
Exposed shafts:	1.150 m^2	2.000
Dome:	4.830 m^2	2.700
Bilge keel	11.960 m^2	1.400
Bow thruster diameter:	0.570 m	0.005

Notes:
1 Wetted surface areas estimated from 'Proposed Hull Modifications' drawing.
2 Drag coefficients were all estimated using NavCad™.
3 Bow thruster measured from the 'Docking Plan' drawing.

The Holtrop 1984 prediction method [10] was used to calculate the resistance for the bare hull as well as to estimate the values for the correlation allowance and the 3-D corrected form factor. This method was employed because it had the best ranking according to NavCAD™ 'Method Expert's' ranking of prediction methods. However, it is noted in the program that Holtrop 1984 tends to under predict its results. This was taken into consideration in the final design of the instrumentation installed in measuring the shaft strains. In addition, it should be noted that Holtrop 1988 prediction method was employed to predict the hull resistance with attached appendages.

The appropriate propeller information was input to derive the delivered power. Since there was little data available from the current ship operators or the Canadian Coast Guard (CCG) on the type of propeller fitted on the 'Lauzier', the propeller attributes were estimated by visually examining various photographs taken while the vessel was on dry dock. Even though the propeller was not a standard B-series prop, two B4.65 series props (4 blades with an expanded area ratio, EAR, of 0.65) were used as a best case scenario in the prediction with a pitch / diameter ratio (P/D) of 0.5625. The P/D value was varied until the analysis produced a shaft RPM closest to that experienced on the 'Lauzier' at full speed (~415 RPM @ 11.5 knots). In order to run the analysis, Holtrop 1984 prediction method was used to incorporate the wake fraction, thrust deduction and relative rotative efficiency into the power prediction calculation. Table 3-3 displays the predicted power that the 'Lauzier' should experience per shaft while in operation. The summary of the NavCAD™ shaft power prediction output is also provided in the IMD

report describing the full scale sea trials on the 'Lauzier' [12]. This prediction is not corrected for hull roughness or hull fouling effects.

Table 3-3: NavCAD™ Power Prediction Summary

Power Prediction Summary							
Vel kts	Fn	Rtotal N	PEtotal kW	PropRPM RPM	Thrust N	Torque kNm	PD/prop kW
3.00	0.081	3841	5.9	122.2	2014.95	0.47	6
5.00	0.136	9025	23.2	196.8	4735.28	1.02	21
6.00	0.163	12145	37.5	233.1	6372.82	1.39	34
7.00	0.190	15624	56.3	269.1	8198.12	1.81	51
8.00	0.217	19493	80.2	305.0	10228.4	2.29	73
9.00	0.244	23801	110.2	340.9	12489.3	2.80	100
10.00	0.271	28698	147.6	377.3	15058.7	3.39	134
11.00	0.298	34112	193.0	413.7	17899.6	4.02	174
12.00	0.325	39770	245.5	449.7	20869.1	4.69	221
13.00	0.352	46241	309.3	486.4	24264.7	5.46	278

Based on the estimate of thrust generated, a prediction of the thrust strain on the shaft was made by IMD electronics staff. With a predicted maximum thrust loading of only 2.5 μstrain, it was not deemed feasible to measure the thrust load on the 'Lauzier' using a shaft mounted strain gage based system as the thrust strain level was beyond the capability of even the most sensitive strain gauges to measure accurately.

2.1.2 Description of Shaft Torque Instrumentation Installation

To measure shaft torque, strain gauges were bonded to the shaft and a shaft mounted Acurex WDC Model 1216C strain transmitter module used to condition and transmit the strain signal. A rotor/stator antenna assembly mounted close to the strain gauge installation was required to transmit power to the strain transmitter using a 160 kHz power carrier and to transmit the FM strain signal using a 10 MHz carrier. The module provided a 6-Volt DC excitation signal to the strain gage bridge, thus providing

self-contained excitation, signal conditioning and signal transmission. The strain transmitter module was fitted in a recessed pocket in a two-piece wooden collar that included a rotary antenna. An Acurex model 1206D demodulation and display unit was used in conjunction with a stationary antenna loop and model 1211a induction power supply to provide the 160 kHz power carrier and receive the FM Modulated signal from the rotating shaft electronics. The demodulation and display unit took the FM Modulated signal and converted it to a voltage linearly proportional to gauge strain. This output voltage was then fed through an IMD signal conditioner to the data acquisition system. A schematic diagram of the torque measurement system is provided in Figure 3-1.

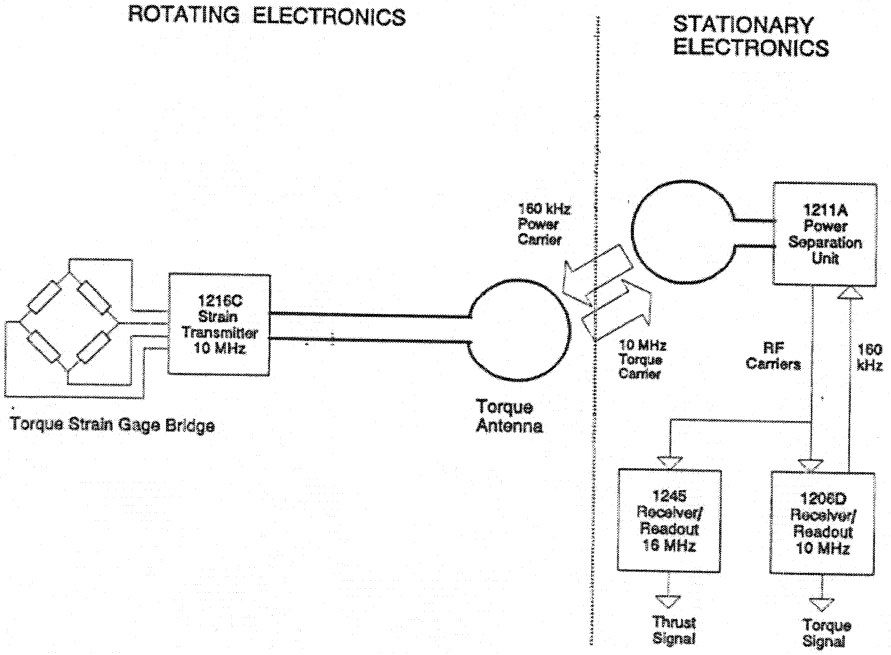

Figure 3-1: Schematic of Torque Instrumentation

A detailed description of the installation/calibration of the shaft torque measurement system is provided in an IMD work instruction manual [11]. The torque

signal is calibrated by placing a shunt resister across the ¼ of the bridge simulating a shaft torsion load.

2.2 Other Measured Parameters

For a full list of the parameters required, refer to Table 3-4. The instrumentation, signal cabling, and data acquisition system used along with the calibration method employed for each parameter is described in the IMD report of the full scale sea trials [12]. The data acquisition system was set up on the countertop located in the Biology Wet Lab on the starboard side of the Wheelhouse Deck of the 'Lauzier', as seen in Figure 3-2.

Table 3-4: Full Scale Instrumentation Plan

List of Instrumentation

Signal	Device	Units	Calibrated Range	Critical for: Man. Trial	Skp Trial	Prop. Trial
Forward Speed	DGPS	m/s	0 - 6	X	X	X
Heading Angle	DGPS	deg. TRUE	0 - 360	X	X	X
Planar Position	DGPS	Lat., Long.	-	X	X	X
Heading Angle	Ship's Sperry Gyro	degree(s)	0 - 360	X	X	X
Roll Angle	electro-mechanical gyro	degree(s)	+/- 35	X	X	X
Pitch Angle	electro-mechanical gyro	degree(s)	+/- 12	X	X	X
Yaw Rate	electro-mechanical gyro	degree(s)/second	+/- 5	X		X
Roll Rate	Stable Platform	degree(s)/second	+/- 20		X	
Pitch Rate	Stable Platform	degree(s)/second	+/- 20		X	
Yaw Rate	Stable Platform	degree(s)/second	+/- 5		X	
Heave Accel.	linear accelerometer	m/s^2	+/- 20		X	
Surge Accel.	linear accelerometer	m/s^2	+/- 20		X	
Sway Accel.	linear accelerometer	m/s^2	+/- 20		X	
Rudder Angle	yo-yo potentiometer	degree(s)	0 - 35	X	X	X
Shaft rpm (P)	tap off ship's remote indicator	rpm	0 - 450	X	X	X
Shaft rpm (S)	tap off ship's remote indicator	rpm	0 - 450	X	X	X
Shaft Torque (P)	strain gages	kN-m	7		X	X
Shaft Torque (S)	strain gages	kN-m	7		X	X

NOTES: Sampling rate is 50 Hz (filter 10 Hz) for all analog channels with the exception of shaft torque which will be sampled at a min. of 800 Hz. (filter 200 Hz) for the calm water propulsion trials ONLY.

A	DGPS Receiver	D	Signal Conditioner	F	DC Power Supply
B	NavGyro Interface	E	Computer	G	Rate Gyros
C	Monitor				

Figure 3-2: 'Lauzier' Biology Wet Lab – DAS

3.0 Powering Trials

The powering runs were carried out in central Conception Bay between the North coastline and Bell Island on the 22nd of August with select repeat runs performed on the 23rd. Powering runs were carried out at speeds from 5.5 knots to 11.5 knots in one knot increments. Powering runs were also performed astern but these runs will not be analyzed as they are outside the scope of this thesis.

The typical powering run follows the guideline outlined by ITTC [13] and is described in the IMD technical report on the full scale sea trials [12]. For each test speed, three powering runs were executed along the same course path, achieved by implementing a Williamson Turn at the end of each run. A Williamson turn is typically carried out in an 'immediate action' situation as in recovering a man overboard. This is depicted in Figure 3-3. The purpose of the runs travelling over identical path lines was to mitigate any drift effects due to the wind and current when the runs were analyzed together. However, due to the calm testing conditions (wind < 5 knots) and the low ambient current (< 0.5 knots), there were generally little differences in the mean test values for each test run at a given vessel speed.

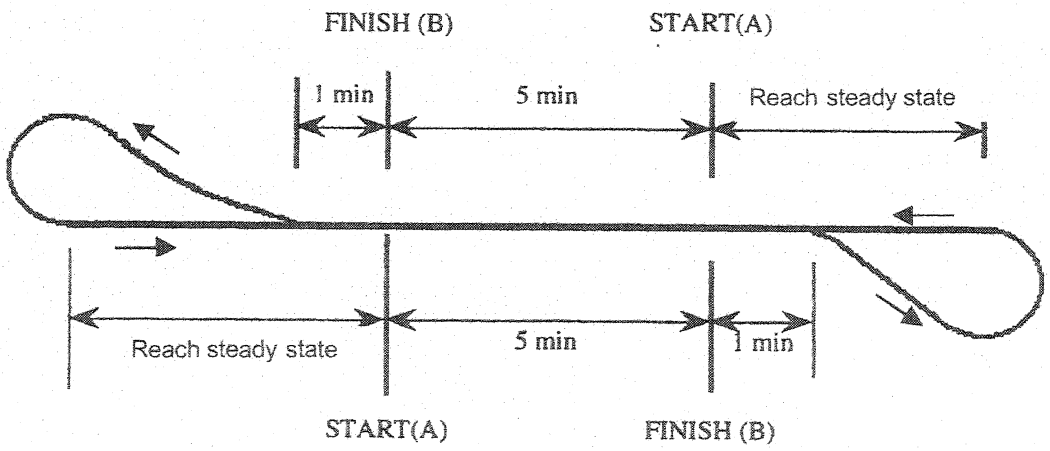

Figure 3-3: Path of Ship During a Typical Powering Manoeuvre

3.1 Powering Online Analysis

During testing, a torque and RPM versus Speed over Ground (SOG) plot was generated to check the integrity of the results. The trials director used this plot to verify

data from repeat runs and to see if there was increasing torque with an increase in RPM. This plot can be seen in Figure 3-4.

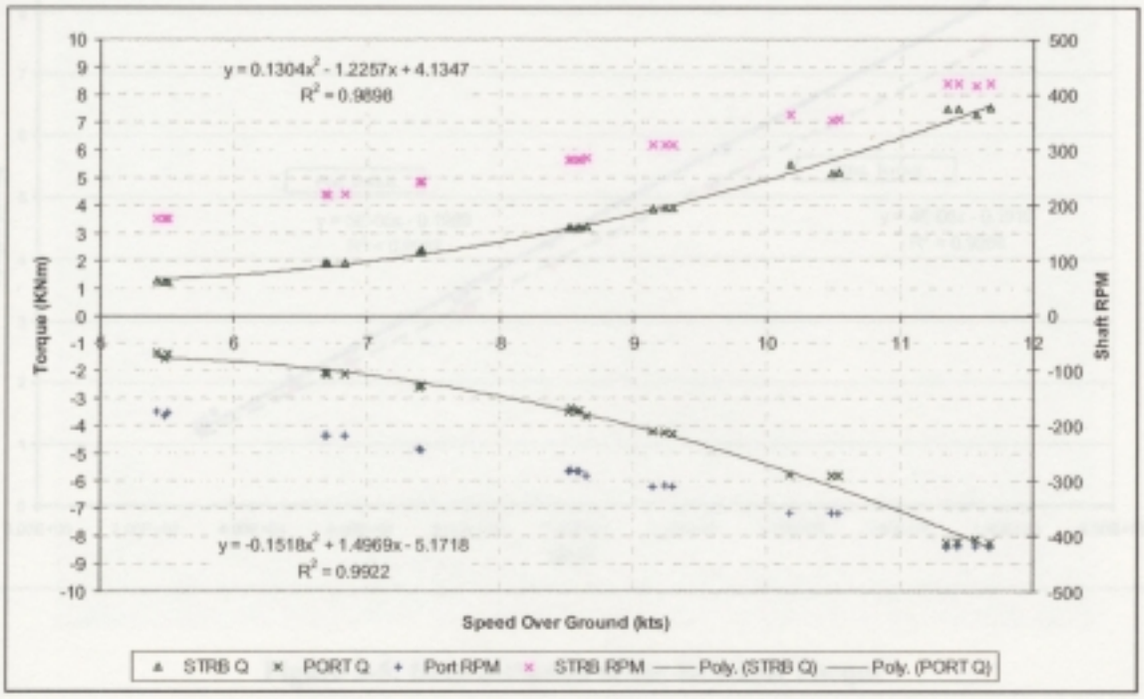

Figure 3-4: Online Analysis – Powering

3.2 Powering Offline Analysis

Once the propulsion trials were complete, the data was analyzed to calculate the power delivered to the propellers by the engines. First, the residual torque incorporated in the shafts was determined by plotting torque versus RPM^2 for all the powering runs and fitting a line through the data. It was extrapolated through the y-axis with the residual torque as the y-axis offset. From this graph, Figure 3-5, the starboard torque offset was -0.1919 kN-m, while the port torque offset was -0.1989 kN-m. The residual torque was then subtracted from the mean torque values for each powering run.

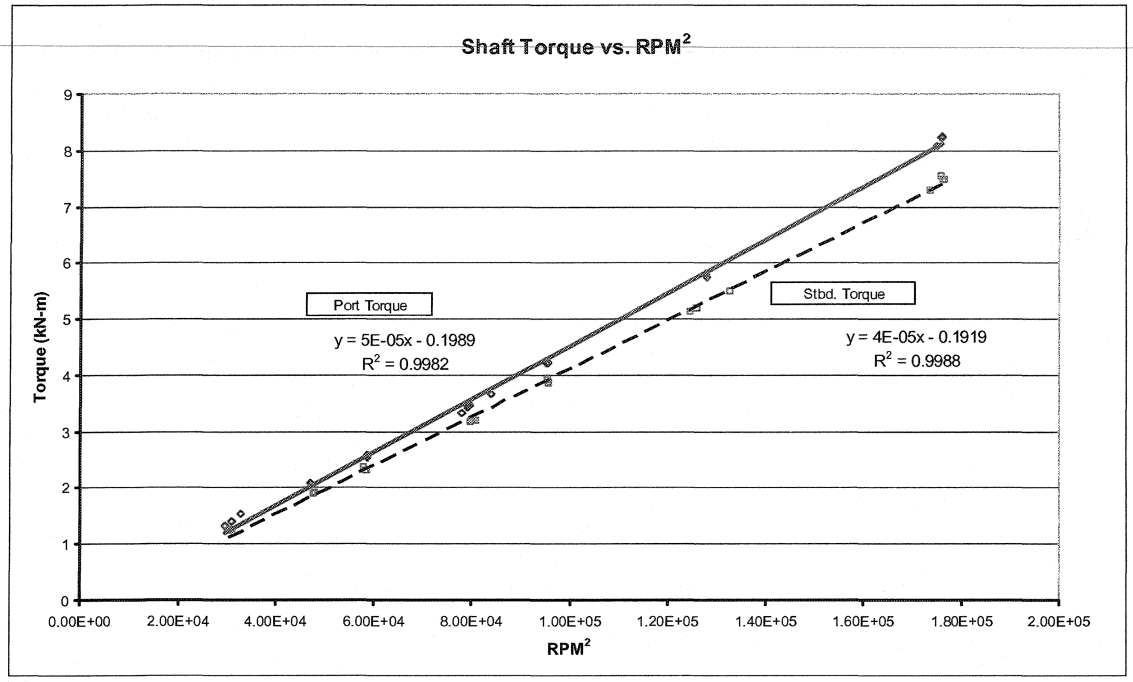

Figure 3-5: Determination of the Residual Torque

As seen above, the torque on the port shaft was consistently ~8.5% higher than the torque measured on the starboard shaft. It was speculated that the torque difference is due to a disparity in the incident flow into the propeller. The most likely cause is due to the large sounder caisson mounted on the starboard side of the hull (Figure 1-3). Another indication of the difference in fluid flow was seen when the 'Lauzier' was put on dry dock in March 2002. At that time, flow induced pitting on the starboard propeller (Figure 3-6) and underneath the hull in way of the starboard propeller was noticed while the port side had no such damage. During this time, the propeller blades were measured in order to develop geometrically similar propellers during model testing. Due to this hypothesis, a wake survey was planned during model testing to provide further insight into this issue.

Figure 3-6: Damaged Starboard Propeller

Once the shaft torques were finalized, the shaft power was computed for each forward speed as follows:

$$P_D = 2\pi \cdot \frac{AverageShaftRPM}{60} \cdot (PortTorque + StbdTorque) \qquad \textbf{(3-1)}$$

For each run, a form was generated containing basic information on the trial and statistical information on the data acquired. The offline powering tables can be seen in the full scale IMD report [12].

Although three runs were performed at each speed and some repeat runs were executed, the final power calculation for the 'Lauzier' only used the average values of the first two runs of each manoeuvre. The other runs were used primarily for verification

purposes only. The average powering values and the shaft power calculations can be seen in Table 3-5.

Table 3-5: Summary Table of Powering Data

M/V Louis M. Lauzier - Summary Table - Powering Data

August 2001 **IMD Proj. #: 01960**

Speed (knots)	Speed (m/s)	Port Shaft RPM	Stbd. Shaft RPM	Average Shaft RPM	Port Torque (kN-m)	Stbd. Torque (kN-m)	Total Shaft Power (kW)
5.47	2.81	176.69	175.42	176.06	1.6327	1.4272	56.41
6.73	3.46	216.98	218.61	217.80	2.2786	2.0947	99.75
7.34	3.78	242.32	241.69	242.01	2.7566	2.5263	133.88
8.56	4.40	281.57	282.64	282.11	3.6606	3.3729	207.78
8.59	4.42	284.52	283.90	284.21	3.6979	3.3799	210.65
9.23	4.75	308.81	309.14	308.98	4.4247	4.0638	274.65
10.38	5.34	357.43	358.59	358.01	5.9751	5.5005	430.23
11.59	5.96	419.42	419.70	419.56	8.4300	7.6991	708.65

Polynomials were fit to the above data in order to predict the delivered power at 0.5 knot increments. The delivered power equalled the shaft power times 0.96. The reduction in power is to take into account the frictions caused by the stern tubes and A-brackets. The polynomials can be seen in Figure 3-7 and Figure 3-8 with the tabulated powering prediction in Table 3-6. The computed polynomials are below, where 'x' represents the ship speed:

Average Port and Starboard Shaft RPM: $1.6826x^2 + 10.445x + 70.523$

Port Shaft Torque (kN-m): $0.0184x^3 - 0.3234x^2 + 2.4477x - 5.0927$

Starboard Shaft Torque (kN-m): $0.0172x^3 - 0.3131x^2 + 2.4385x - 5.3692$

Total Shaft Power (kW): $2.8179x^3 - 53.317x^2 + 374.58x - 859.87$

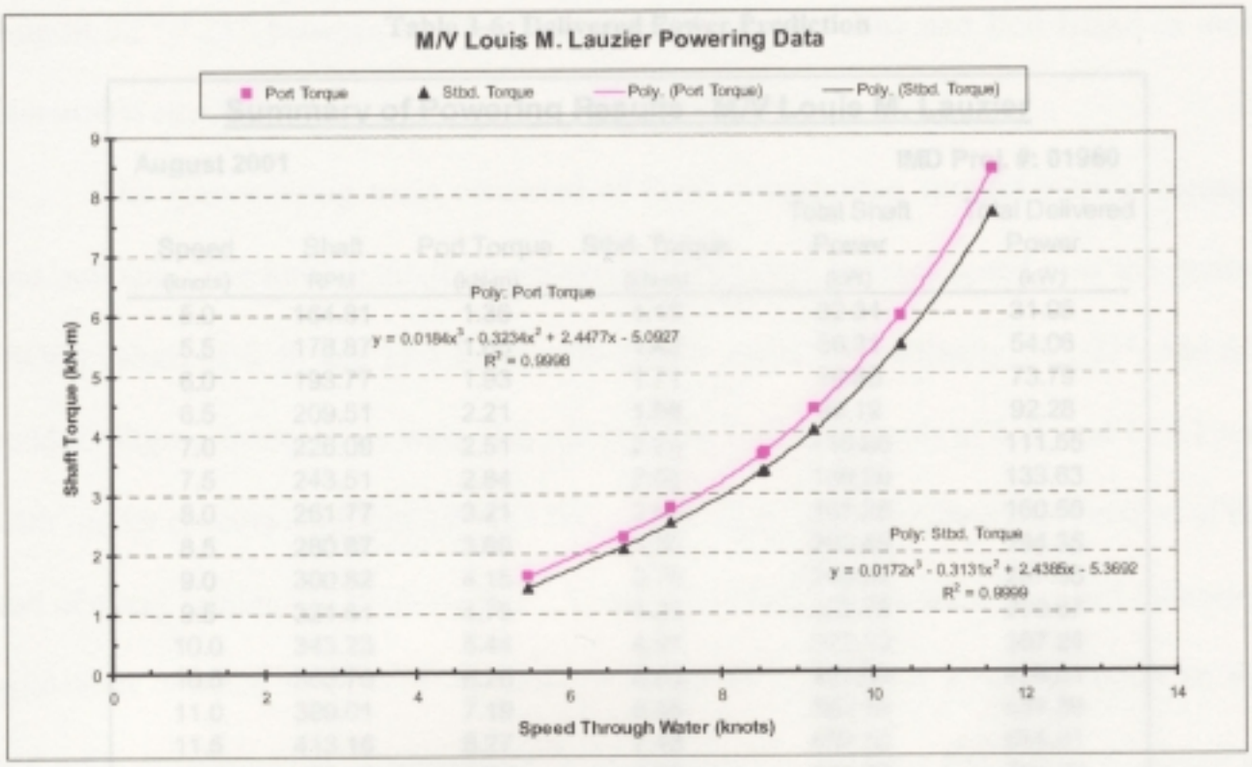

Figure 3-7: Plot of Shaft Torque vs. Speed Through Water

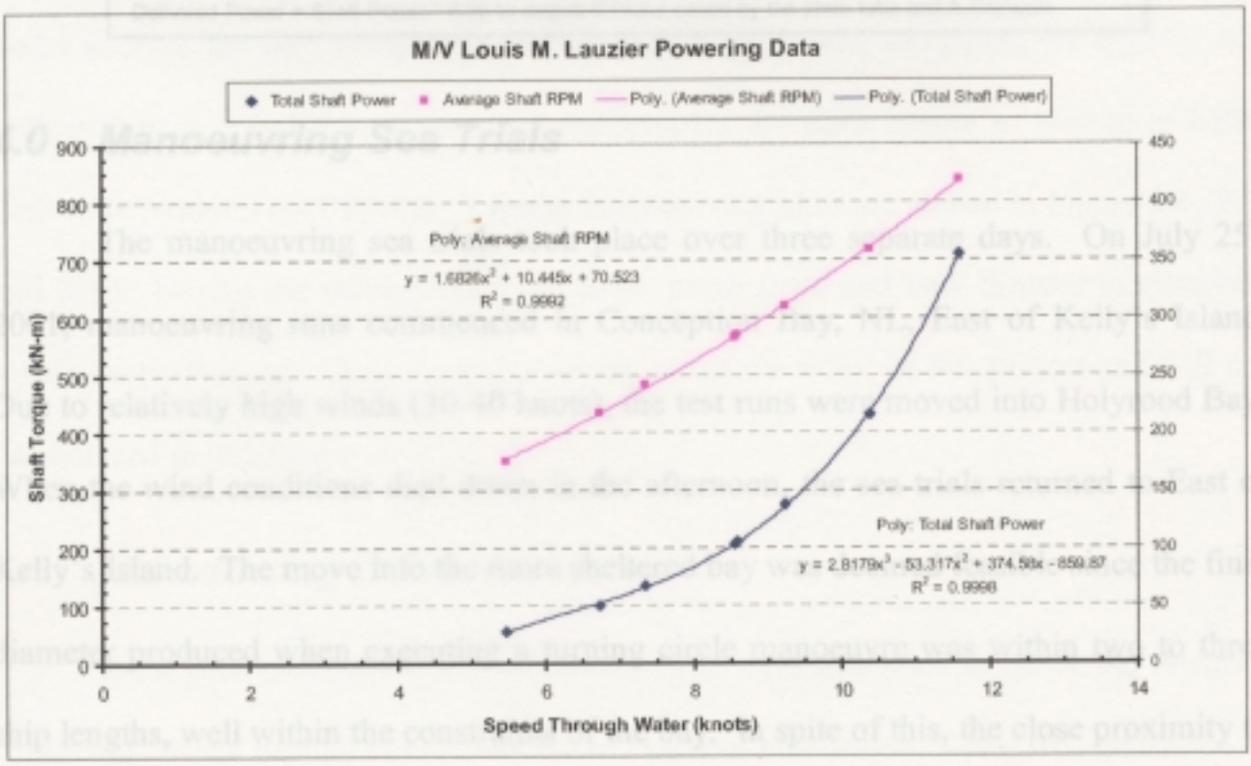

Figure 3-8: Plot of Shaft RPM / Power vs. Speed Through Water

Table 3-6: Delivered Power Prediction

Summary of Powering Results - M/V Louis M. Lauzier

August 2001 **IMD Proj. #: 01960**

Speed (knots)	Shaft RPM	Port Torque (kN-m)	Stbd. Torque (kN-m)	Total Shaft Power (kW)	Total Delivered Power (kW)
5.0	164.81	1.36	1.15	32.34	31.05
5.5	178.87	1.65	1.43	56.31	54.06
6.0	193.77	1.93	1.71	76.86	73.79
6.5	209.51	2.21	1.98	96.12	92.28
7.0	226.09	2.51	2.26	116.20	111.55
7.5	243.51	2.84	2.56	139.20	133.63
8.0	261.77	3.21	2.91	167.25	160.56
8.5	280.87	3.65	3.30	202.45	194.35
9.0	300.82	4.15	3.76	246.92	237.05
9.5	321.61	4.75	4.29	302.78	290.67
10.0	343.23	5.44	4.91	372.13	357.24
10.5	365.70	6.25	5.63	457.09	438.81
11.0	389.01	7.19	6.46	559.78	537.39
11.5	413.16	8.27	7.43	682.30	655.01
12.0	438.16	9.51	8.53	826.77	793.70

Notes:

Computed using polynomial regression equations.

Delivered Power = Shaft Power * 0.96 to deduct frictions cause by the stern tube and A-Brackets

4.0 Manoeuvring Sea Trials

The manoeuvring sea trials took place over three separate days. On July 25th 2001, manoeuvring runs commenced in Conception Bay, NL, East of Kelly's Island. Due to relatively high winds (30-40 knots), the test runs were moved into Holyrood Bay. When the wind conditions died down in the afternoon, the sea trials returned to East of Kelly's Island. The move into the more sheltered bay was deemed feasible since the final diameter produced when executing a turning circle manoeuvre was within two to three ship lengths, well within the constraints of the bay. In spite of this, the close proximity to the land meant that the vessel was also dealing with drift caused by the tide, on top of the drift created by the wind and current. Additional manoeuvring testing was carried out on

August 22nd / 23rd between the North coast of Conception Bay and Bell Island in more favourable environmental conditions.

The manoeuvring trials consisted of three manoeuvres: turning circles, zigzags, and pullouts. The turning circles were executed at initial forward speed over the ground (SOG) values of 6, 8, and 11.5 knots with rudder angles of nominally 15°, 25°, and full rudder. Zigzag manoeuvres were also run at initial forward speeds of 6, 8, and 11.5 knots with rudder execute angles of 10° and 20°. The pullout manoeuvres were executed at the end of every turning circle manoeuvre. These three manoeuvres were executed following guidelines outlined by ITTC [13], and are described in the IMD technical report on the full scale sea trials [12]. Although ITTC stated that for a turning circle only a change of 540° in heading is required; for the sea trials, this was later increased to 720° in order to better analyze the drift component in the manoeuvre. Also, the zigzag manoeuvre was increased from 5 rudder executes to 7 executes for the same reason as well as to better derive the Nomoto coefficients. Typical manoeuvring plots are shown in Figure 2-6, 2-9, and 2-10. During the manoeuvring sea trials, crash stops and bow thruster manoeuvres were also performed. These manoeuvres are out of the scope of this project and will not be analyzed in this thesis.

4.1 Manoeuvring Online Analysis

After each manoeuvre was complete, plots were generated to check the integrity of the run. For a turning circle manoeuvre / pullout manoeuvre, a plot was generated to check the rudder angle as well as an X-Y planar position plot. If the graph showed the rudder not keeping its angle, then the run was noted to be repeated. The rudder was

controlled using hydraulic pumps and over a course of a turning circle manoeuvre, these pumps appeared to leak hydraulic pressure, creating a change in rudder angle. If the angle decreases by a few degrees, the hydraulic controllers recognized the drop in pressure and increased the pressure again in order to bring the rudder back to the desired angle. A plot of a typical turning manoeuvre with a decreasing rudder angle is seen in Figure 3-9.

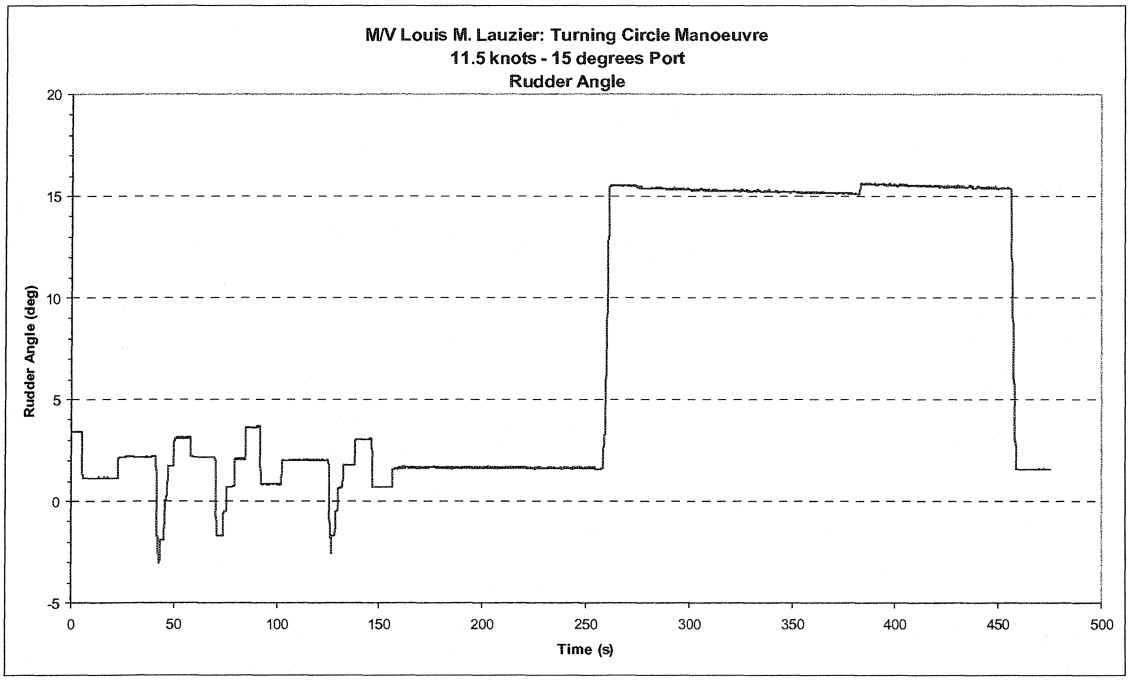

Figure 3-9: Turning Circle Manoeuvre - Erratic Rudder Signal

During the first two days of testing, two hydraulic pressure pumps were used to control the rudder angle. On the third day, only the port pump was active. This mitigated the rudder problem. A plot of a typical X-Y plot is seen in Figure 3-10.

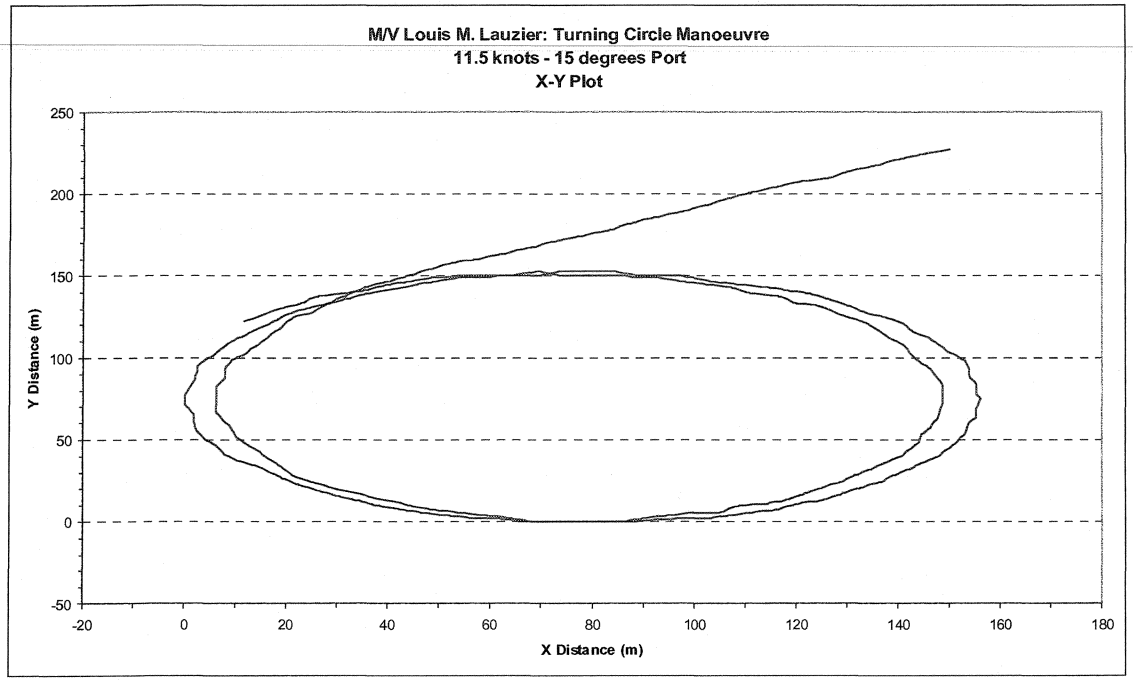

Figure 3-10: Turning Circle Manoeuvre: Typical X-Y Plot

After a zigzag manoeuvre, a plot of the rudder angle superimposed over the change in heading angle was generated. The plot was checked for integrity in the rudder signal as well as the response time for rudder turn over, i.e. once the change in heading angle reaches the rudder angle, then the helmsman reverses the rudder to the other side of amidships. An example of an online zigzag plot can be seen in Figure 3-11.

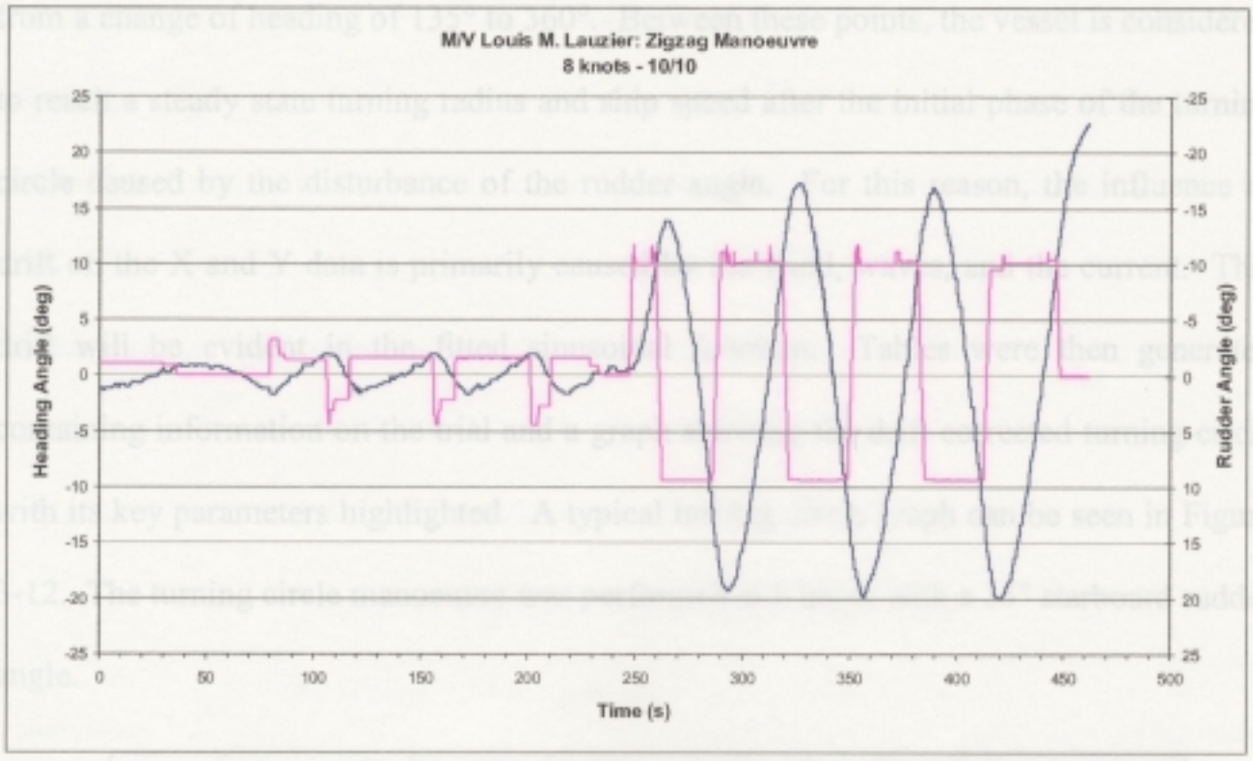

Figure 3-11: Zigzag Manoeuvre: Typical Online Plot

4.2 Manoeuvring Offline Analysis

The post processing of the manoeuvring trials were done using Igor Pro[2], a software package that is an integrated program for visualizing, analyzing, transforming, and presenting data. Procedure files were created for each manoeuvre to analyze the run and generate appropriate tables and graphs.

In analyzing a turning circle manoeuvre, the first command was transforming the X and Y distances from the Global Positioning System (GPS) antenna to the Centre of Gravity (CG) of the 'Lauzier' and then correcting it for drift effects. To correct for drift, Igor Pro™ fits a sinusoidal function to the X and Y data. The sinusoidal typically starts

[2] Igor Pro is copyrighted by Wave Metrics Inc. of Lake Oswego, OR, USA

from a change of heading of 135° to 360°. Between these points, the vessel is considered to reach a steady state turning radius and ship speed after the initial phase of the turning circle caused by the disturbance of the rudder angle. For this reason, the influence of drift on the X and Y data is primarily caused by the wind, waves, and the current. This drift will be evident in the fitted sinusoidal function. Tables were then generated containing information on the trial and a graph showing the drift corrected turning circle with its key parameters highlighted. A typical turning circle graph can be seen in Figure 3-12. The turning circle manoeuvre was performed at 8 knots with a 15° starboard rudder angle.

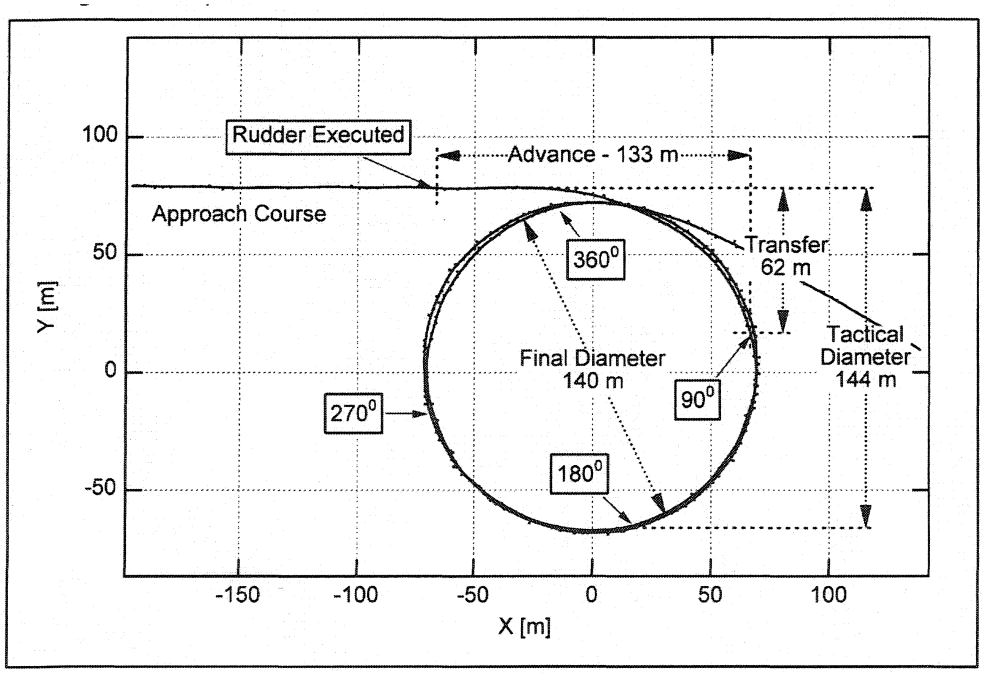

Figure 3-12: Typical Drift Corrected Turning Circle

The 'Advance' is the distance by which the CG of the 'Lauzier' advances in the first quadrant of the turning circle manoeuvre. It was measured from the CG position at the start of the rudder deflection to the CG position when the heading angle of the

'Lauzier' has changed by 90°. The 'Transfer' is the lateral offset of the CG at the point where the advance is measured. The 'Tactical Diameter' is the distance travelled by the CG of the 'Lauzier' perpendicular to the approach path when the heading is changed by 180°. The 'Final Diameter' is the diameter of the turning circle once it reaches its steady turning state. A summary of all turning circle manoeuvres with their manoeuvring parameters is provided in Table 3-7. The Igor Pro™ generated plots for a turning circles can be seen in the full scale IMD technical report [12].

Table 3-7: Summary Table of Turning Circle Data

M/V Louis M. Lauzier - Summary Table - Turning Circle Data

July/August 2001 — IMD Proj. # 01960

File Name	NF Time	Forward Speed (kts)/(m/s)	Nominal Rudder Angle (deg. P/S)	Advance (m)	Transfer (m)	Tactical Diameter (m)	Final Diameter (m)	Yaw Rate in Turn (deg./s)	Rudder Angle in Turn (deg.)	Heel Angle in Turn (deg.)	Forward Speed in Turn (m/s)	Comments
FS8_15S_200107251943	19:43	8.7/4.48	15 S	137.65	82.54	170	168	2.70	-13.39	-1.14	3.02	inconsistant rudder angle
FS8_15P_200107251047	10:47	7.4/3.81	15 P	81.61	54.47	123	116	-2.37	14.48	0.39	2.73	inconsistant rudder angle
FS8_15P_200107251930	19:30	8.6/4.42	15 P	118.56	57.79	131	128	-2.85	14.44	0.89	3.29	inconsistant rudder angle
FS7_25S_200107251415	14:15	7.0/3.60	25 S	92.58	40.68	105	109	2.98	-20.98	-0.78	2.44	inconsistant rudder angle
FS8_25P_200107251427	14:27	8.0/4.12	25 P	93.34	36.22	90	87	-3.25	24.15	0.33	2.71	
FS7_35S_200107251441	14:41	7.2/3.70	35 S	87.52	30.38	78	78	3.31	-29.36	-0.51	2.04	steps noted in rudder angle
FS7_35P_200107251455	14:55	7.0/3.60	35 P	89.24	26.55	73	69	-3.31	31.93	2.06	2.34	step noted in rudder angle
FS11_15S_200107251512	15:12	11.7/6.02	15 S	178.67	66.40	168	170	3.53	-13.24	-2.80	4.60	uneven rudder execute
FS11_15P_200107251543	15:43	11.5/5.92	15 P	140.11	56.03	139	139	-3.89	14.54	1.13	5.01	
FS11_25S_200107251609	16:09	11.5/5.92	25 S	108.92	42.11	106	103	4.59	-20.73	-2.09	3.75	
FS11_25P_200107251556	15:56	11.3/5.81	25 P	107.20	41.07	100	96	-4.69	21.52	2.06	4.39	
FS11_35S_200107251643	16:43	11.1/5.71	35 S	101.58	28.95	77	77	5.10	-28.20	-2.56	3.06	step noted in rudder angle
FS11_35S_200107251628	16:28	11.3/5.81	35 S	94.78	28.45	75	77	5.21	-28.79	-1.86	3.07	
FS11_35P_200107251617	16:17	11.4/5.86	35 P	72.97	19.75	55	54	-5.26	31.11	1.89	3.75	
FS6_15S_200108221903	19:03	6.0/3.09	15 S	125.11	77.67	156	147	1.96	-11.71	-0.81	2.29	
FS6_15S_200108231820	18:20	6.10/3.14	15 S	130.27	60.73	143	136	2.05	-13.46	-1.39	2.28	
FS6_15P_200108231834	18:34	5.90/3.03	15 P	153.11	47.65	130	129	-2.10	14.52	1.09	2.55	uneven rudder execute
FS6_FullS_200108231744	17:44	6.10/3.14	Full S	83.59	27.51	73	74	2.72	-28.24	-0.95	1.62	1 step in rudder angle
FS6_FullP_200108231756	17:56	6.10/3.14	Full P	82.28	24.41	71	69	-2.69	30.22	0.68	1.89	1 step in rudder angle
FS8_15S_200108231547	15:47	8.20/4.22	15 S	132.80	61.50	144	140	2.60	-13.08	-1.25	3.06	
FS8_15P_200108231559	15:59	8.00/4.12	15 P	132.13	57.05	136	127	-2.71	13.78	1.74	3.24	2 steps in rudder angle
FS8_FullS_200108231612	16:12	7.90/4.06	Full S	87.87	29.27	74	73	3.58	-28.62	-0.80	2.10	2 steps in rudder angle
FS8_FullP_200108231624	16:24	7.90/4.06	Full P	85.34	26.02	73	69	-3.55	30.33	1.14	2.49	3 steps in rudder angle
FS11P5_15S_200108231712	17:12	11.4/5.86	15 S	146.76	78.46	175	170	3.42	-12.21	-2.69	4.81	glitch in rudder angle
FS11P5_15P_200108231723	17:23	11.4/5.86	15 P	139.31	59.37	150	144	-3.34	13.60	2.07	5.02	1 step in rudder angle
FS11P5_FullS_200108231852	18:52	11.6/5.97	Full S	97.69	29.01	79	80	5.22	-28.25	-1.09	3.35	1 step in rudder angle
FS11P5_FullP_200108231943	19:43	11.8/6.07	Full P	98.31	29.03	77	76	-5.29	30.27	1.02	3.85	1 step in rudder angle

In analyzing the zigzag manoeuvre, a drift correction was also performed on the yaw angle data, typically from the third rudder execute to the fifth execute. Tables were then generated containing information on the trial and a graph showing the drift corrected turning circle with its key parameters highlighted. Besides the normal zigzag parameters,

the zigzag manoeuvre was analyzed to produce the Nomoto coefficients [7] that characterize the manoeuvrability of the 'Lauzier'. In order to properly analyze the manoeuvre to achieve the Nomoto coefficients, there has to be at least four rudder executes. Using these Nomoto coefficients, a calculated heading angle was produced and plotted against the measured heading angle. If the two headings overlap, then it is considered a good Nomoto match. An important parameter influencing the match is the amount of rudder lag during the run. Rudder lag is the time from when the change in heading reaches the rudder angle to the time the helmsman changes the rudder angle.

A typical zigzag graph with a good Nomoto match can be seen in Figure 3-13. The Igor Pro™ generated plots featuring the key zigzag parameters and the Nomoto coefficients can be seen in IMD technical report of the full scale sea trials [12]. A summary of all zigzag manoeuvres with their manoeuvring parameters is provided in Table 3-8.

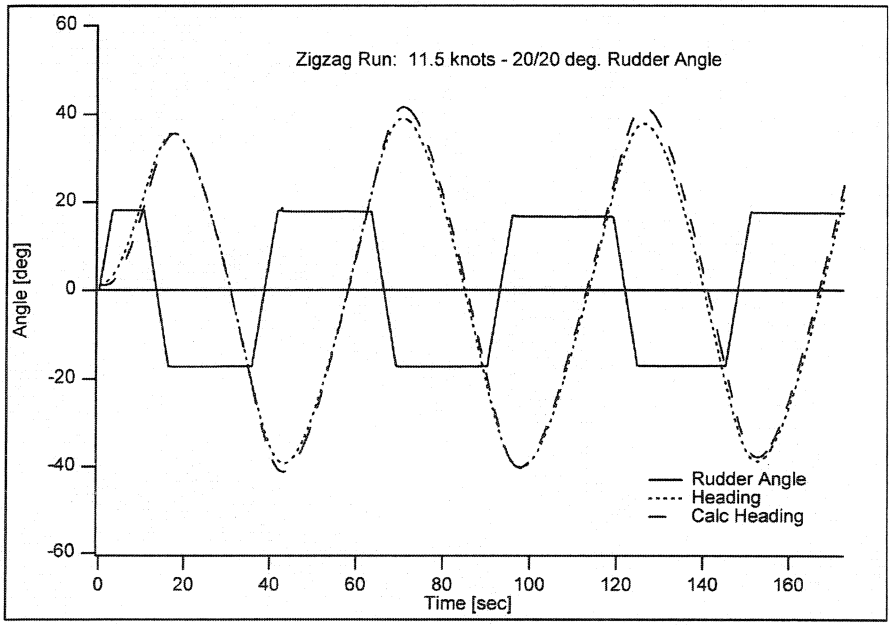

Figure 3-13: Typical Zigzag Manoeuvre with a Good Nomoto Match

Table 3-8: Summary Table of Zigzag Data

M/V Louis M. Lauzier - Summary Table - ZigZag Manoeuvring Data

July/August 2001 — IMD Proj. # 01960

File Name	NF Time	Nominal		Run Heading			Nomoto Coefficients			Calculated Heading			Comments
		Forward Speed (kts)/(m/s)	Zigzag	Time to Reach Execute (s)	Reach (s)	Period (s)	Delta R (deg)	K(mean) (1/s)	T(mean) (s)	Time to Reach Execute (s)	Reach (s)	Period (s)	
ZZ_FS8_10S10P_200107251717	17:17	8.2 / 4.22	10 / 10	14.84	33.22	67.31	-3.13	0.2199	12.275	N/A	30.80	N/A	Calculated heading never match stbd rudder angle due to large wind acting on the port beam.
ZZ_FS8_10S10P_200107251727	17:27	8.5 / 4.37	10 / 10	5.84	25.80	56.91	-0.81	0.1437	2.854	7.72	29.14	54.76	Average rudder lag of 5.5 s / 3rd execute higher than the rest.
ZZ_FS8_10S10P_200107251741	17:41	7.9 / 4.06	10 / 10	12.09	33.20	62.70	-0.18	0.2128	10.185	14.73	32.08	61.50	Overshoot of measured heading continued to increase, therefore hard to match.
ZZ_FS8_20S20P_200107251758	17:58	8.5 / 4.37	20 / 20	11.71	42.90	70.54	-0.78	0.2137	11.459	12.52	42.30	70.49	Manoeuvre started to port / Good Nomoto match.
ZZ_FS8_20S20P_200107251811	18:11	8.0 / 4.12	20 / 20	6.31	32.94	70.93	-0.66	0.1474	3.108	10.29	34.78	66.35	Average rudder lag of 7.4 s.
ZZ_FS11P5_10S10P_200107251827	18:27	11.3 / 5.81	10 / 10	9.25	25.38	46.45	-0.14	0.2574	5.967	10.20	25.20	46.39	6 executes / correlation slightly offset.
ZZ_FS11P5_10S10P_200107251838	18:38	11.4 / 5.86	10 / 10	5.12	21.44	45.14	-0.52	0.1835	0.808	6.51	22.82	42.96	Average rudder lag of 4.9 s / 3rd & 5th rudder executes were erratic.
ZZ_FS11P5_20S20P_200107251846	18:46	11.4 / 5.86	20 / 20	6.87	28.16	53.95	-0.56	0.2071	3.274	9.36	27.74	52.38	Average rudder lag of 3.4 s / Good Nomoto match.
ZZ_FS11P5_20S20P_200107251856	18:56	11.5 / 5.92	20 / 20	9.12	29.80	53.91	-0.45	0.2438	5.921	10.07	29.84	52.22	Average rudder lag of 1.1 s / Good Nomoto match.
ZZ_FS6_10S10P_200108221656	16:56	6.0 / 3.09	10 / 10	14.86	59.25	109.54	-0.34	0.1603	14.416	18.90	56.88	105.66	Large rudder lag (7.6 s) at the beginning / Good Nomoto match in the middle of the run.
ZZ_FS6_10S10P_2_200108221709	17:09	6.0 / 3.09	10 / 10	15.95	42.88	81.04	-1.06	0.1491	13.001	20.50	40.63	78.95	Good Nomoto match at the end of the run.
ZZ_FS6_10S10P_3_200108221726	17:26	6.0 / 3.09	10 / 10	19.61	45.88	77.78	-0.21	0.1253	9.558	21.55	45.00	74.57	Drift in calculated heading.
ZZ_FS6_20S20P_200108221738	17:38	6.0 / 3.09	20 / 20	17.52	53.75	90.62	-0.60	0.1505	14.833	19.80	52.13	89.24	Good Nomoto match at the end of the run.
ZZ_FS6_20S20P_2_200108221754	17:54	5.9 / 3.03	20 / 20	14.38	49.25	92.82	-0.22	0.1659	16.450	16.85	49.13	90.86	Average rudder lag of 1.6 s.
ZZ_FS6_20S20P_200108231808	18:08	6.1 / 3.14	20 / 20	15.66	52.88	93.71	-0.19	0.1726	16.549	19.23	50.00	92.23	5 executes / Average rudder lag of 1.7 s.
ZZ_FS8_10S10P_200108231204	12:04	8.2 / 4.22	10 / 10	12.88	32.00	58.81	-0.64	0.1792	7.756	13.82	32.50	55.97	Stbd rudder executes were erratic / drift in calculated heading.
ZZ_FS8_10S10P_2_200108231218	12:18	7.9 / 4.06	10 / 10	10.42	31.12	58.64	-0.26	0.1937	9.311	11.68	32.88	55.62	Stbd rudder executes were erratic / drift in calculated heading.
ZZ_FS8_10S10P_200108231523	15:23	7.7 / 3.96	10 / 10	13.95	34.25	62.56	-1.06	0.1743	7.561	17.99	31.50	60.54	Large offset in calculated heading.
ZZ_FS8_10S10P_200108231536	15:36	8.4 / 4.32	10 / 10	12.21	34.75	60.08	0.91	0.1734	7.657	13.26	35.13	57.83	Stbd rudder executes were erratic / Good Nomoto match.
ZZ_FS8_20S20P_200108231458	14:58	8.1 / 4.17	20 / 20	11.19	48.50	80.67	0.03	0.2162	11.781	12.37	48.63	79.73	Large rudder lag of 5.1 s in 1st execute / drift in calculated heading.
ZZ_FS8_20S20P_2_200108231512	15:12	8.0 / 4.12	20 / 20	12.50	39.00	70.20	-0.33	0.2013	10.437	14.60	37.88	69.13	Calculated heading does not match on the port executes.
ZZ_FS11P5_10S10P_200108231652	16:52	11.5 / 5.92	10 / 10	9.01	25.75	45.41	0.07	0.2293	4.656	9.67	25.88	43.48	Drift in calculated heading.
ZZ_FS11P5_20S20P_200108231701	17:01	11.5 / 5.92	20 / 20	9.22	30.88	53.14	-0.51	0.2538	6.134	10.05	30.75	52.39	Good Nomoto match.

The 'Time to Reach Execute' (TRE) is the time from initial rudder movement until the heading angle first reaches the selected rudder angle. The 'Reach' is the elapsed time from the initial rudder movement to the time the heading angle returns to the initial course after the first helm reversal. The 'Period' of a zigzag cycle is measured from the TRE until the corresponding point in the next positive half-cycle. Finally, the 'Overshoot Angle' is the difference between the maximum rudder angle and the maximum heading angle for a given rudder execute.

Although the pullout manoeuvre was performed at the termination of every turning circle, the manoeuvre was only analyzed at the end of the 15° turning circle runs. This is in accordance to the guidelines set out by ITTC [13]. Seeing that the analysis requires a port and starboard pullout manoeuvre, there were only three quality pullout manoeuvres analyzed: 4.5 knots, 6 knots, and 9.5 knots. A typical pullout plot can be seen in Figure 3-14. As seen in this graph, the 'Lauzier' was slightly unstable to the port side. This was seen in the other 2 manoeuvres as well. The Igor Pro™ generated tables can be seen in the IMD technical report of the full scale sea trials [12].

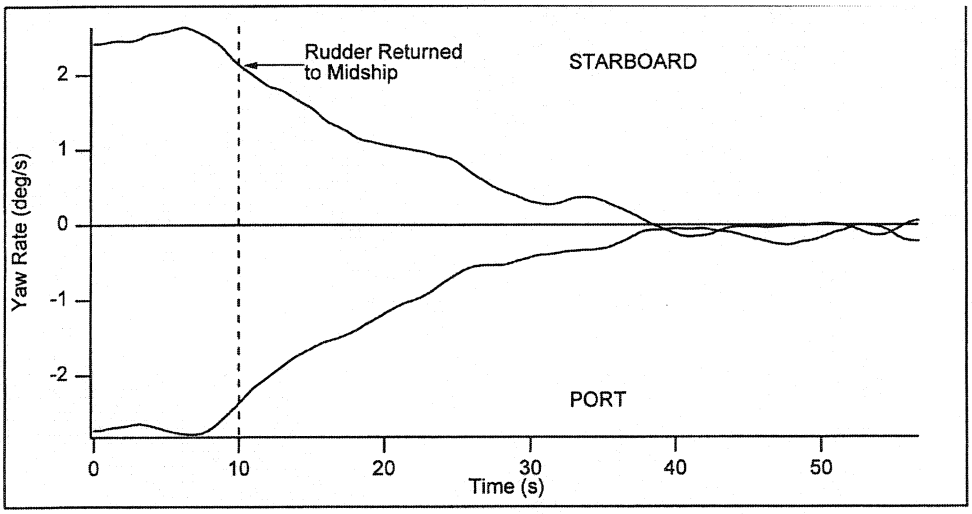

Figure 3-14: Typical Pullout Manoeuvre

5.0 Seakeeping Sea Trials

The seakeeping sea trials were attempted on four different days, all roughly 17 nautical miles East of St. John's. To measure the sea conditions, a small directional wave

buoy[3] was used during the trials. The first attempt on September 10th was carried out in unsuitable environmental conditions. For seakeeping experiments on the 'Lauzier', a minimal sea state of 3 is required to produce significant roll and pitch amplitudes. For this sea trial attempt, the winds were calm and the sea conditions were only characterized as a sea state 1. After a few runs, the sea trials were cancelled until a more suitable day. On September 28th, the second attempt had more favourable conditions with sea state 3-4 wave conditions. Although the wave buoy passed all checks prior to departure from the dock, unfortunately once deployed, there was no communication between the 'Lauzier' and the buoy. The wave buoy was retrieved and subsequently shipped back to the manufacturers for repair. The third attempt on October 24th was similar to the first attempt with less than ideal sea conditions (sea state 2). Nonetheless, a full set of seakeeping trials were completed due to the uncertainty if there will be another occasion when there would be suitable sea conditions.

On November 6th, the fourth and final set of trials was performed. The sea conditions were characterized as a sea state 3 that produced a 3 metre significant wave height swell being propelled ahead of a storm front. A total of 12 runs were carried out including five heading angles represented by head, bow, beam, quartering, and following seas with respect to the incident waves at 6.5 and 10.5 knots plus 2 zero speed beam runs. These runs were based on the guidelines outlined by ITTC [13] and described in the IMD technical report [12] on the full scale sea trials. During the sea trials however, the

[3] The wave buoy was manufactured by Neptune Sciences, Inc. of Slidell, Louisiana. For additional information see the wave buoy operation manual [14].

'Lauzier' performed the changing of the heading angle based on a pentagon pattern around the wave buoy. This resulted in some runs being carried out at an unacceptable long distance from the wave buoy. Also, at times the sea direction did not appear to conform to the expected direction either because the sea direction was changing or the original direction determination was incorrect. Consequently, this problem could not accurately be cross checked with the wave buoy due to the substantial distance between wave buoy and the 'Lauzier'. Therefore, in the future, IMD will follow the recommendation set out by ITTC of the acceptable seakeeping testing pattern as seen in Figure 3-15, where 1 thru 5 represent head, following, bow, beam, and quartering seas.

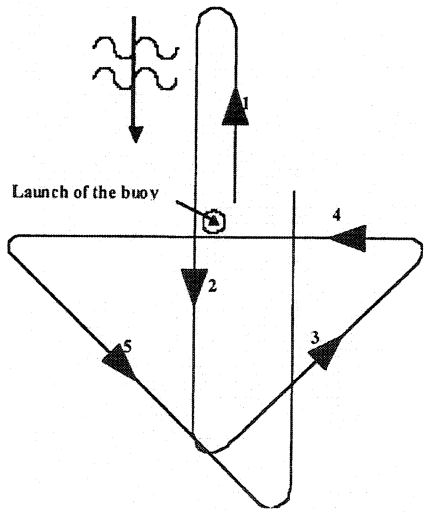

Figure 3-15: ITTC Recommended Seakeeping Testing Pattern

5.1 Seakeeping Online Analysis

After each seakeeping run, time series plots of the roll angle, pitch angle, and heave acceleration were generated. These plots were analyzed for acceptable amplitude

given the sea state and the direction of the ship relative to the incident waves. A typical online plot can be seen in Figure 3-16 for roll, pitch, and heave.

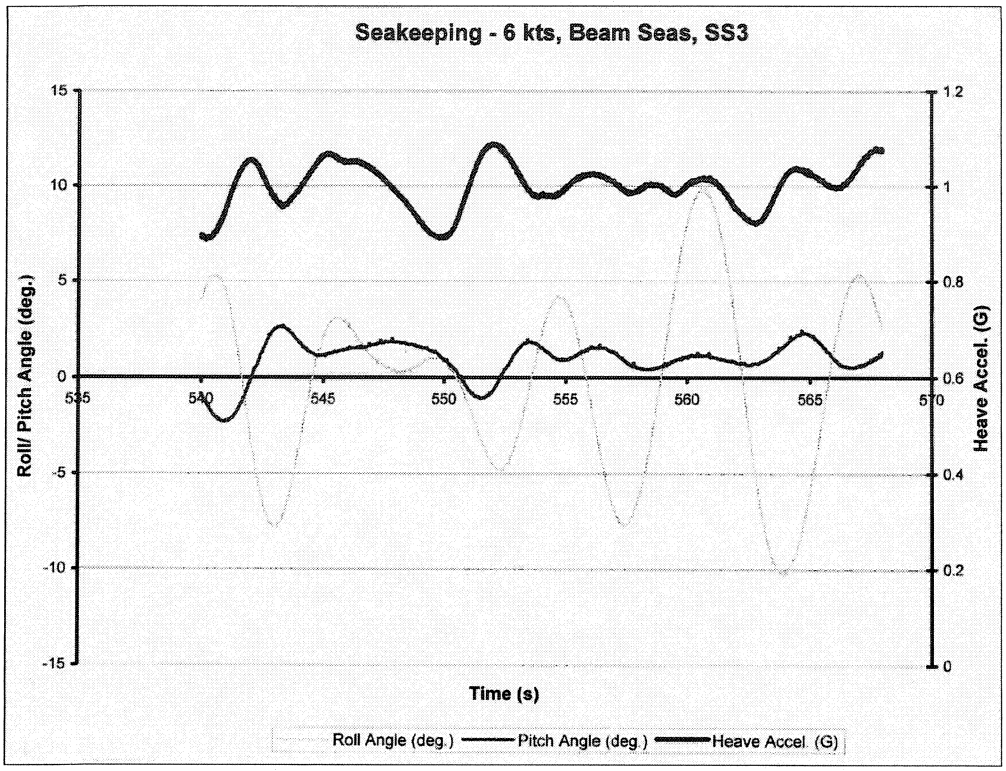

Figure 3-16: Seakeeping Test Run: Typical Online Plot

5.2 Seakeeping Offline Analysis

Once the trials were complete, the wave buoy was retrieved and the wave data downloaded. The buoy was configured to acquire information on the wave conditions every half hour during the sea trials. A summary of the wave statistics acquired on November 6th is provided in Table 3-9. Note that within the wave buoy, sea direction is measured using a flux gate compass and thus the data is generated in degrees magnetic. The magnetic deviation for St. John's approaches during the trials was 22.3 degrees West and this correction was applied to derive wave direction in degrees TRUE.

Table 3-9: Summary of Wave Statistics

Summary of Wave Statistics Collected Using MUN Directional Wave Buoy

Date	NF Time	Sig. Wave Height (m)	Dominant Wave Freq. (Hz)	Average Wave Freq. (Hz)	Dominant Wave Period (s)	Average Wave Period (s)	Dominant Wave Dir. (deg. mag.)	Average Wave Dir. (deg. mag.)	Dominant Wave Dir. (deg. TRUE)	Average Wave Dir. (deg. TRUE)
Nov. 6	12:00	3.19	0.08	0.12	12.34	8.41	192.7	179.0	170.4	156.7
Nov. 6	12:30	2.94	0.08	0.13	12.34	7.90	195.4	180.2	173.1	157.9
Nov. 6	13:00	2.98	0.09	0.13	10.89	7.73	191.0	182.3	168.7	160.0
Nov. 6	13:30	3.22	0.08	0.12	12.34	8.29	197.6	185.1	175.3	162.8
Nov. 6	14:00	3.07	0.09	0.13	10.89	7.90	193.5	182.5	171.2	160.2
Nov. 6	14:30	3.23	0.08	0.12	12.34	8.24	210.4	187.0	188.1	164.7
Nov. 6	15:00	3.01	0.08	0.12	12.34	8.09	176.5	169.8	154.2	147.5
Nov. 6	15:30	3.17	0.09	0.12	10.89	8.34	186.0	175.5	163.7	153.2
Nov. 6	16:00	2.70	0.08	0.13	12.34	7.61	165.1	155.0	142.8	132.7
Nov. 6	16:30	3.18	0.08	0.12	12.34	8.39	182.9	169.5	160.6	147.2
Nov. 6	17:00	3.23	0.08	0.12	12.34	8.49	165.2	161.0	142.9	138.7

The difference between dominant and average from the statistical information provided by the wave buoy is that the dominant term refers to the non-directional wave spectrum directly while the average term is a calculation based on the spectrum. For example, the dominant wave frequency is the frequency associated with the highest peak of the spectrum. The average frequency, on the other hand, is calculated by m_1/m_0 where m_0 and m_1 are the first and second derivative of the spectrum, respectively. For further details on the wave spectrum and its properties, refer to the wave buoy manual [14]. These spectra are useful, for they show in detail the dominant wave direction in which the 'Lauzier' is travelling against throughout the trials.

The motions of the 'Lauzier' were analyzed and computed statistically for the CG of the ship as well as for the middle of the external aft deck and the helmsman's position on the Bridge. All motions were calculated based on the earth coordinate system. Since the data was available, statistics on the propulsion parameters were also computed. It should be noted that in this process, the same residual torque values calculated during the powering trials were used. The statistical data along with information on the trial run were outputted on a generic form. The seakeeping tables can be seen in the IMD

technical report of the full scale sea trials [12]. A summary table of the ship motion standard deviation values is presented in Table 3-10. The relationship between the roll angle, pitch angle, and the accelerations versus the heading angle with respect to the incident wave are provided in Figure 3-17 and Figure 3-18 for the two forward speeds. The added power analysis is provided in Table 3-11.

Table 3-10: Summary of Ship Motions

Ship Motion Analysis

November 6, 2001 — M/V Louis M. Lauzier — IMD Proj.#01960

Speed (kts)	Heading	Roll Angle (deg)	Pitch Angle (deg)	Yaw Angle (deg)	Sway Displ. (m)	Heave Displ. (m)	Surge Accel. (m/s^2)	Sway Accel. (m/s^2)	Heave Accel. (m/s^2)
6.5	Head	2.777	1.895	1.213	0.975	0.749	0.467	0.954	0.589
6.5	Bow	4.025	1.841	1.283	1.201	0.855	0.444	1.360	0.645
6.5	Beam	4.729	1.297	1.373	1.633	0.916	0.318	1.514	0.578
6.5	Quartering	3.868	1.417	1.475	1.815	0.969	0.316	1.215	0.450
6.5	Following	2.617	1.699	1.300	1.112	0.674	0.351	0.892	0.353
10.5	Head	2.971	2.112	1.261	1.086	0.798	0.564	1.053	0.849
10.5	Bow	3.208	1.756	1.248	1.198	0.785	0.468	1.092	0.777
10.5	Beam	4.546	1.207	1.446	1.960	0.865	0.314	1.493	0.653
10.5	Quartering	3.763	1.350	2.110	2.457	0.787	0.277	1.257	0.456
10.5	Following	2.696	1.616	2.284	2.460	0.826	0.327	0.932	0.369

Note: The above values are Standard Deviation values of the particular motion.
The accelerations were measured for the center of gravity of the vessel.

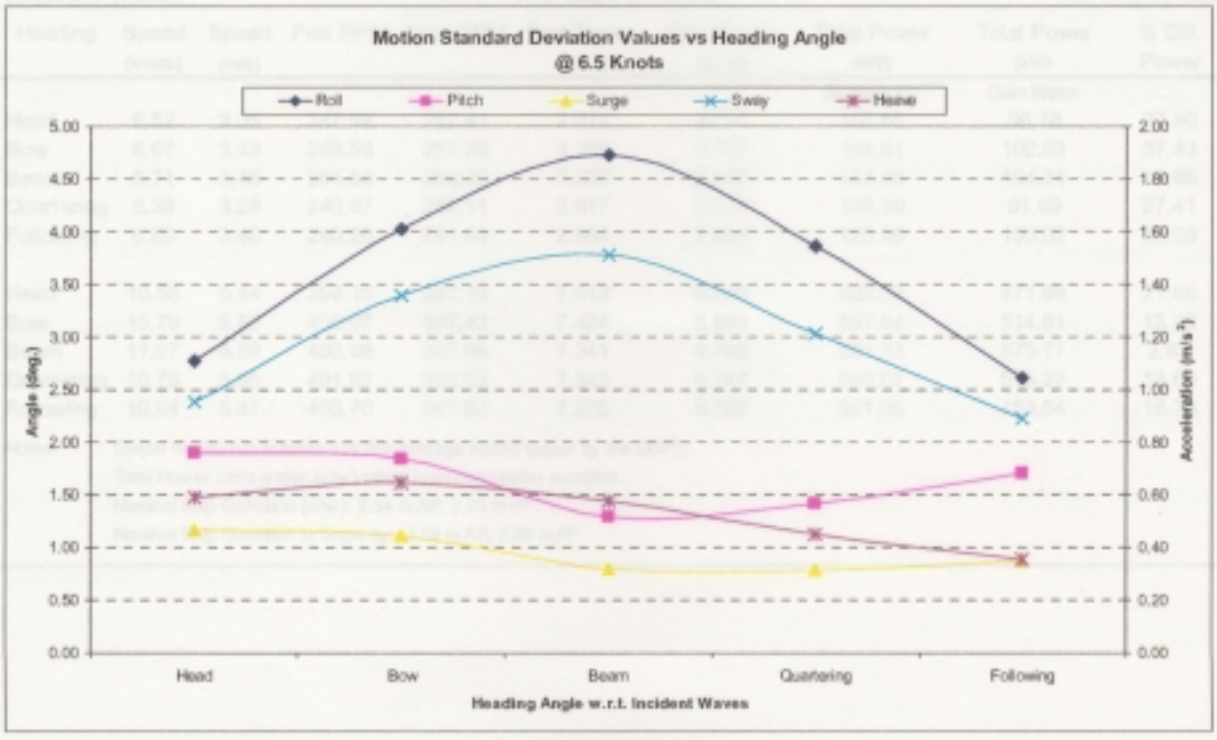

Figure 3-17: Ship Motions vs. Wave Direction - 6.5 knots

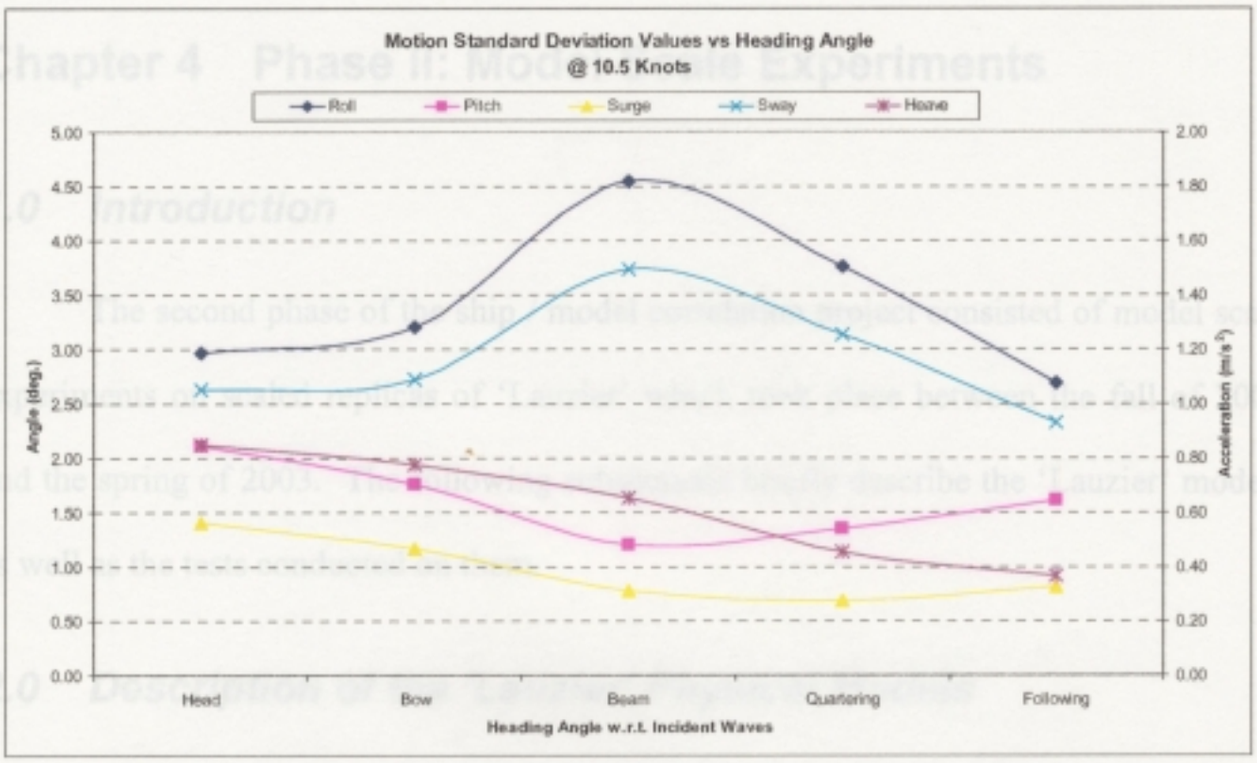

Figure 3-18: Ship Motions vs. Wave Direction - 10.5 knots

Table 3-11: Added Power Analysis

Added Power Analysis

November 6, 2001 — M/V Louis M. Lauzier — IMD Proj.#01960

Heading	Speed (knots)	Speed (m/s)	Port RPM	Stbd RPM	Port Torque (kN-m)	Stbd Torque (kN-m)	Total Power (kW) Seakeeping	Total Power (kW) Calm Water	% Diff. Power
Head	6.52	3.35	247.94	257.41	2.874	3.016	155.85	96.78	37.90
Bow	6.67	3.43	263.53	257.86	3.289	2.737	164.51	102.93	37.43
Beam	6.71	3.45	264.59	258.30	3.230	2.507	157.08	104.21	33.66
Quartering	6.38	3.28	240.67	242.11	2.617	2.379	126.30	91.69	27.41
Following	6.60	3.40	240.20	241.64	2.584	2.408	125.95	100.02	20.59
Head	10.58	5.44	399.15	397.15	7.512	6.940	602.52	471.99	21.66
Bow	10.79	5.55	400.07	397.42	7.424	6.893	597.84	514.61	13.92
Beam	11.07	5.69	400.98	397.85	7.341	6.796	591.33	575.77	2.63
Quartering	10.79	5.55	401.82	398.03	7.343	6.747	590.07	515.22	12.69
Following	10.64	5.47	400.70	397.83	7.275	6.622	581.05	483.54	16.78

Notes: Speed for the run is taken has the average speed output by the DGPS.
Total Power calm water (c/w) taken from regression equation.
Nominal Ship Condition (c/w): 2.34 m AP, 2.70 m FP
Nominal Ship Condition in Seaway: 2.39 m AP, 2.86 m FP

Chapter 4 Phase II: Model Scale Experiments

1.0 Introduction

The second phase of the ship / model correlation project consisted of model scale experiments on scaled replicas of 'Lauzier' which took place between the fall of 2002 and the spring of 2003. The following subsections briefly describe the 'Lauzier' models as well as the tests conducted on them.

2.0 Description of the 'Lauzier' Physical Models

As part of the 'Ship-Model Correlation Study', two model scale replicas were constructed of the 'Lauzier'. These models were used to carry out tests that would characterize the different components of the ship's performance. A 1:6 scale model, designated IMD597, was used to generate results for calm water resistance and propulsion, while a 1:12 scale model, designated IMD605, was used for seakeeping and manoeuvring experiments. Both scale model hulls were constructed using a foam mould with a fibreglass shell that conformed to a set of faired lines using IMD's standard model construction procedure [15]. The lines were measured by hand from a paper drawing (drawing #2175-1 / June 11, 1993) provided by the Marine Institute of Memorial University, the operators of the 'Lauzier'. The faired lines plan for the two models is depicted in Figure 4-1.

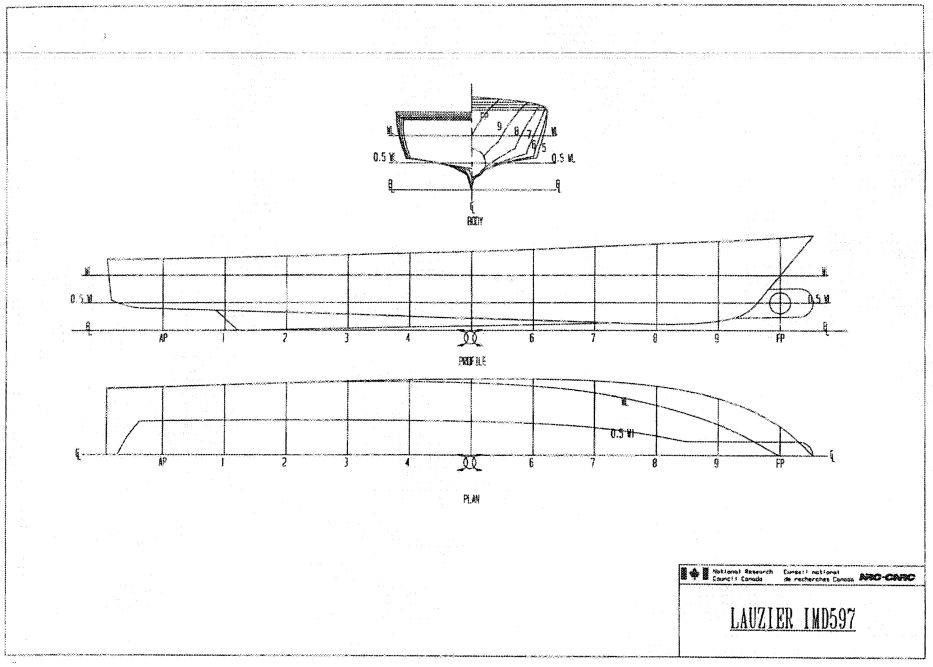

Figure 4-1: 'Lauzier' Lines Plan

2.1 1:6 Scale Model

The 1:6 scale model was designed to operate in a tow tank environment fitted to a tow post. The principle dimensions for the model are given below:

Length overall (LOA):	6.67 m
Length between perpendiculars (LBP):	5.67 m
Maximum breadth:	1.37 m
Draft at midships:	0.420 m
Displacement:	1118 kg

The hull was painted white and marked with standard sections and waterline markings [15]. The model included eleven reference blocks and five trim pads fitted to the gunnels and milled flat to a known elevation relative to the baseline. This was a

source of confusion during the resistance and propulsion test program, performed in August/September 2002, as it caused the appended hull resistance and self-propulsion test programs to be tested at a larger displacement. Due to this, those two test programs were repeated in November 2002. At the time of construction, the hull was measured, for quality assessment, at key locations throughout its length to verify dimensional accuracy. It was within the specified allowable IMD tolerance of ± 0.05% on length and ± 1mm on section shape.

Like the hull, the appendages were scaled versions of those on the 'Lauzier'. All the appendages, except the skeg and the bulbous bow, were designed to be detachable. Also, the 1:6 scale propellers were geometrically similar to the 'Lauzier' propellers. For the model powering experiments, turbulence stimulators were fitted to the hull and bulbous bow [15]. For these set of model experiments, it was not necessary to model the superstructure of the 'Lauzier'. A photograph of the 1:6 model is provided in Figure 4-2.

Figure 4-2: 1:6 Scale Model - Hull

The model was designed to be self-propelled. The drive system for the model test consisted of two Aerotech 1960 DC motors and the DS160 series servo amplifier motor

controller. The 1960 motors were used in this test due to the thrust and torque requirements needed to drive a model of this scale, maximum required thrust of 400 N and torque of 20 Nm. The model was also equipped with an instrumented gimble that interfaced with the tow post, which was used to measure the sinkage and trim, an anchor for the grasshopper unit in the bow of the model, and ballast. Photograph of the fully outfitted motor can be seen in Figure 4-3.

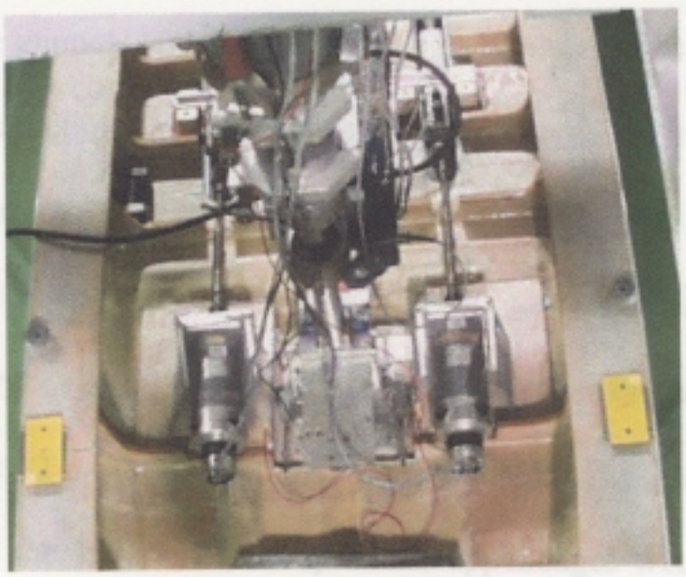

Figure 4-3: 1:6 Scale Model - Motors and Tow Post

2.2 1:12 Scale Model

The 1:12 scale model was designed to be radio controlled while operating in the IMD OEB. The principle dimensions for the model are given below:

Length overall (LOA):	3.33 m
Length between perpendiculars (LBP):	2.83 m
Maximum breadth:	0.68 m
Seakeeping Condition	
Draft at midships:	0.219 m

Displacement:	155 kg
Manoeuvring Condition	
Draft at midships:	0.212 m
Displacement:	145 kg

The hull was painted white and marked with standard sections and the waterline was marked for the seakeeping condition only. The model included eight reference blocks fitted to the gunnels and milled flat at a known elevation relative to the baseline. At the time of construction, the hull was measured for quality assessment at key locations throughout its length to verify dimensional accuracy. It was determined to be within the specified allowable IMD tolerance of ± 0.05% on length and ± 1mm on section shape.

Like the larger model size, the appendages were scaled versions of those on the 'Lauzier'. The 1:12 scale propellers were geometrically similar to the 'Lauzier' propellers. Unlike the 1:6 model, many of the appendages were permanently attached (the propeller, rudders and the sonar caisson were not).

For the seakeeping and manoeuvring experiments, no turbulence stimulators were added to the hull. Modifications were added to the hull to reinforce the local structural strength during the seakeeping trials. Renshape reinforcement was bonded to the stern to support an eyebolt that accommodated a lightweight tow line required to arrest the model at the end of a test run. Renshape was also bonded to the hull port and starboard adjacent to the LCG and above the waterline to accommodate 203.2 mm (8.0 in) long – 19.1 mm (0.75 in) aluminium pins. These pins were designed to interface with the model acceleration system that was used to maximize the available run length in the OEB.

For the set of seakeeping experiments, it was not necessary to model the superstructure of the 'Lauzier'. Instead, a 15 cm high lexan bulwark was constructed around the perimeter of the entire main deck, extending to 30 cm at the stern, a reasonable height as the testing sea state for the model only produced limited amounts of spraying and/or green water. The bulwarks were also modified in the bow, extended laterally port and starboard, in order to accommodate two large - 24 V batteries. The batteries were mounted in this fashion to match, within reason, the scale GM and the target roll radius of gyration. These properties are an important aspect in seakeeping trials since the purpose of the experiments was to try to accurately measure the motions of the vessel.

The 1:12 model was designed to be a self-propelled, free running model; therefore, the shafts were driven using electric propulsive motors activated by the 24 V batteries, described above. The electric motors consisted of two small Faulhaber motors (model #: 3564k024B) with an integral 3.75:1 gearbox, which gave the recommended maximum continuous rating of 18 rps. The motors can achieve revolutions as high as 22 rps for short periods of time. Small aluminium water catches were installed under the inboard end of each stern tube to retain any water that might ingress through them. The model was also equipped with radio controller / telemetry electronics, instrumentation, single rudder servo unit, several batteries of different size and type, and ballast. The battery capacity was sufficient enough to operate the model for an extended working day (16 hr) without recharging. Photographs of the fully outfitted model for the seakeeping and manoeuvring conditions are shown in Figure 4-4 and Figure 4-5. It should be noted

from Figure 4-5 that the large 24 V batteries were raised by 4 inches (~10 cm) on large pieces of styrofoam and two small weights were raised to sit on top of the stern bulwarks. These changes, along with the removed of 10 kg of weights, lowered the GM of the vessel to represent the quasi-static effects of the free surface in all of the tanks during the full scale sea trials, which is important during the model manoeuvring experimentation.

Figure 4-4: 1:12 Scale Model - Seakeeping

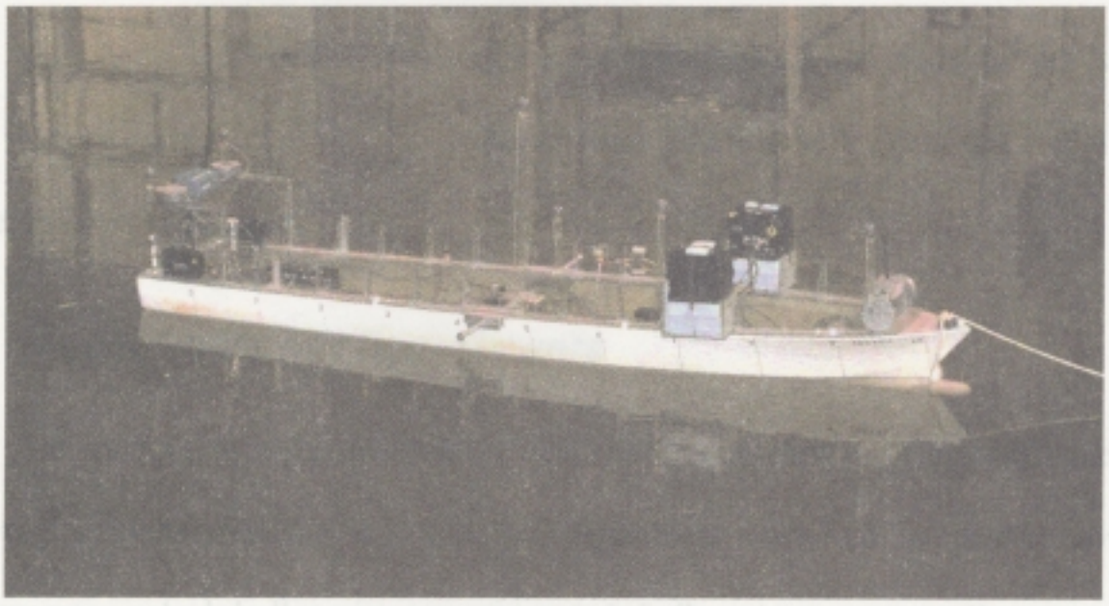

Figure 4-5: 1:12 Scale Model - Manoeuvring

The fully outfitted model was swung in air for both test conditions, as well as inclining experiments to achieve / verify the vessel's mass properties. The summary of the swing and inclining results are presented in Table 4-1. The target values were based on the closest load condition available from the 'Lauzier' stability booklet.

Table 4-1: Summary Results of the Swing and Inclining Experiments

FINAL SEAKEEPING RESULTS			
	Measured	Target	Error
VCG (Pitch) From keel (m)	***0.324***	***0.309***	4.64%
VCG (Roll) From keel (m)	***0.333***	***0.309***	7.10%
Radius of Gyration (Pitch) (m)	***0.961***	***0.990***	3.05%
Radius of Gyration (Roll) (m)	***0.297***	***0.315***	6.05%
GMT (m)	***0.169***	***0.180***	6.51%

FINAL MANOEUVRING RESULTS			
	Measured	Target	Error
VCG (Pitch) From keel (m)	***0.377***	***0.309***	18.01%
VCG (Roll) From keel (m)	***0.387***	***0.309***	20.25%
Radius of Gyration (Pitch) (m)	***0.971***	***0.990***	1.97%
Radius of Gyration (Roll) (m)	***0.323***	***0.315***	2.55%
GMT (m)	***0.118***	***0.120***	1.69%

As mentioned above, it was important to match the GM of model to the 'Lauzier' in the manoeuvring condition. This is achieved by altering the VCG of the model had to be altered beyond its target.

3.0 Model Powering Experiments

The model powering experiments were carried out using the 1:6 scale model. The following sections describe the different experiments required to predict powering requirements: naked hull resistance, appended hull resistance, propeller open water experiments, and self-propulsion experiments.

3.1 Resistance Experiments

The naked hull resistance experiments were completed at the Institute for Marine Dynamics in September 2002, while the appended hull resistance experiments were completed in November 2002. The model resistance experiments were executed in the IMD Towing Tank and the IMD Ice Tank. The model was instrumented to measure the tow force along with its sinkage and trim. Data was also collected on the water temperature and the carriage speed. For details on the instrumentation and calibration methodology, refer to the IMD technical report of the model resistance and propulsion experiments [16]. The following sections describe the experimental set-up necessary to get the required facility and the model 'test ready' along with the resistance testing procedure and the online and offline data analysis.

3.1.1 Towing Tank Configuration

For the resistance testing, the Towing Tank was filled up to 7 metres and side beaches were installed to aid in the bow wave energy absorption. Test runs were carried out with the carriage running towards the beach.

3.1.2 Ice Tank Configuration

For the resistance testing, the thermal doors were open for complete access to the entire tank. No ice sheet was required and the tank was operating at +15°C. The service carriage was not in use and was docked over the melt pit while the underwater carriage was disconnected and stationed at the far end of the setting up area. Side beaches were

installed for bow wave energy absorption. Test runs were carried out with the carriage running towards melt pit.

3.1.3 Model Preparation

For the appended hull resistance test, the model was fitted with all the designed appendages except the propellers and the rudders. The propellers were replaced with a propeller hub and a fairing cone. The propeller hub had the exact diameter as the designed propeller's hub, without the blades. This enabled water to pass through the propeller face without propeller fin interaction. It should be noted that for models, a centerline skeg and bulbous bow are considered part of the hull, therefore, for the bare hull resistance test, the skeg and bulbous bow were not removed. The appendages removed were: the bilge keels, the sonar dome, the twin propeller shafts, the set of 'A' brackets, the propeller hubs, and the fairing cones. The model was also outfitted with turbulence stimulators on the bow and the bulbous bow. The stimulators transformed the water from a laminar state to a turbulent state by disturbing the flow across them. Turbulent flow was required because it is the particular flow that the full scale ship experienced since the transition to turbulence occurred closer to the bow at higher Reynolds Number (higher speeds).

The displacement of the model was taken as the weight of the bare hull model plus the weights of all outfit, cables, and ballast that is placed in the model. The measured weight was within the IMD tolerance of ±1.0% from the value derived by the computed hydrostatics. The displacement for the appended model included the

displacement of the appendages. Adjustments were made to the ballast to accommodate the removal of the appendages. The weight of the bare hull model was 1118 kg, while the weight of the appended model is 1130.5 kg. In addition to the bare hull test condition, experiments were performed on a secondary test condition, called the Prohaska Method. These experiments involved removal of ballast in order to raise the transom out of the water, while still retaining the forward draft. This displacement was recorded was 734 kg.

Along with displacement, care was taken to ensure that the model had the correct static trim. To obtain this, the model's freeboard, rather than the draft, was measured using trimming hooks seated on milled reference pads at the following five locations: aft perpendicular (port and starboard side), forward perpendicular (starboard side), and amidships (port and starboard side). The ballast was redistributed in order to be within the IMD tolerance of ±3 mm. Displacement was not changed to bring the draft within these limits. The measurements for all three testing conditions are presented in Table 4-2.

Table 4-2: Trim Hook Measurements

Resistance and Propulsion Experiments
Trim Hook Measurements

Condition	Hook Placement	Required Freeboard (mm)	Measured Freeboard (mm)	
Bare Hull (Standard)	Port Aft Perpendicular	303	303	
	Stbd Aft Perpendicular	303	303	
	Port Amidships	273	274	
	Stbd Amidships	273	274	
	Stbd Fwd Perpendicular	242	243	
Bare Hull (Prohaska)	Port Aft Perpendicular	404	405	
	Stbd Aft Perpendicular	404	405	
	Port Amidships	323	324	
	Stbd Amidships	323	325	
	Stbd Fwd Perpendicular	242	242	
Appended Hull	Port Aft Perpendicular	303	304	
	Stbd Aft Perpendicular	303	-	*
	Port Amidships	273	272	
	Stbd Amidships	273	274	
	Stbd Fwd Perpendicular	242	241	

*- As per IMD standard [17], trim measurements are only required in the four nominal locations measured during the appended hull experiments.

Once the model was trimmed, the model was attached to the testing carriage of the Towing Tank for the bare hull resistance test. For the appended hull resistance test, the model was connected to the carriage in the Ice Tank. A tow post was connected to the gimble onboard the model, located at the LCB of the model. The tow post and gimble combination allowed the model to heave, pitch, and roll. To prevent the model from yawing, a single K&R grasshopper guider was fitted forward of the tow post to restrain any lateral and surge motion of the model. To complete the installation, all instrumentation cables were connected to the carriage's data acquisition system and the

motor cables were connected to the motor control system onboard the carriage. A picture of the installed model is provided in Figure 4-6.

Figure 4-6: Installed 1:6 Scale Model for Resistance Testing

3.1.4 Hull Resistance Test Program

The hull resistance test program followed the guidelines set out by IMD [17] to obtain the resistance (drag), sinkage, and dynamic trim of the 1:6 scale model of the 'Lauzier'. In order to obtain the hull resistance, the test program was broken up into three components: Appended Hull Resistance, Bare Hull Resistance (Standard Test Method), and Bare Hull Resistance (Prohaska Method). The Prohaska method is performed with the transom out of the water. The method was used strictly to determine the form factor of the hull, while the standard bare hull resistance in conjunction with the appended hull resistance was used to isolate the increase in the model's resistance due to the appendages.

The Appended and Standard Bare Hull Resistance test programs were identical. The test matrix consisted of speeds ranging from 5% below the minimum speed produced

by the full scale 'Lauzier' at which reliable data can be obtained, to 5% above the highest speed the 'Lauzier' can maintain. The test matrix does not evenly divide the speed range. In order to define any humps and hollows in the resistance curve, more testing speeds at the lower end of the speed range were required. However, as the slope of the resistance curve is greater at the high end of the speed range, only a few testing speeds were required.

Bare Hull Resistance: Prohaska Method test program consisted of tests conducted at nine speeds that correspond approximately to the Froude Number, *Fn*, range of 0.12 – 0.20 in steps of 0.01. Since these tests were at such low speeds that may result in scatter, each test was repeated.

To ensure the integrity of the results, the test matrix was developed so that the experiments were run at every other speed, starting at the lowest speed to the highest speed and then continued from highest to lowest, filling in the gaps. Repeat runs were also added to the matrix to verify the data.

Two rough-up runs were performed at the beginning of each day of testing at the median test speed. A rough-up run was performed as a calibration check to ensure that all instrumentation was performing properly and to disturb the perfectly calm water. A single rough-up run was also performed after any breaks in the test program that allowed the tank to settle to calm.

The test matrix for each test program can be seen in the Table 4-3 & Table 4-4. The tests were carried out following IMD guidelines [17] to ensure the highest quality of results.

Table 4-3: Bare Hull / Appended Hull Resistance Test Program

Run No.	Fn	Speed (knots FS)	Speed (m/s MS)
1	0.216	8.00	1.680
2	0.216	8.00	1.680
3	0.108	4.00	0.840
4	0.121	4.50	0.945
5	0.135	5.00	1.050
6	0.135	5.00	1.050
7	0.148	5.50	1.155
8	0.162	6.00	1.260
9	0.189	7.00	1.470
10	0.216	8.00	1.680
11	0.243	9.00	1.890
12	0.243	9.00	1.890
13	0.270	10.00	2.100
14	0.324	12.00	2.520
15	0.297	11.00	2.310
16	0.256	9.50	1.995
17	0.229	8.50	1.785
18	0.202	7.50	1.575
19	0.175	6.50	1.365
20	0.155	5.75	1.208
21	0.155	5.75	1.208
22	0.142	5.25	1.103
23	0.128	4.75	0.998
24	0.114	4.24	0.891

Table 4-4: Prohaska Test Program

Run No.	Fn	Speed (knots FS)	Speed (m/s MS)
1	0.15	5.56	1.168
2	0.15	5.56	1.168
3	0.12	4.45	0.934
4	0.14	5.19	1.090
5	0.16	5.93	1.246
6	0.18	6.67	1.402
7	0.2	7.42	1.557
8	0.19	7.04	1.480
9	0.17	6.30	1.324
10	0.15	5.56	1.168
11	0.13	4.82	1.012
12	0.12	4.45	0.934
13	0.14	5.19	1.090
14	0.16	5.93	1.246
15	0.18	6.67	1.402
16	0.2	7.42	1.557
17	0.19	7.04	1.480
18	0.17	6.30	1.324
19	0.15	5.56	1.168
20	0.13	4.82	1.012

3.1.5 Resistance Online Analysis

Before the online analysis began, an information file (*.inf) was created. This file contained the information about the project such as project number and title, as well as links to the model particular file (*.mdl) and the tank particular file (*.tnk). The model particular file expressed the scale of the model and its associated particulars such as displacement and block coefficient. The tank particular file expressed the dimensions of the filled tank along with the cross-sectional area.

Also performed before the test program is initiated was an estimate of the resistance and the total resistance coefficient over the speed range of the test program to provide a comparison curve during online analysis. This was obtained from published data using NavCAD™, for example, or from previous IMD model tests. For the initial appended hull resistance test program was performed at the end of August 2002, a NavCAD™ prediction was implemented using Holtrop 1988 method based on particulars of the model including all of its appendages. For the two bare hull resistance test programs, the results from the first set of appended hull resistance program were used as an estimate. For the appended hull resistance program performed in November 2002, the results from the first set of experiments were used as an estimate.

Although the NavCAD™ prediction was originally used, the results were unreliable. The Holtrop prediction was based only on the hull form with the added appendages. This returned a resistance curve that does not rapidly increase until higher in the speed range, speed that is out of the speed range of the 'Lauzier'. This made sense because the ship was originally designed to perform in the +20 knot speed range. Later

in its life, the ship was installed with new engines that restricted the ship to only perform at a top speed of 11.5 knots and its aft was extended, which in turn increased resistance. Consequently, this modification created a larger slope of the resistance earlier in the speed range. The NavCAD™ results with comparison to the full scale results can be seen in Figure 4-7.

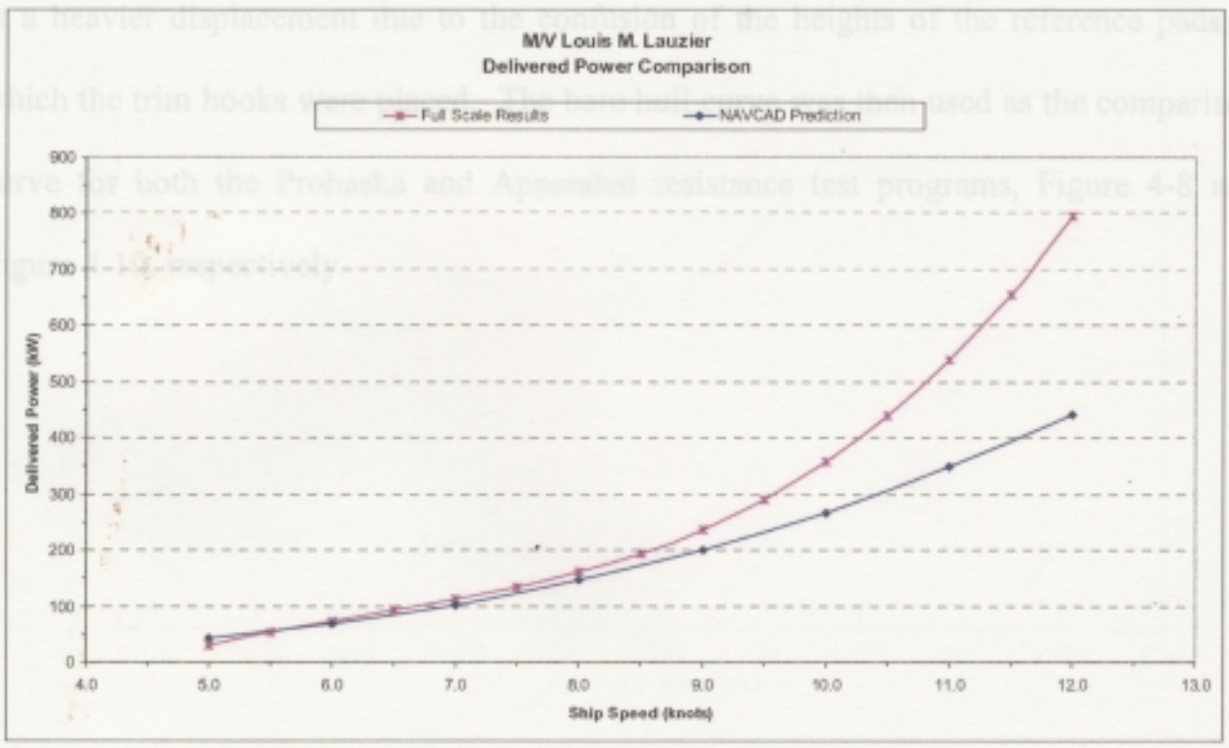

Figure 4-7: NavCAD™ Power Prediction

The online analysis [16] was carried out on a workstation in the control room onboard the carriage immediately after each run to verify the integrity of the acquired data. The data was checked for integrity by:

- Comparing the results with the comparison curve;
- Comparing the results from repeat runs;
- Ensuring that the data was increasing in a reasonable manner with increased speed; and

- During the step down in speed process of the test program, the data was 'filling in' the gaps between the data obtained during the step up in speed.

Figure 4-8, Figure 4-9, and Figure 4-10 are the resistance curves produced during the testing procedure. The comparison curve in Figure 4-9 was the appended resistance curve generated in August 2002. However, that particular set of experiments was tested at a heavier displacement due to the confusion of the heights of the reference pads at which the trim hooks were placed. The bare hull curve was then used as the comparison curve for both the Prohaska and Appended resistance test programs, Figure 4-8 and Figure 4-10, respectively.

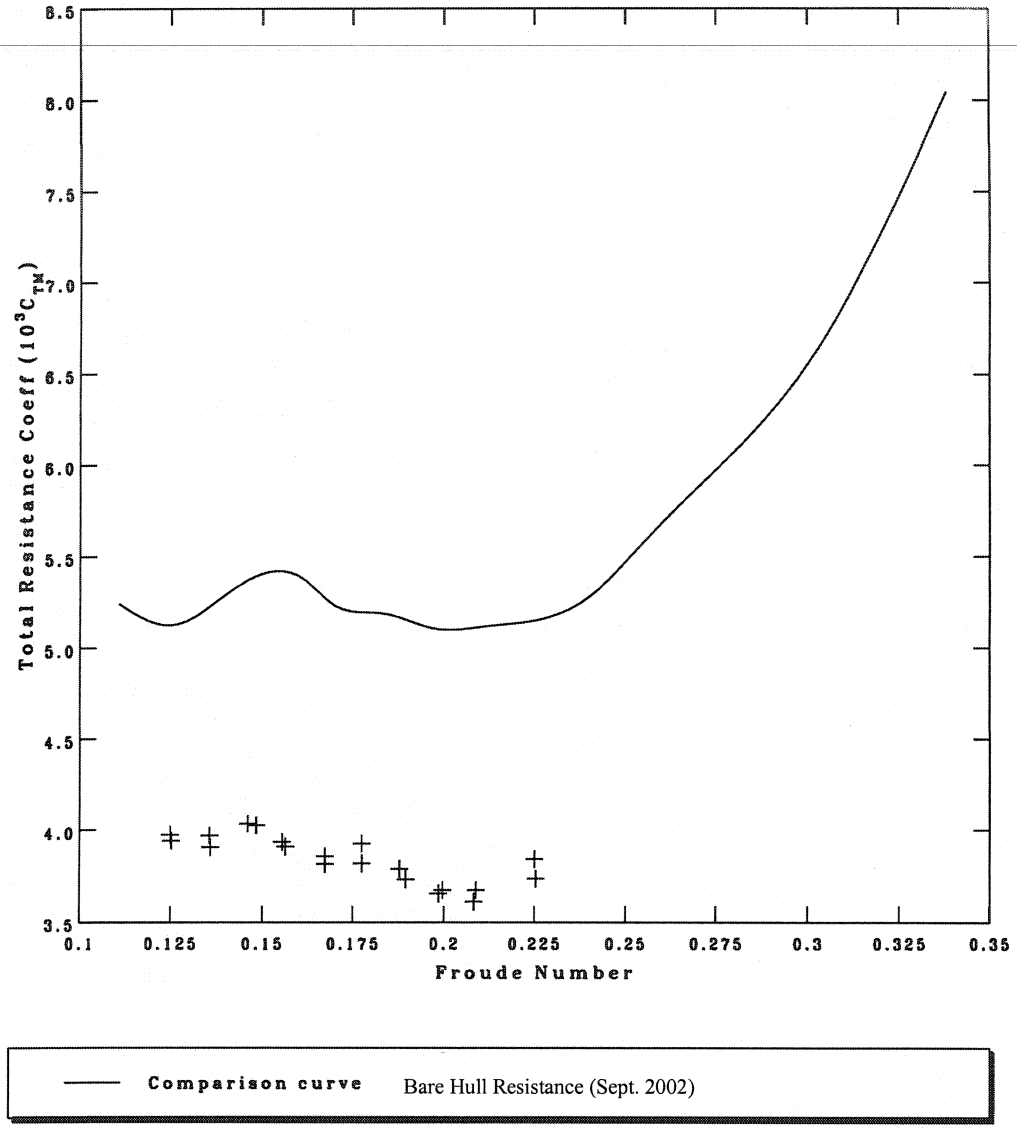

Figure 4-8: Online Analysis - Model Resistance (Prohaska)

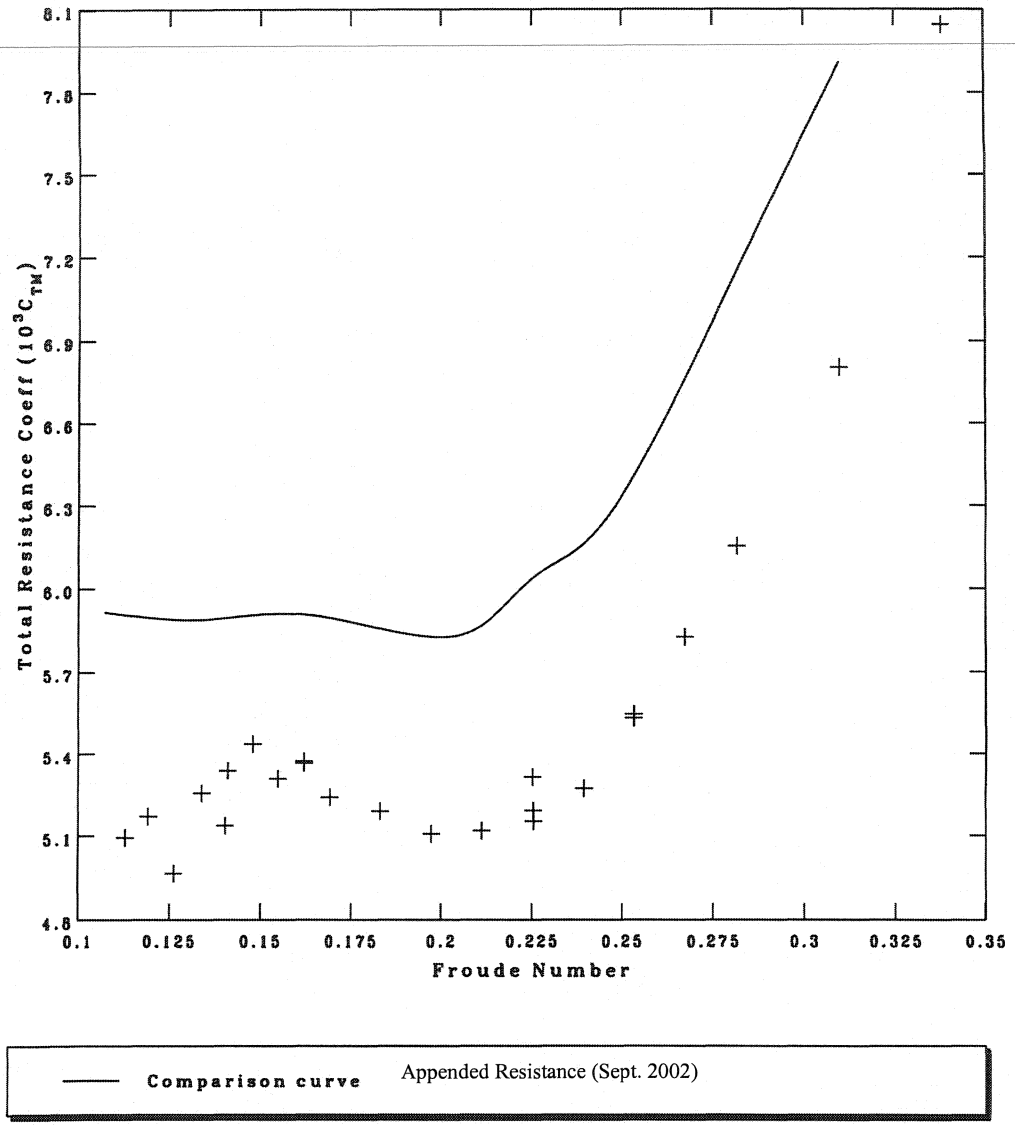

Figure 4-9: Online Analysis - Model Resistance (Bare Hull)

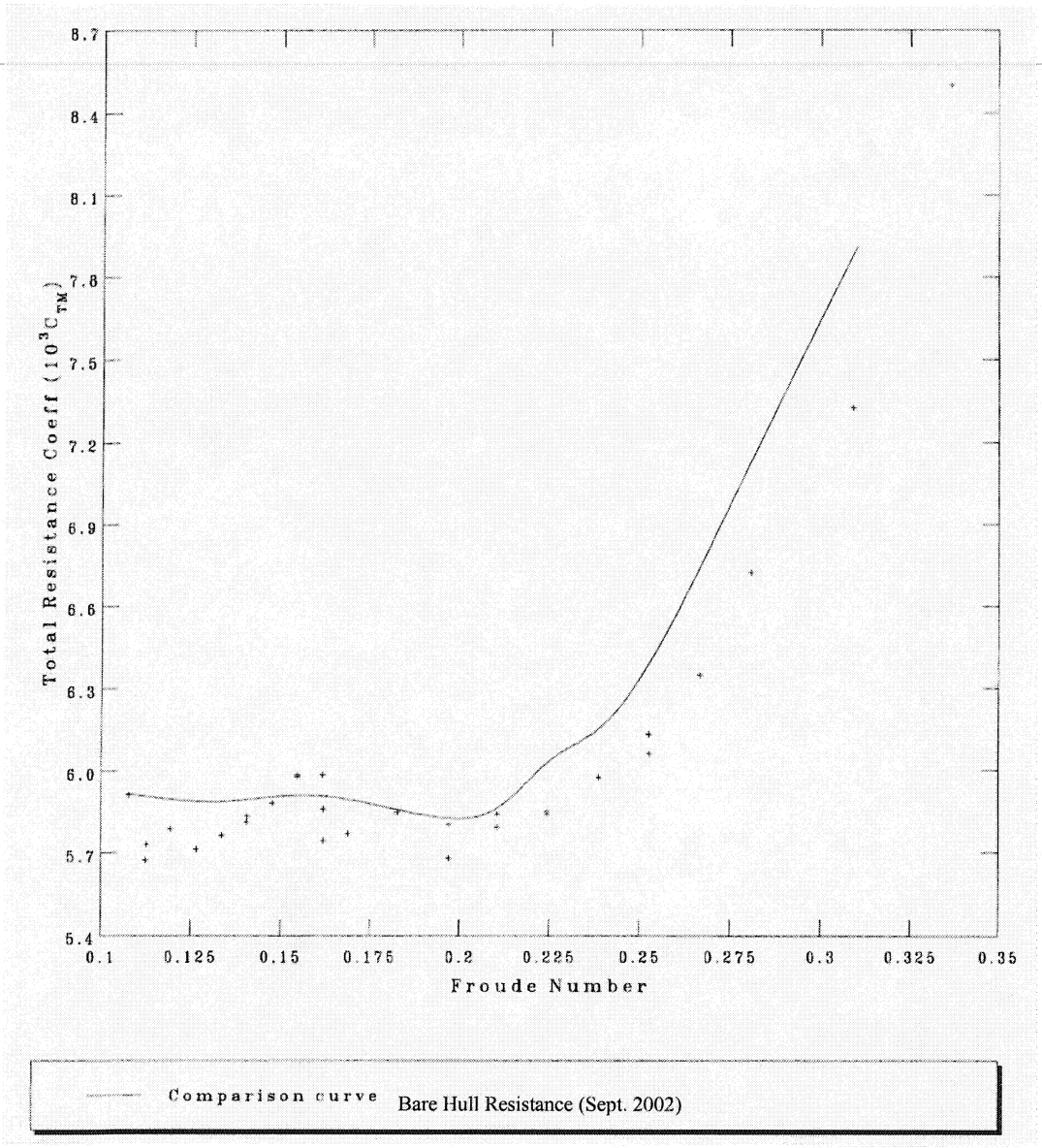

Figure 4-10: Online Analysis - Model Resistance (Appended)

Figure 4-11 displays a comparison curve between the naked resistance and the appended resistance. The resistance was calculated based on the total resistance coefficients as outlined in Equation 2-14.

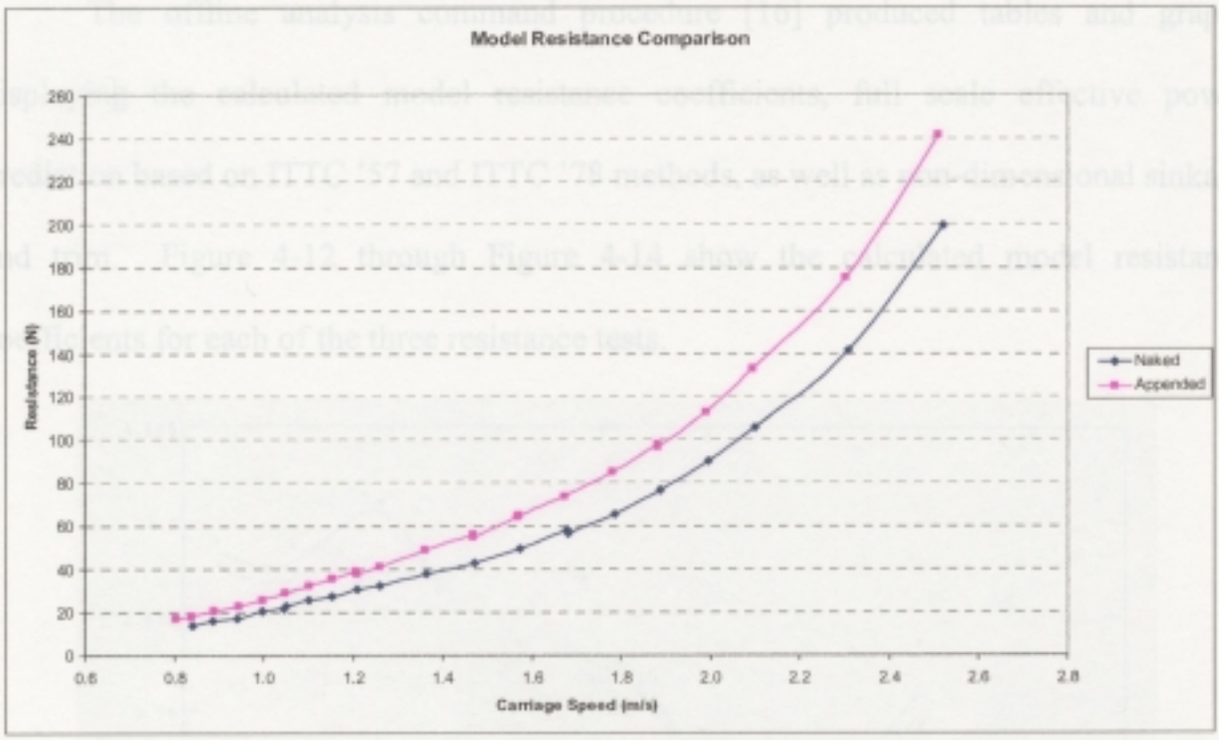

Figure 4-11: Model Resistance Comparison - Appended vs. Bare Hull

The complete online tables and graphs are provided in the model scale IMD technical report focussed on the resistance and propulsion experiments [16].

3.1.6 Resistance Offline Analysis

The offline data analysis for the model resistance data was performed on all three of the resistance experiments. Although the command procedure to analyze the experiments is the same with only the input and output file names being different, the analysis was carried out on the Prohaska set of experiments strictly to obtain the form factor. This form factor was then manually added to the header of the point files for the other two experiments. Therefore, in the command procedure the user is prompted to predict the form factor, the user will skip this computation and the program will read the experimental derived value.

The offline analysis command procedure [16] produced tables and graphs displaying the calculated model resistance coefficients, full scale effective power prediction based on ITTC '57 and ITTC '78 methods, as well as non-dimensional sinkage and trim. Figure 4-12 through Figure 4-14 show the calculated model resistance coefficients for each of the three resistance tests.

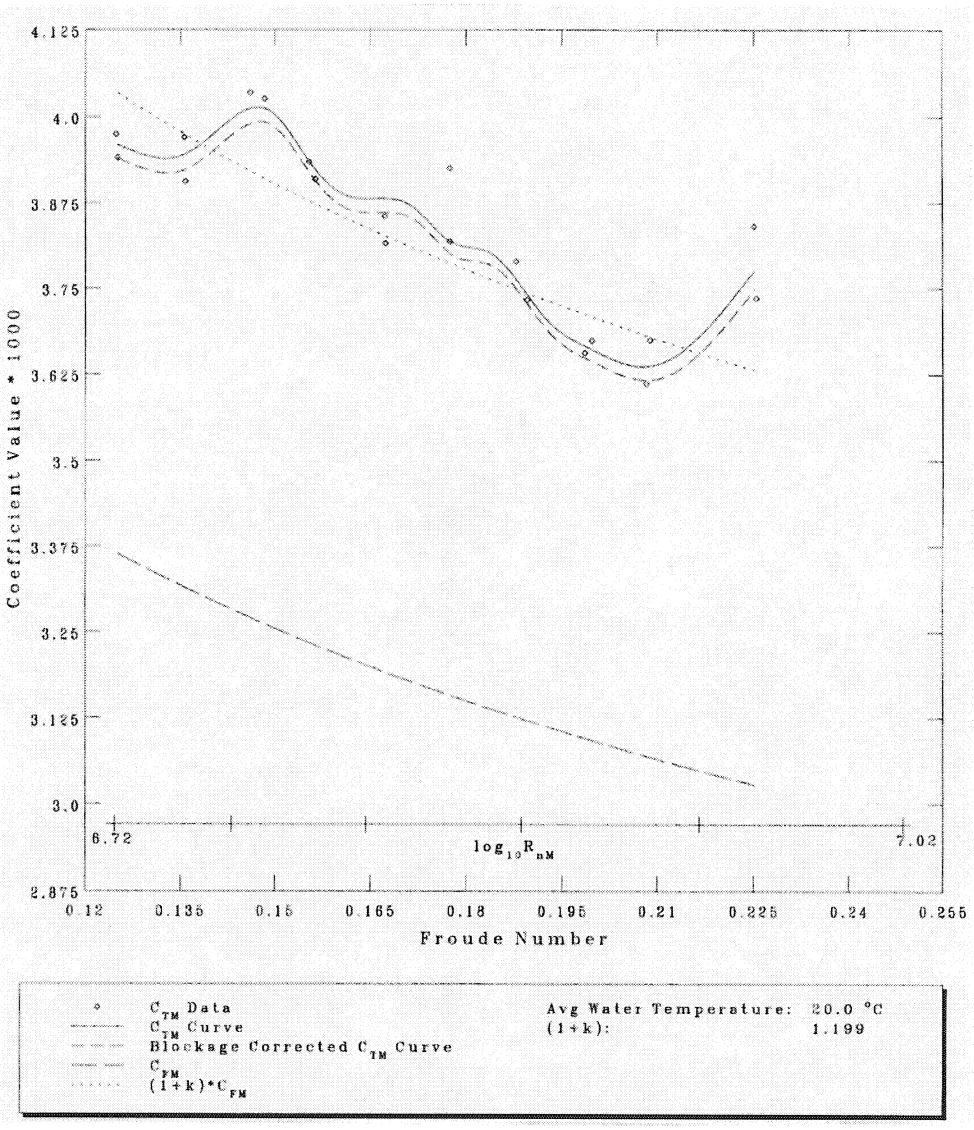

Figure 4-12: Offline Analysis - Model Resistance Coefficients (Prohaska)

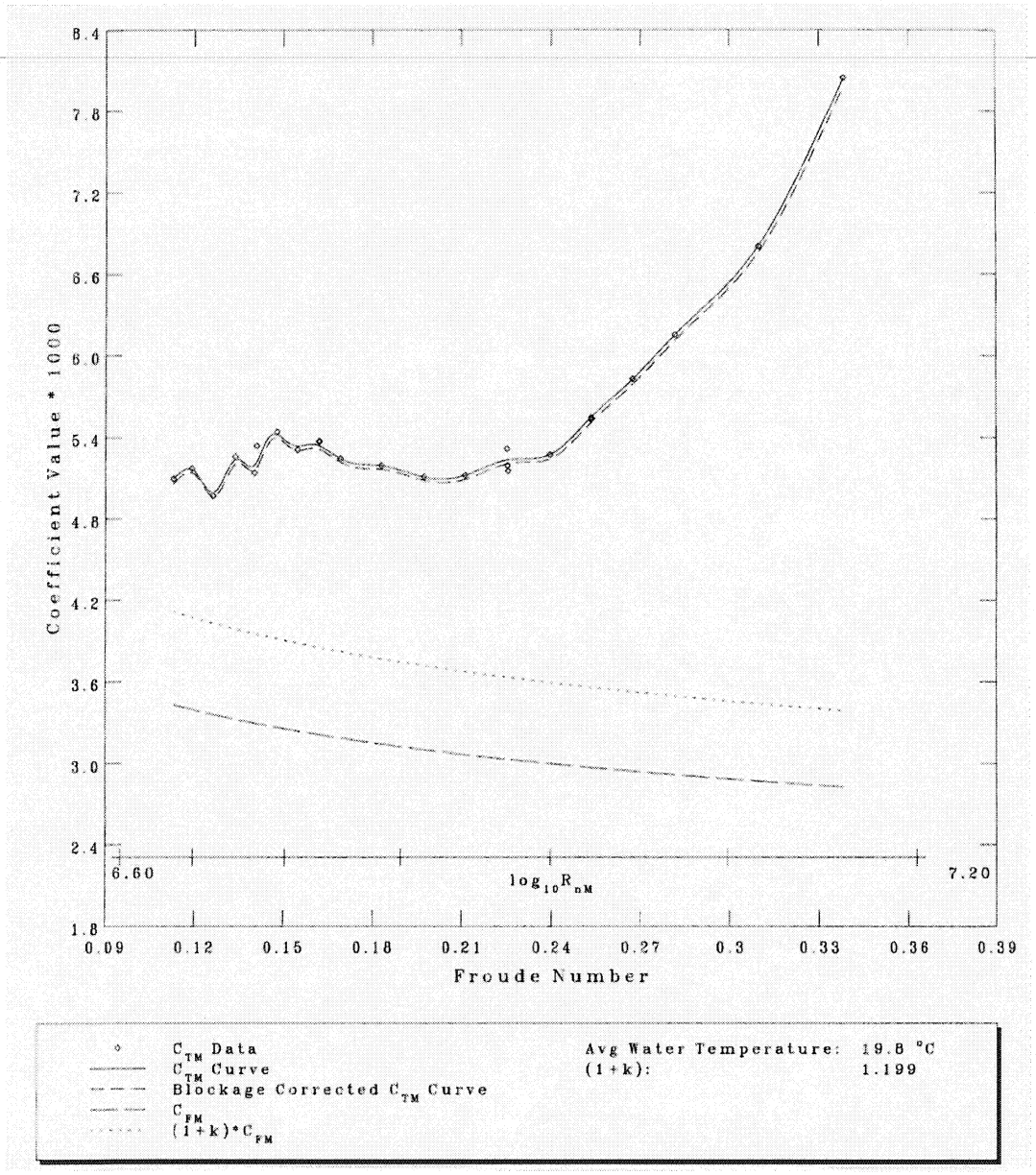

Figure 4-13: Offline Analysis - Model Resistance Coefficients (Bare Hull)

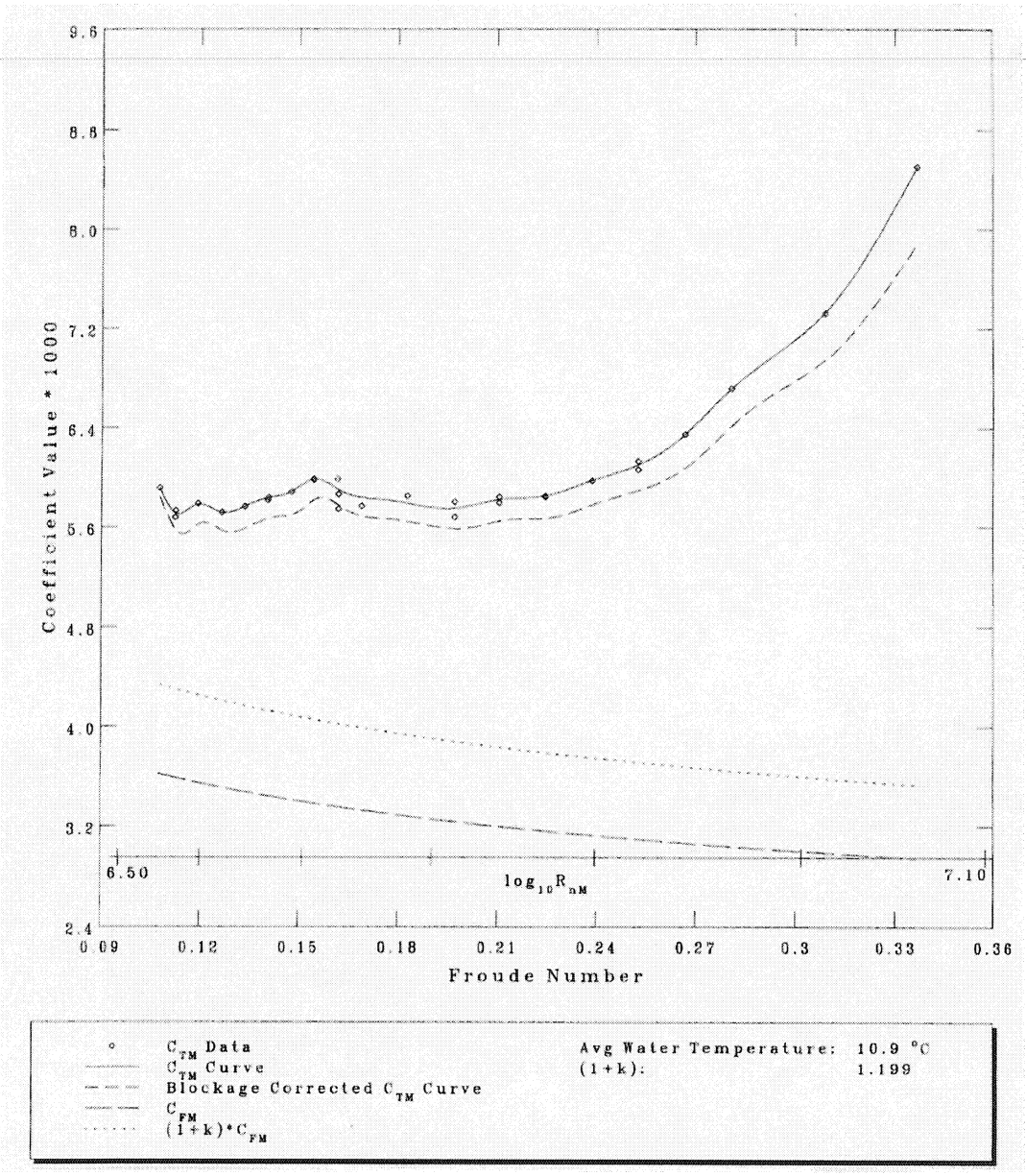

Figure 4-14: Offline Analysis - Model Resistance Coefficients (Appended)

The complete offline tables and graphs are provided in the model scale IMD technical report focussed on the resistance and propulsion experiments [16].

3.2 Propeller Open Water Experiments

The propeller open water experiments on the geometrically similar 1:6 scale propellers were completed in the MUN Towing Tank in November 2002. For these set of experiments, the experimenter used an apparatus specially designed for propeller open water experiments: MUN's Opens Boat. The Opens Boat was instrumented to measure the shaft speed, the propeller thrust and torque. Data was also collected on the water temperature and the carriage speed. For details on the instrumentation and calibration methodology, refer to the IMD technical report of the model resistance and propulsion experiments [16]. The following sections describe the experimental set-up necessary to get the required facility and the model 'test ready', and the propeller open water testing procedure, along with the online and offline data analysis.

3.2.1 Towing Tank Configuration

For the propeller open water experiments, MUN's Opens Boat was installed underneath the carriage as done previously during the R-Class propeller open water experiments [18]. The water level was raised to approximately 1.5x the diameter of the 'Lauzier' model propeller (0.318m) above the centerline of the propeller and the bow wave absorbers were installed along the sides of the tank. Test runs were carried out with the carriage running towards the wavemaker.

3.2.2 Description of MUN's Opens Boat

MUN's Opens Boat is a boat specially designed for propeller open water experiments. The narrow stainless steel Opens Boat, which is installed underneath the

Towing Tank's carriage, has a long shaft protruding forward where the propeller is attached. The long shaft enables the propeller to experience uniform flow entering the propeller blade area. The Opens Boat can be seen in Figure 4-15 and Figure 4-16. The Opens Boat is equipped with a motor, dynamometer, propeller shaft and propeller arranged as seen in Figure 4-17. The propeller shaft extends from the propeller through the outer bearing to be connected to the universal coupling that connects the shaft to the dynamometer. A drive belt is used to transfer power from the motor to the drive shaft in front of the dynamometer.

Figure 4-15: Profile View of the Opens Boat

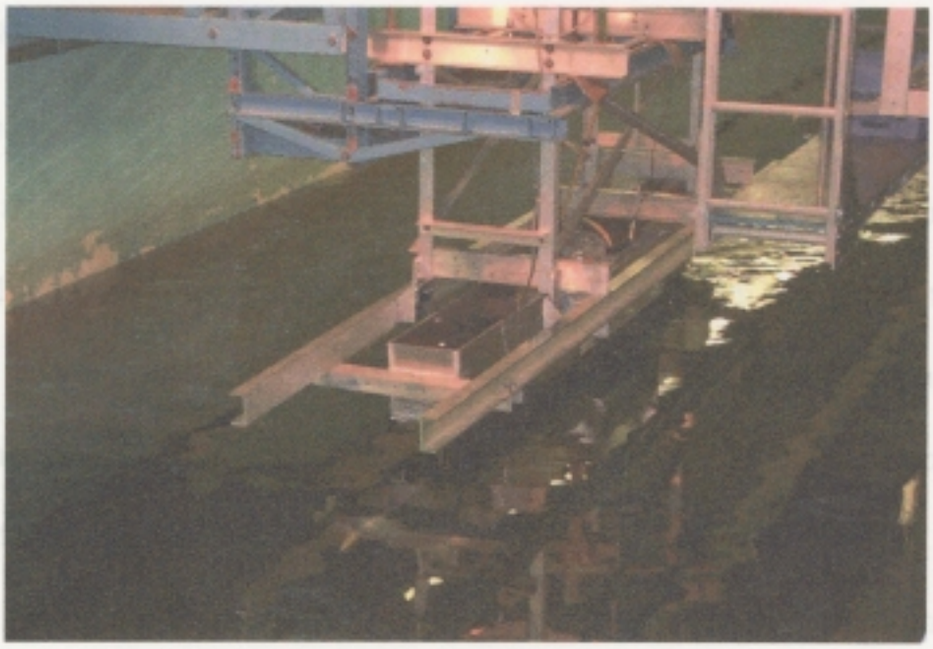

Figure 4-16: Opens Boat Connected to the Carriage

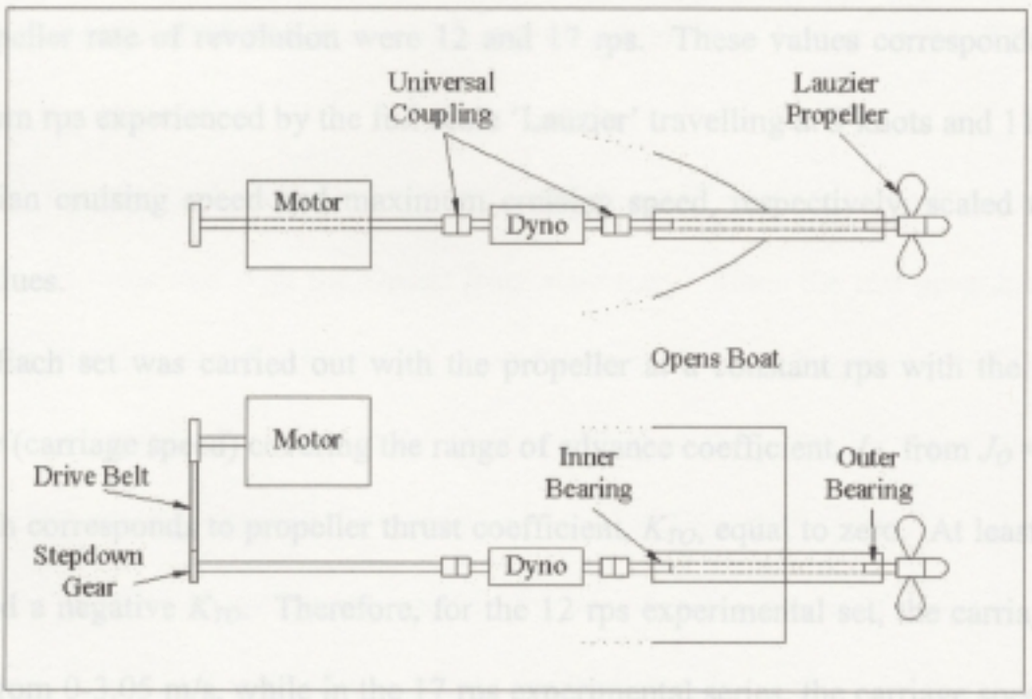

Figure 4-17: Opens Boat Schematic

3.2.3 Propeller Open Water Test Program

The open water test plan program followed the guidelines set out by IMD [19] to determine the performance characteristics for the 1:6 scale 'Lauzier' propellers in unrestricted uniform flow. Tests were completed on both the port and starboard propellers. These propellers, designated P304L and P304R, are outward turning props with a diameter of 0.212 m, a pitch / diameter ratio of 1.1 @ 0.7R, and an expanded blade area ratio of 0.65.

The test program consisted of two sets of experiments for each propeller, where each set corresponds to a different propeller rate of revolution (rps). The two values for the propeller rate of revolution were 12 and 17 rps. These values corresponded to the maximum rps experienced by the full scale 'Lauzier' travelling at 9 knots and 11.5 knots, its median cruising speed and maximum cruising speed, respectively, scaled to model scale values.

Each set was carried out with the propeller at a constant rps with the speed of advance (carriage speed) covering the range of advance coefficient, J_O, from $J_O = 0$ to the J_O which corresponds to propeller thrust coefficient, K_{TO}, equal to zero. At least one run produced a negative K_{TO}. Therefore, for the 12 rps experimental set, the carriage speed varied from 0-3.05 m/s, while in the 17 rps experimental series, the carriage speed varied from 0-4.32 m/s. The full test program can be seen in Table 4-5. The tests were carried out following IMD guidelines [19] which ensure the highest quality of results.

Table 4-5: Propeller Open Water Test Program

Run. No.	n = 17 rps Carriage Speed (m/s)	n = 12 rps Carriage Speed (m/s)	J
1	0.00	0.00	0.00
2	0.29	0.20	0.08
3	0.86	0.61	0.24
4	1.44	1.02	0.40
5	2.02	1.42	0.56
6	2.59	1.83	0.72
7	3.17	2.24	0.88
8	3.75	2.65	1.04
9	4.32	3.05	1.20
10	4.04	2.85	1.12
11	3.46	2.44	0.96
12	2.88	2.04	0.80
13	2.31	1.63	0.64
14	1.73	1.22	0.48
15	1.15	0.81	0.32
16	0.58	0.41	0.16

As seen in Table 4-5, for each set of experiments, the carriage speed varied from lowest to highest speed, and then continued from highest to lowest speed, filling in the gaps.

At the start and end of the test program, the shaft frictional torque caused by the bearings was measured with the Opens Boat stationary. Since the test program spanned more than one day, the frictional torque was measured at the beginning and the end of every day of testing. To measure the frictional torque, the propeller was replaced with the 'Lauzier' dummy hub and the torque was measured for shaft rps values ranging from 10% below to 10% above the rps used in the set of experiments, 10.8 rps to 18.7 rps. The dummy hub was also fitted to calibrate the shaft speed.

In addition to the friction test, a set of rough-up runs was performed at the beginning of each day. A rough-up run was performed as a calibration check to ensure that the instrumentation was performing properly and to disturb the perfectly calm water. The carriage speed was chosen to correspond to the middle of the speed range in the test

program for that particular shaft rps. A rough-up run was also performed after an extended span of downtime, i.e. after a break for lunch, as well as at the beginning of a new test program. It is standard practice to perform 2 rough-up runs concurrently. This was a good measure of the test repeatability.

3.2.4 Propeller Open Water Online Analysis

The online analysis was carried out on a workstation onboard the Towing Tank's carriage and performed immediately after every run. This verified the integrity of the acquired data. It was also compared to the propeller curves developed for a B-Series propeller with the same diameter and pitch / diameter ratio. The computed propeller coefficients can be seen in Table 4-6, while the comparison graphs can be seen in Figure 4-18 and Figure 4-19 for the two different shaft speeds.

Table 4-6: Online Analysis: Computed Propeller Coefficients

Propeller 304L						Propeller 304R					
Raw 12 rps 2002			Raw 17 rps 2002			Raw 12 rps 2002			Raw 17 rps 2002		
J	KT	10KQ	J	KT	10KQ	J	KT	10KQ	J	KT	10KQ
0.0000	0.5258	0.7714	0.0000	0.5410	0.8181	0.0002	0.5493	0.8448	0.0000	0.5618	0.8554
0.0776	0.5014	0.7692	0.0822	0.5125	0.7809	0.0774	0.5262	0.8189	0.0820	0.5304	0.8107
0.1602	0.4712	0.7591	0.1655	0.4815	0.7369	0.1614	0.4948	0.7676	0.1652	0.5019	0.7771
0.2380	0.4415	0.7110	0.2451	0.4479	0.7024	0.2408	0.4627	0.7358	0.2454	0.4683	0.7349
0.3211	0.4089	0.6773	0.3282	0.4134	0.6650	0.3206	0.4287	0.6905	0.3274	0.4333	0.6899
0.4067	0.3725	0.6388	0.4096	0.3774	0.6193	0.4028	0.3959	0.6550	0.4090	0.3975	0.6474
0.4784	0.3412	0.6100	0.4919	0.3433	0.5764	0.4814	0.3614	0.6067	0.4901	0.3609	0.6060
0.5571	0.3079	0.5326	0.5730	0.3053	0.5310	0.5591	0.3246	0.5693	0.5714	0.3247	0.5610
0.5997	0.2885	0.5100	0.6115	0.2881	0.5105	0.6026	0.3059	0.5472	0.6130	0.3061	0.5390
0.6364	0.2740	0.5104	0.6139	0.2875	0.5098	0.6026	0.3056	0.5463	0.6172	0.3061	0.5381
0.7158	0.2377	0.4334	0.6556	0.2748	0.4923	0.6403	0.2919	0.5242	0.6525	0.2889	0.5172
0.7975	0.2008	0.4032	0.7317	0.2398	0.4447	0.7180	0.2558	0.4835	0.7308	0.2560	0.4753
0.8740	0.1642	0.3145	0.8129	0.2064	0.4014	0.8002	0.2183	0.4248	0.8106	0.2217	0.4241
0.9523	0.1301	0.3090	0.8922	0.1708	0.3533	0.8776	0.1805	0.3670	0.8921	0.1867	0.3819
1.0315	0.0892	0.2352	0.9726	0.1332	0.3072	0.9547	0.1480	0.3317	0.9707	0.1491	0.3336
1.1086	0.0500	0.2105	1.0521	0.0931	0.2464	1.0353	0.1033	0.2754	1.0495	0.1079	0.2792
1.1841	0.0100	0.1403	1.2549	-0.0250	0.0812	1.1126	0.0681	0.2250	1.1206	0.0683	0.2229
1.2242	-0.0132	0.1086				1.1882	0.0251	0.1646	1.2525	-0.0093	0.1140
						1.2454	-0.0093	0.1145			

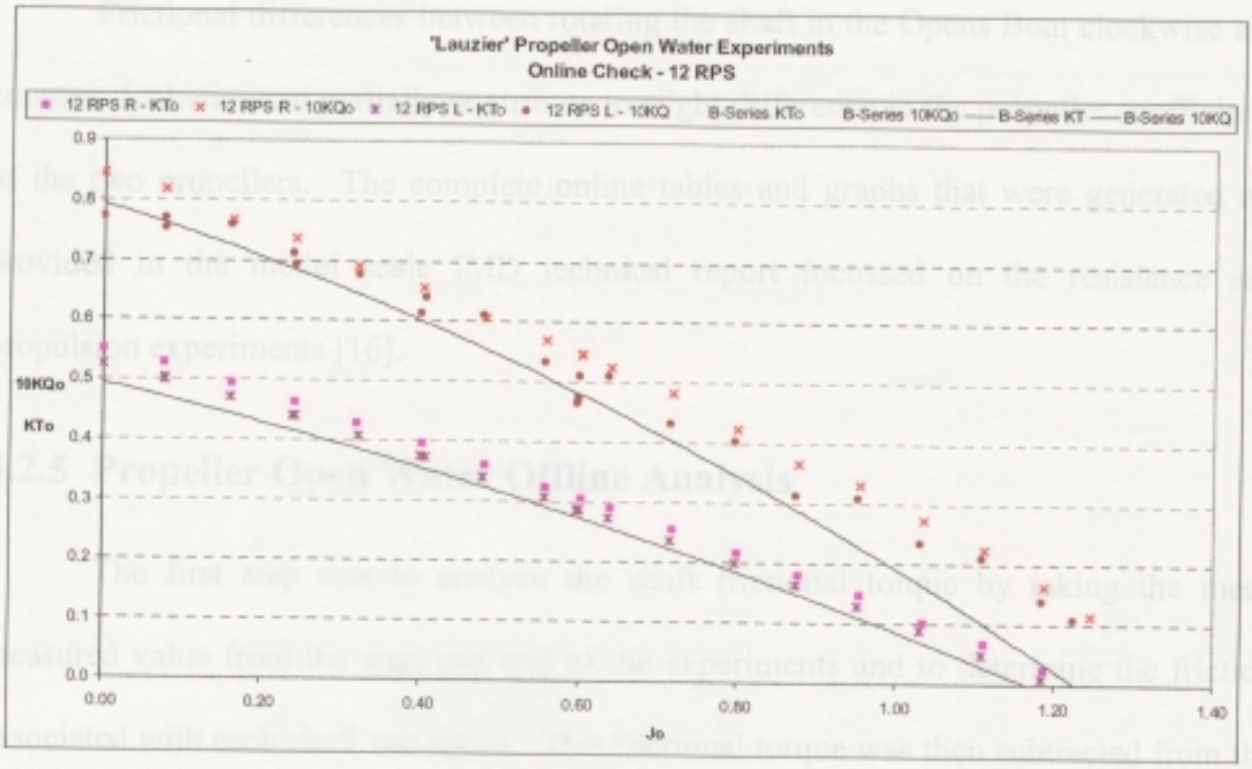

Figure 4-18: Online Analysis - Propeller Open Water (12 RPS)

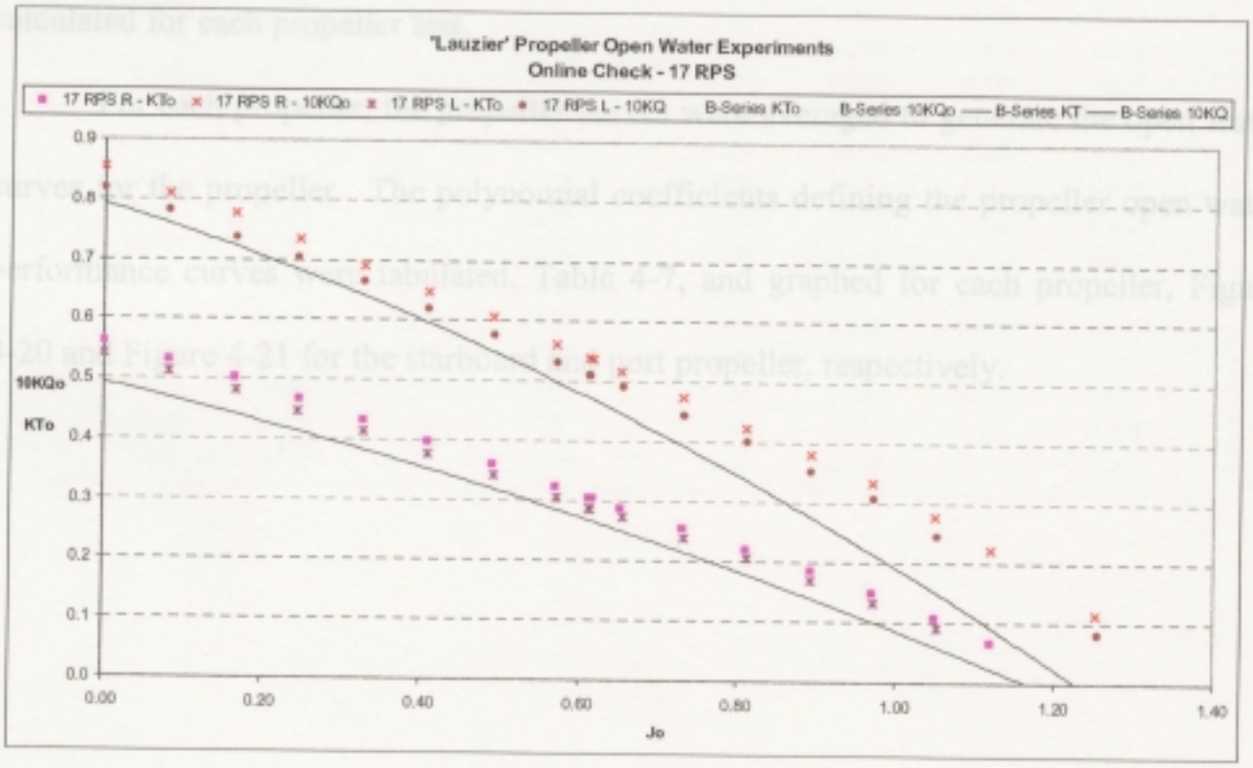

Figure 4-19: Online Analysis – Propeller Open Water (17 RPS)

Frictional differences between rotating the shaft in the Opens Boat clockwise and counter clockwise can partially contribute to slight difference in the propeller coefficients of the two propellers. The complete online tables and graphs that were generated are provided in the model scale IMD technical report focussed on the resistance and propulsion experiments [16].

3.2.5 Propeller Open Water Offline Analysis

The first step was to analyze the shaft frictional torque by taking the mean measured value from the start and end of the experiments and to determine the friction associated with each shaft test speed. This frictional torque was then subtracted from the original torque values obtained during the test run. New propeller coefficients were then calculated for each propeller test.

For each propeller, the propeller curves were averaged to generate the open water curves for the propeller. The polynomial coefficients defining the propeller open water performance curves were tabulated, Table 4-7, and graphed for each propeller, Figure 4-20 and Figure 4-21 for the starboard and port propeller, respectively.

Table 4-7: Offline Analysis - Propeller Open Water Coefficients

M/V Louis M. Lauzier **Propeller Open Water Experiments**
November 2002

IMD #304R / #304L
P/D = 1.1 @ 0.7R

Mean Propeller Revolution (RPS):
12.0 / 17.0

Left				Right			
J	K_T	$10K_Q$	η_o	J	K_T	$10K_Q$	η_o
0.001	0.534	0.806	0.001	0.001	0.557	0.846	0.001
0.050	0.516	0.787	0.052	0.050	0.539	0.825	0.052
0.100	0.498	0.766	0.103	0.100	0.520	0.803	0.103
0.150	0.479	0.745	0.153	0.150	0.500	0.780	0.153
0.200	0.460	0.723	0.202	0.200	0.481	0.756	0.202
0.250	0.440	0.701	0.250	0.250	0.461	0.732	0.250
0.300	0.420	0.677	0.296	0.300	0.441	0.708	0.297
0.350	0.400	0.653	0.341	0.350	0.420	0.683	0.343
0.400	0.380	0.628	0.385	0.400	0.399	0.657	0.387
0.450	0.359	0.603	0.427	0.450	0.378	0.631	0.430
0.500	0.338	0.576	0.466	0.500	0.357	0.604	0.470
0.550	0.316	0.549	0.504	0.550	0.335	0.576	0.509
0.600	0.294	0.521	0.539	0.600	0.313	0.548	0.545
0.650	0.272	0.493	0.572	0.650	0.290	0.519	0.579
0.700	0.250	0.463	0.601	0.700	0.268	0.489	0.609
0.750	0.227	0.433	0.625	0.750	0.245	0.459	0.636
0.800	0.204	0.403	0.645	0.800	0.221	0.429	0.657
0.850	0.181	0.371	0.658	0.850	0.197	0.397	0.672
0.900	0.157	0.339	0.663	0.900	0.173	0.365	0.680
0.950	0.133	0.306	0.656	0.950	0.149	0.333	0.677
1.000	0.108	0.272	0.633	1.000	0.124	0.300	0.661
1.050	0.083	0.237	0.588	1.050	0.099	0.266	0.625
1.100	0.058	0.202	0.506	1.100	0.074	0.232	0.561
1.150	0.033	0.166	0.363	1.150	0.049	0.197	0.453
1.200	0.007	0.129	0.107	1.200	0.023	0.161	0.269
1.250	-0.019	0.092	-0.409	1.250	-0.004	0.125	-0.056

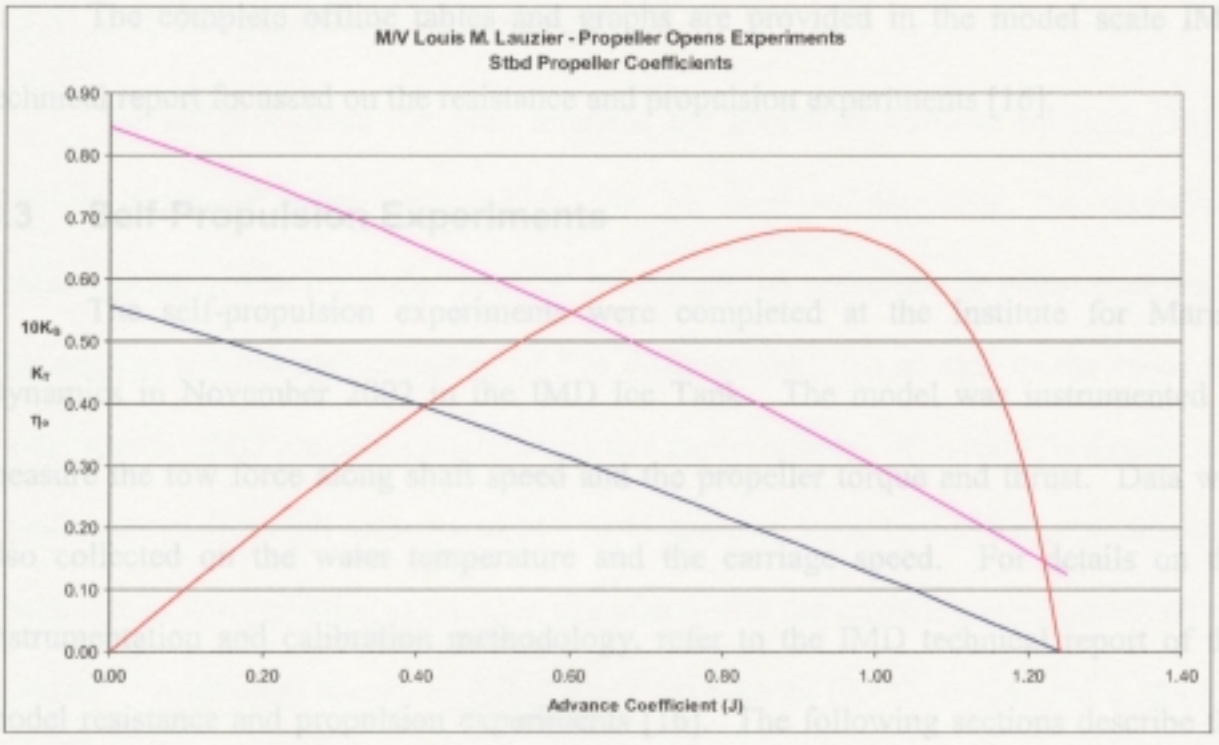

Figure 4-20: Offline Analysis - Propeller Open Water Curves (Stbd Propeller)

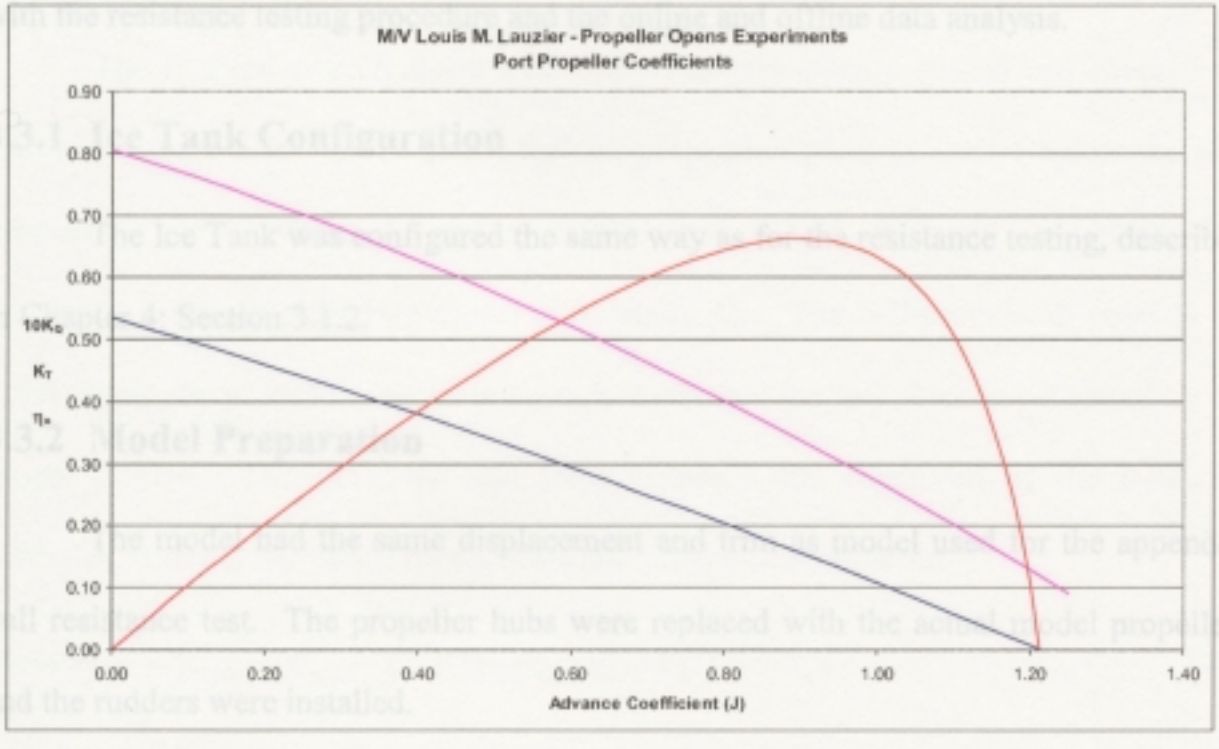

Figure 4-21: Offline Analysis - Propeller Open Water Curves (Port Propeller)

The complete offline tables and graphs are provided in the model scale IMD technical report focussed on the resistance and propulsion experiments [16].

3.3 Self-Propulsion Experiments

The self-propulsion experiments were completed at the Institute for Marine Dynamics in November 2002 in the IMD Ice Tank. The model was instrumented to measure the tow force along shaft speed and the propeller torque and thrust. Data was also collected on the water temperature and the carriage speed. For details on the instrumentation and calibration methodology, refer to the IMD technical report of the model resistance and propulsion experiments [16]. The following sections describe the experimental set-up necessary to get the required facility and the model 'test ready' along with the resistance testing procedure and the online and offline data analysis.

3.3.1 Ice Tank Configuration

The Ice Tank was configured the same way as for the resistance testing, described in Chapter 4: Section 3.1.2.

3.3.2 Model Preparation

The model had the same displacement and trim as model used for the appended hull resistance test. The propeller hubs were replaced with the actual model propellers and the rudders were installed.

3.3.3 Self-Propulsion Test Program

The self-propulsion test plan followed the guidelines outlined by IMD [20] to develop a set of experiments which can be used to determine the propulsion characteristics of the 1:6 scale 'Lauzier' model and its propellers in calm open water. The original test program consisted of five different shaft rps at each of the seven test model speeds (IMD standard only required five model speeds). The test speed range was equally spaced from full-scale speed of 5 to 11 knots or 1.050 to 2.310 m/s model scale. These speeds corresponded to the ones associated with the powering experiments on the 'Lauzier'. Additional speeds of 3.7, 4.4 and 10.4 knots (0.777, 0.924, and 2.184 m/s model scale) were added to enhance research and development for Sue Molloy, a MUN Ph. D candidate.

The five rps at each speed were approximately equally spaced and covered the tow force range from 0.0012 above the self-propulsion point to 0.0004 below the self-propulsion point, where the values 0.0004 and 0.0012 represent the incremental resistance coefficient for ship-model correlation, C_A. The self-propulsion point is the point where the propellers generate enough thrust that the tow force experienced by the model is zero. Therefore, the tow force expected was calculated by the following formulas, where $_M$ represents model scale and $_S$ represents full scale:

$$TowForce = \left(C_{FM} - C_{FS} - C_A\right) \cdot \left(\tfrac{1}{2} \cdot \rho_M \cdot S_M \cdot V_M^2\right) \quad \text{(4-1)}$$

$$C_F = \frac{0.075}{\left(\log(Rn) - 2\right)^2} \quad \text{(4-2)}$$

$$Rn = \frac{VL}{\nu} \qquad (4\text{-}3)$$

where: ρ = Density of the water;

S = Wetted surface area of the model;

V = Velocity of the ship/model;

L = Length of the ship/model; and

ν = Kinematic viscosity of the water.

Reynolds number, Rn, was calculated for model scale, $_M$, and full scale, $_S$.

The best estimate for the nominal shaft revolution for the self propulsion point is by converting the full scale measured RPM during the powering trials to model scale rps.

In addition to the five shaft speeds per model speed, a zero shaft thrust condition was added. This test involved turning the shafts at a very low rps, enough to overcome the drag of the slowly rotating propeller, i.e. producing zero thrust. This was added for research being conducted by Dr. N. Bose, a MUN engineering professor. Also added to the test program was a testing methodology proposed by Holtrop to predict the propulsive characteristics [21]. This methodology involved varying the shaft revolutions manually from 1 rps above to 1 rps below the nominal model self-propulsion point in one test run. These test program additions are out of the scope of this project and the data will not be analyzed.

To ensure the integrity of the results, the test matrix was developed so that the experiments were run at every other speed starting at the lowest speed to the highest

speed and then continued from highest to lowest, filling in the gaps. Also, the shaft speeds at each model speed were in order of increasing speed.

Two rough-up runs were performed at the beginning of each day of testing at the median test speed, 1.544 m/s. A rough-up run was performed as a calibration check to ensure that all instrumentation was performing properly and to disturb the perfectly calm water. A single rough-up run was also performed after any breaks in the test program that allowed the tank to settle to calm.

The full propulsion test program is provided the IMD technical report of the model resistance and propulsion experiments [16]. A summary of that test program can be seen in the following table.

Table 4-8: Propulsion Test Program

Fn	Nom. Speed (knots FS)	Speed (m/s MS)	Shaft Speed (rps MS)
0.198	7.35	1.544	9.8
0.198	7.35	1.544	9.8
0.100	3.7	0.777	Zero shaft thrust
0.100	3.7	0.777	5 shaft rps: nominal 4.2 rps
0.100	3.7	0.777	Holtrop procedure
0.135	5	1.050	Zero shaft thrust
0.135	5	1.050	5 shaft rps: nominal 6.7 rps
0.135	5	1.050	Holtrop procedure
0.189	7	1.470	Zero shaft thrust
0.189	7	1.470	5 shaft rps: nominal 9.2 rps
0.189	7	1.470	Holtrop procedure
0.243	9	1.890	Zero shaft thrust
0.243	9	1.890	5 shaft rps: nominal 12.3 rps
0.243	9	1.890	Holtrop procedure
0.280	10.4	2.184	Zero shaft thrust
0.280	10.4	2.184	5 shaft rps: nominal 14.6 rps
0.280	10.4	2.184	Holtrop procedure
0.297	11	2.310	Zero shaft thrust
0.297	11	2.310	5 shaft rps: nominal 15.9 rps
0.297	11	2.310	Holtrop procedure
0.270	10	2.100	Zero shaft thrust
0.270	10	2.100	5 shaft rps: nominal 14 rps
0.270	10	2.100	Holtrop procedure
0.216	8	1.680	Zero shaft thrust
0.216	8	1.680	5 shaft rps: nominal 10.7 rps
0.216	8	1.680	Holtrop procedure
0.162	6	1.260	Zero shaft thrust
0.162	6	1.260	5 shaft rps: nominal 7.9 rps
0.162	6	1.260	Holtrop procedure
0.119	4.4	0.924	Zero shaft thrust
0.119	4.4	0.924	5 shaft rps: nominal 5.5 rps
0.119	4.4	0.924	Holtrop procedure

At the start and end of the self-propulsion test program, the shaft frictional torque caused by the bearings was measured. Since the test program spanned more than one day, the frictions were measured at the beginning and the end of every day of testing on the stationary model. To measure the frictional torque, the propellers were replaced with the 'Lauzier' dummy hubs and the torques were measured at ten values that are evenly spaced over the shaft rps range of 10% below to 10% above the rps used in the set of

experiments, 3.8 rps to 17.5 rps. The dummy hub was the same one fitted to calibrate the shaft speed.

In addition to the propulsion experiments, a set of bollard tests was conducted to achieve the bollard characteristics of the model. These tests were carried out with the carriage positioned approximately midway up the tank. With the carriage held stationary, the tests were conducted at nine equally spaced values of rps. The bollard test program was conducted at the beginning of the propulsion test program, as seen in Table 4-9.

Table 4-9: Bollard Test Program

No.	rps MS	RPM FS
1	4.5	110
2	6.1	150
3	7.3	178
4	8.5	207
5	9.6	235
6	10.7	263
7	11.9	292
8	13.1	320
9	14.2	348

All the propulsion experiments are carried out following IMD guidelines [20] to ensure the highest quality of results.

3.3.4 Self-Propulsion Online Analysis

Before the online analysis began, an information file (*.inf) was created. This file contained the information about the project such as project number and title, as well as links to the model particular file (*.mdl), the tank particular file (*.tnk), and the port and starboard propeller particular files (*.prp). The model particular file expressed the scale of the model and its associated particulars such as displacement and block coefficient.

The tank particular file expressed the dimensions of the filled tank along with the cross-sectional area. The propeller particular file contained the designated name of the propeller and its particulars such as rotation direction and diameter.

The online analysis was carried out on a workstation in the control room onboard the carriage immediately after each run to verify the integrity of the acquired data. The checks that were carried out manually by reviewing the plots and tables produced during the analysis include:

- Verifying that the both shafts were rotating at the same rate;
- Ensuring that the propeller coefficients were decreasing in a reasonable manner with increased speed;
- Ensuring that the nominal tow force values were met for the self-propulsion experiments;
- Ensuring that the zero shaft thrust was met for N. Bose research; and
- Ensuring that the shaft rps was increasing at a steady rate during the Holtrop experimentation.

A typical online plot (carriage speed = 1.189 m/s) can be seen in Figure 4-22. Since no previous tests have been done on these propellers, no propulsion curves were available for comparison.

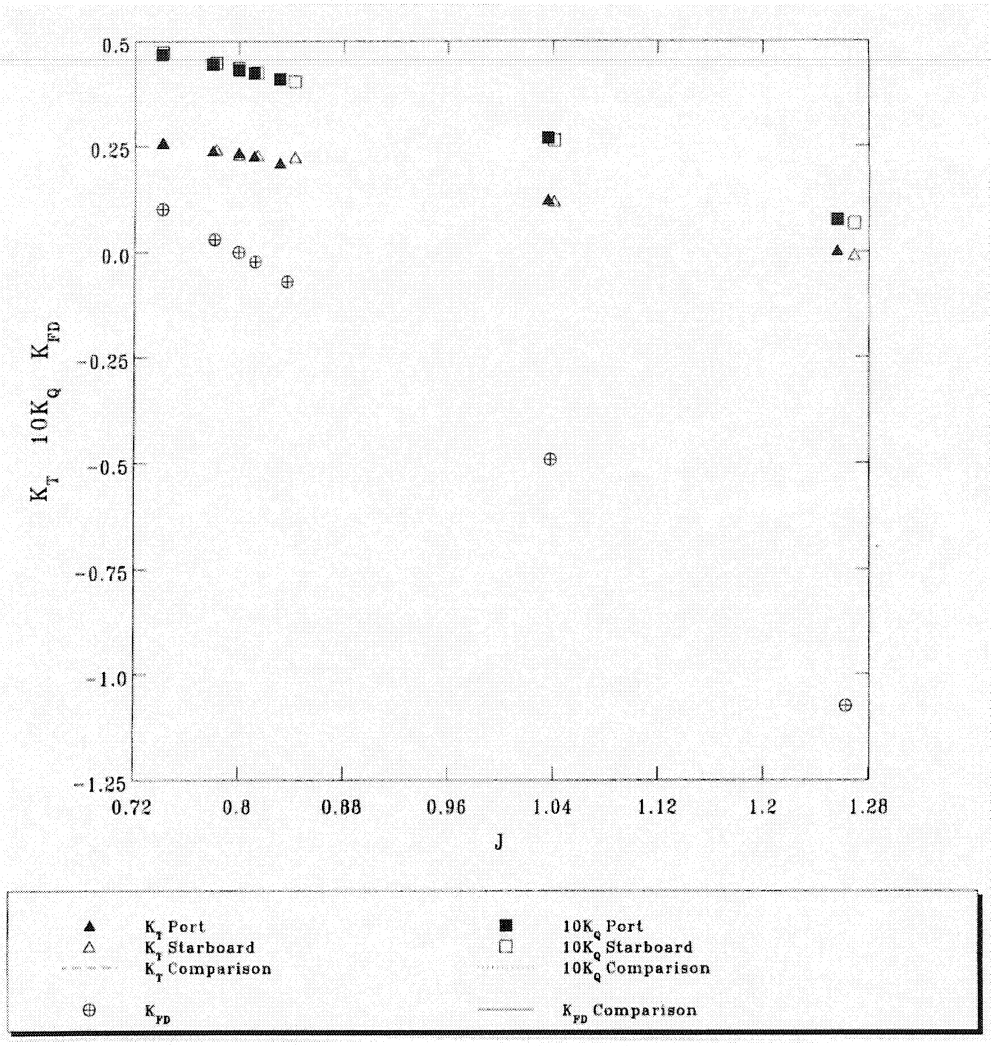

Figure 4-22: Online Analysis - Typical Self-Propulsion Plot

The complete online tables and graphs for the friction tests, bollard test and the self-propulsions experiments are provided the IMD technical report of the model resistance and propulsion experiments [16].

3.3.5 Self-Propulsion Offline Analysis

Before the offline propulsion data analysis was carried out, offline analysis was completed on the shaft frictions. The command procedure for the frictional analysis

calculated the average port and starboard friction from the two port friction curves and the two starboard friction curves. The inputted friction curves represented the friction lines calculated immediately before and after the propulsion experiments. Two plots were created, representing the port and starboard friction curves. Each plot contained the before and after friction curves as well as the average friction curve.

Since the online propulsion analysis created a separate point file for each model speed, the files were merged before the offline propulsion analysis was completed. During the merging process, all data obtained for the zero shaft thrust and Holtrop methodology experiments were excluded from the new file.

The offline analysis fitted polynomial curves to the propulsion curves at each speed and generated a table of their coefficients. When fitting the polynomial curves to the propulsion data, care was given to ensure that all the curves are gradually decreasing. If there was a slight increasing slope in the curve, the full scale powering prediction would be unreliable. A typical plot of the fitted polynomial curves (carriage speed 1.189 m/s) is shown in Figure 4-23. The complete set of polynomial curves along with the table of the polynomial coefficients can be seen the IMD technical report of the model resistance and propulsion experiments [16].

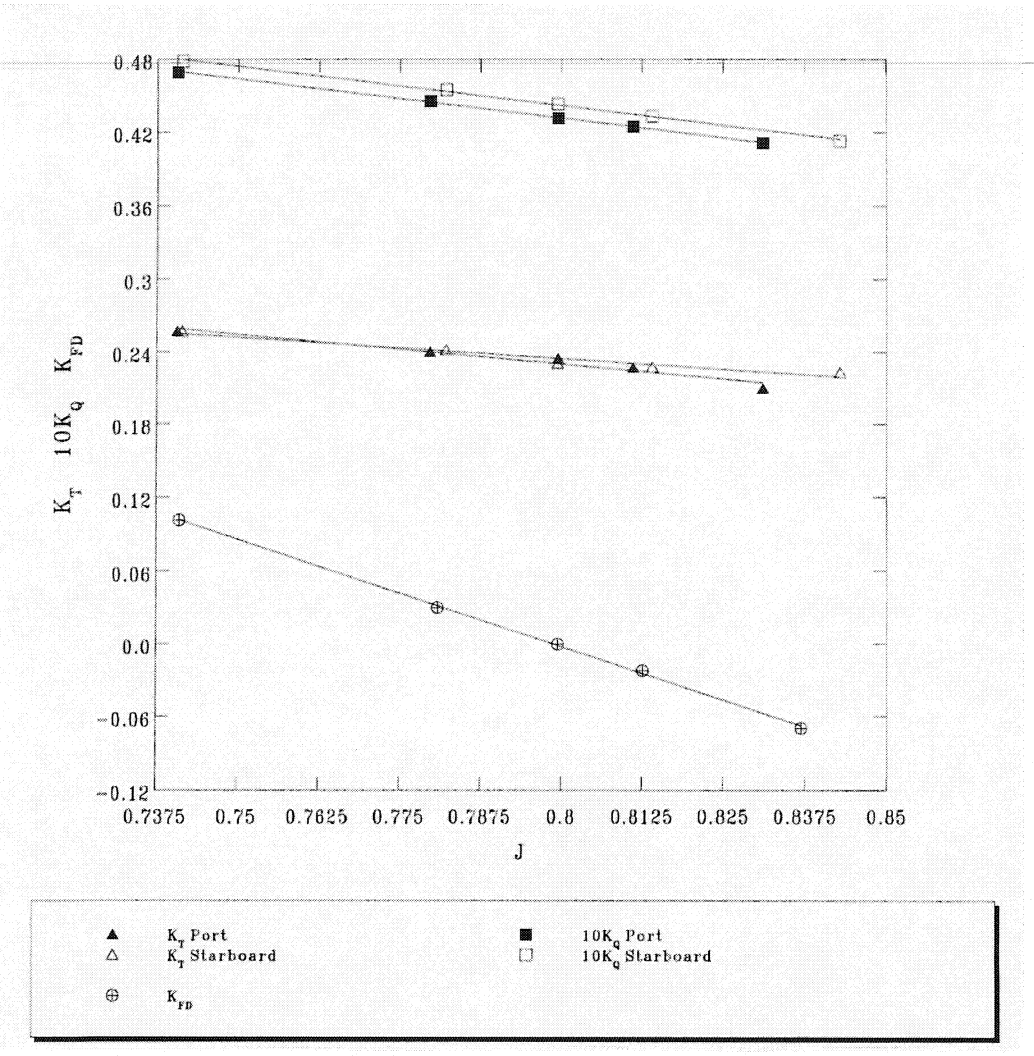

Figure 4-23: Offline Analysis - Typical Propulsion Curves

3.4 Full Scale Powering Prediction

Once the offline analysis for the resistance, propeller open water, and the propulsion experiments had been completed, preparation was carried out in order to predict the full-scale powering requirements for the 'Lauzier'. Following the IMD standard, I predicted the powering performance of the 'Lauzier' using ITTC '57 Ship Model Correlation Line with a correlation allowance [2]. Since resistance experiments

were carried out with both the naked and appended model, the increase in ship resistance coefficient due to appendages was predicted by multiplying the increase in model resistance by an appendage scale factor. The ship resistance coefficient is given by:

$$C_{TS}(app) = C_{TS}(naked) + \beta[C_{TM15}(app) - C_{TM15}(naked)] \quad (4\text{-}4)$$

The model resistance coefficients were corrected to the standard temperature of 15°C in the above equation to allow for any differences in water temperature between the two model tests. At IMD, standard predictions are made with the appendage scale factor $\beta = 0.5$.

I also performed a prediction using ITTC '78 Performance Prediction Method [3]. Since the resistance experiments were carried out with both the naked and appended model, a new form factor was calculated for the appended hull by adding the increase in form factor due to the appendages to the form factor obtained during the Prohaska method. This produced a form factor, k, of 0.36, an increase of 0.161 from the form factor obtained using the Prohaska method.

The powering prediction methodology for both the ITTC '57 and ITTC '78 method followed standard IMD guidelines [22] except for the additional calculations needed to account for fouling on the ship hull. As described by a Canadian Navy study [23], an increase of 0.125% in frictional resistance coefficient, C_F, per day the ship was out of dock shall be used to account for hull fouling. In the case of the 'Lauzier', the full-scale powering experiments were conducted approximately 390 days (13 months) since the last time the vessel was dry-docked. This meant the command procedures had to be altered so that there was an increase of 48.75% in C_F., which translated into an overall

increase of ~18% in delivered power for the ITTC '57 method and an increase of ~26% for the ITTC '78 method.

The full scale power prediction using the ITTC '57 method is presented in Table 4-10, while the ITTC '78 prediction is shown in Table 4-11. A comparison of the two methods is displayed in Figure 4-24.

Table 4-10: ITTC '57 Power Prediction

M/V Louis M. Lauzier
Ship Powering Prediction - ITTC 57

Correlation Allowance: 0.0004

Days Out Of Dock:		0		390	
Speed (knots)	Fn	Shaft (RPS)	P_D (kW)	Shaft (RPS)	P_D (kW)
4.39	0.124	2.15	16.04	2.23	18.96
4.99	0.141	2.45	25.16	2.56	30.28
5.99	0.169	2.96	43.78	3.07	51.91
6.99	0.197	3.43	69.80	3.59	85.35
7.97	0.224	3.92	106.91	4.07	126.79
8.97	0.252	4.43	158.77	4.63	190.63
9.96	0.281	5.11	254.23	5.28	292.26
10.36	0.292	5.37	300.44	5.58	350.59
10.96	0.309	5.84	395.45	6.07	459.52

Table 4-11: ITTC '78 Power Prediction

M/V Louis M. Lauzier
Ship Powering Prediction - ITTC 78

Form Factor (1+k): 1.36

Days Out Of Dock:		0		390	
Speed (knots)	Fn	Shaft (RPS)	P_D (kW)	Shaft (RPS)	P_D (kW)
4.39	0.124	2.16	16.72	2.28	21.19
4.99	0.141	2.48	26.68	2.64	34.56
5.99	0.169	2.99	46.79	3.16	59.24
6.99	0.197	3.47	75.19	3.71	98.84
7.97	0.224	3.97	114.36	4.20	144.42
8.97	0.252	4.51	171.97	4.79	220.04
9.96	0.281	5.16	268.16	5.41	325.18
10.36	0.292	5.44	317.76	5.74	393.02
10.96	0.309	5.90	415.58	6.23	511.66

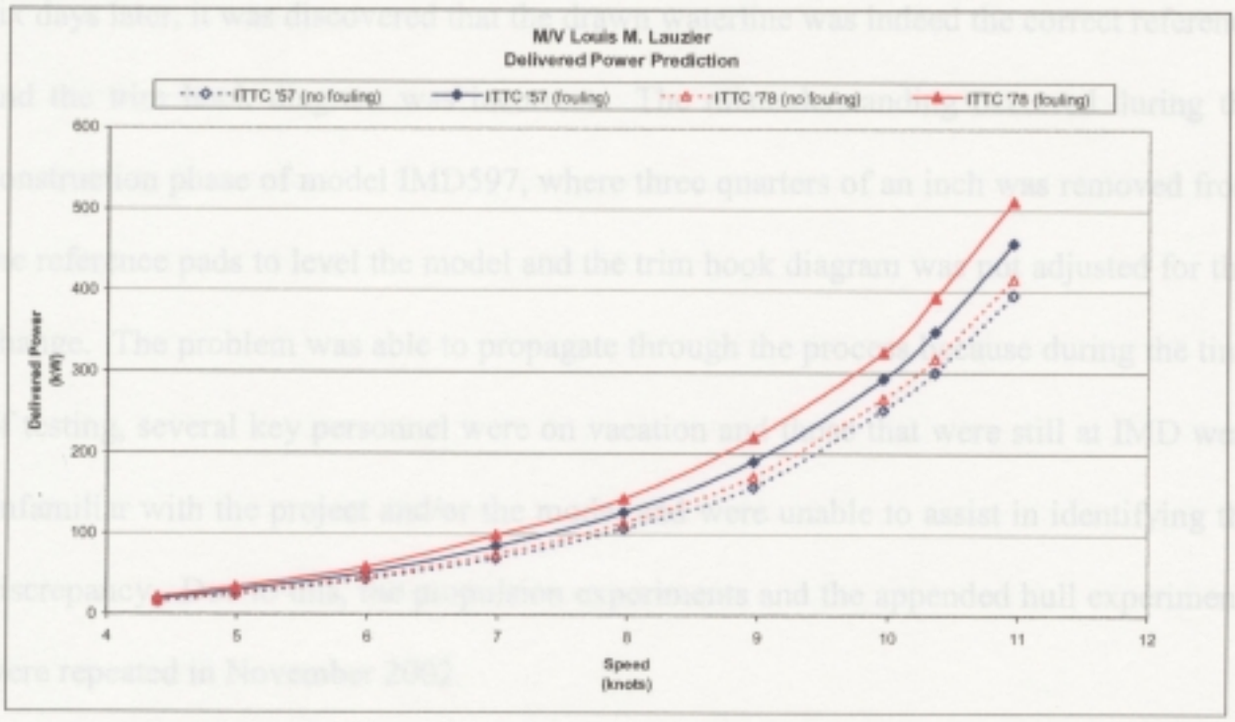

Figure 4-24: Power Prediction Comparison

3.5 Discussion

Although the resistance and propulsion test programs were well documented and easy to implement in the 'Lauzier' test program, the following section discusses some model issues with the test program as well as some observations and comments with respect to the analysis procedures.

Model Issues:

There were several model issues that prevented the test program from running smoothly. One such issue was due to the confusion that occurred when trying to ballast the model in August 2002. When ballasting the model, in accordance to the trim hook diagram supplied, the drawn waterline on the model was ¾ inch below the model waterline. Assuming the trim hook diagram was correct, testing began. Unfortunately,

six days later, it was discovered that the drawn waterline was indeed the correct reference and the trim hook diagram was incorrect. The misunderstanding occurred during the construction phase of model IMD597, where three quarters of an inch was removed from the reference pads to level the model and the trim hook diagram was not adjusted for this change. The problem was able to propagate through the process because during the time of testing, several key personnel were on vacation and those that were still at IMD were unfamiliar with the project and/or the model and were unable to assist in identifying the discrepancy. Due to this, the propulsion experiments and the appended hull experiments were repeated in November 2002.

Another model issue that delayed the model testing in August 2002 was a vibration in the port shafting. When the shafting calibration was being checked at the beginning of the propulsion test program, vibration was noticed at the higher shaft speeds. During the investigation on what particular speed produced the greatest vibration, the universal coupling disconnected between the shaft and the dynamometer. Due to a combination of the vibration and the shaft disconnection from the dynamometer, the internal spring of the dynamometer became twisted, rendering it useless, and had to be replaced. Post inspection of the shafting concluded that the initial cause of the vibration was a tight inboard bearing. However, the initial vibration wore down this bearing making the latter vibration caused by the bearing not as dramatic, enabling the test program to continue without issue.

Due to the worn inboard bearing, water was able to ingress through the stern tube into the port water well of the model. Under constant supervision, the water was

removed from the well after every other test run with an industrial vacuum. Also, at the end of a day of testing, the ballast was removed so that the stern could be raised out of the water. For that reason, at the beginning of the next testing day, the model had to be ballasted and trimmed again, reducing time for testing.

Another model issue arose during some of the propulsion experiments involving the motor control system. At high shaft speeds, the motors would draw too much current causing the breakers of the controller to trip. This was an issue during the testing of the model at the heavier displacement, but a non-issue during the testing performed in November 2002.

Another delay in the overall test program occurred during the propeller open water experiments. During initial set-up of the test program (October 2002), it was brought to the forefront that there is great uncertainty in the torque readings from the Opens Boat. Due to friction fluctuation, there is very low repeatability in these experiments. A slight misalignment in the propeller tube of the Opens Boat caused large frictions to occur and scouring could be seen on the propeller shaft caused by the inner bearing. A decision was made to remove the inboard coupling from the Opens Boat. A set of propeller open water experiments was carried out on a propeller with validated data to verify that the torque problem has been rectified. These experiments were carried out on a R-Class propeller [18]. From these experiments, the modified Opens Boat was deemed reliable and the test program for the 'Lauzier' propellers commenced in November 2002.

Observations:

During the testing of the model, there were interesting observations to note. As mentioned earlier, the NavCAD™ prediction under-predicted the resistance for the model. As noted, this under-prediction can be explained through the redesign of the hull and the propulsion system.

Another interesting observation occurred during the propeller open water experiments. When performing tests for the shaft frictions, the Opens Boat experienced a larger frictional torque when rotating clockwise for the starboard propeller, approximately 0.19 Nm compared to –0.07 Nm when the shaft is rotating counterclockwise for the port propeller. This partly explained why the port propeller experienced lower K_T and K_Q curves in comparison with the starboard propeller.

Also noted during the propulsion test program, the rps needed to reach the self-propulsion point at each model speed was lower than the estimated nominal rps by 7-10%. A possible reason to explain this discrepancy in the test results is the fact that the program used a very clean and smooth model whereas the full scale 'Lauzier' would experience larger frictional resistance due to the marine growth on the hull.

Analysis Comments:

Although it was stated in the IMD test standard for self-propulsion experiments [20] for the test program should be all carried out in one day of testing, the 'Lauzier' propulsion experiments actually spanned two days, with the second day of testing only consisting of two model speeds of the ten. Therefore, during the offline analysis of the propulsion experiments, the program used the average frictional torques from day one

and not the average from the entire test program. This was done because there were minimal differences in the frictions between day one and day two.

As noted in the powering prediction, the use of fouling effects was considered to better predict the required power performance of the 'Lauzier'. Although this is a commonly used practice, the percentage used to increase the frictional coefficient was calculated based on the Royal Navy practise. The actual percentage to use for the 'Lauzier' based on the ship being stationed in the St. John's harbour and the amount of travel that the ship experiences, needs to be further studied.

4.0 Model Manoeuvring Experiments

The following section describes the experimental setup and testing procedure as well as the data analysis for the set of manoeuvring tests completed in the OEB located at the Institute for Marine Dynamics in June 2003. Experiments were performed using the 1:12 scale Lauzier model (IMD605). The model was instrumented to measure the rudder angle and the shaft rotation as well as the ship's motion. The motions were measured using an onboard MotionPak™ and the OEB QUALISYS™ system. A bow accelerometer was added solely as verification for the MotionPak™ analysis algorithm. For details on the instrumentation and calibration methodology refer to the IMD technical report of the model seakeeping and manoeuvring experiments [24].

4.1 Offshore Engineering Basin Configuration

The OEB was configured as follows for these experiments:

Water Depth: The water depth was set at 2.0 m; thus the model was assumed to be operating in deep water.

Blanking Walls: Blanking walls used to cover the beaches on the north side were removed for all experiments.

Segmented Wave Board Configuration: The wavemakers were not used in this experiment.

4.2 Model Preparation

For the manoeuvring experiments, the 1:12 scale model was ballasted and trimmed to the displacement of 145 kg. The free running model was not tethered, allowing it to perform the many manoeuvring trials unimpeded. To operate the model, the shaft speed and rudder angle were controlled and manipulated by software installed on an on-shore computer that communicated with the model via a wireless modem. The computer operator controlled the model using either the levers on the software control panel or a commercial video game steering wheel and foot pedals set. The software used a feedback signal from QUALISYS^{TM} to display the heading of the model.

4.3 Manoeuvring Test Program

The manoeuvring test program consisted of three different test experiments: turning circles, pullouts, and zigzags manoeuvres.

The turning circle manoeuvre test program was carried out with speeds associated with the full-scale tests that were performed at low, medium, and maximum speed: 6, 8, and 11.5 knots, respectively. The manoeuvre was performed with a rudder deflection of 15°, 25°, and 32° to both port and starboard. The 32° rudder deflection represented the maximum rudder deflection experienced on the full-scale Lauzier. The experiment started once the model had achieved the steady state cruising speed. The turning circle was initiated by turning the rudder to the desired angle and allowing the model to rotate in a circle. All turning circles were terminated once the model completed a 720° change in heading, at which time, the pullout manoeuvre was started. This manoeuvre consisted of returning the rudder back to amidships and allowing the vessel to achieve a steady course. The full testing matrix for the required turning circles can be seen in the following table.

Table 4-12: Turning Circle Test Program

Fwd. Speed FS knots	Fwd. Speed MS m/s	Rudder Angle deg. P/S
6	0.891	15P
6	0.891	15S
6	0.891	25P
6	0.891	25S
6	0.891	32P
6	0.891	32S
8	1.188	15P
8	1.188	15S
8	1.188	25P
8	1.188	25S
8	1.188	32P
8	1.188	32S
11.5	1.708	15P
11.5	1.708	15S
11.5	1.708	25P
11.5	1.708	25S
11.5	1.708	32P
11.5	1.708	32S

The zigzag manoeuvre test program consisted of two forward speeds, each containing two zigzags with a change of heading of 10° and 20°. A zigzag manoeuvre started with a steady approach of the desired speed. The rudder was then put over to starboard (first execute) by 10°. Once the heading changed by 10° off its initial course to starboard, the rudder was reversed to port by 10° (second execute). Again, once the heading of the model changed to 10° off its initial course to port, the rudder was then reversed to starboard by 10° (third execute). The manoeuvre continued until at least five executes had been achieved. For the 20° zigzag, the rudder and heading angle changed by 20°. The zigzag test matrix is provided in the following table.

Table 4-13: Zigzag Test Program

Fwd. Speed FS knots	Fwd. Speed MS m/s	Rudder Angle deg. P/S
6	0.891	10S/10P
6	0.891	20S/20P
8	1.188	10S/10P
8	1.188	20S/20P

Due to tank time constraints, the entire manoeuvring test program could not be completed, only the manoeuvres with high importance were executed. For the turning circles, the runs that were carried out were at model speeds of 0.891 and 1.188 m/s with 15° and 32° rudder angle to both the port and starboard side. Only one zigzag was executed: model speed of 0.891 m/s with a 10° port and starboard rudder angle.

4.4 Manoeuvring Online Analysis

The online analysis was carried out on a workstation in the OEB Control Room immediately after each run to verify the integrity of the acquired data. The online command procedure followed that outlined in the IMD technical report of the model manoeuvring and seakeeping experiments [24]. As part of the online analysis, all data was converted to full scale values. The following checks were carried out manually by reviewing the statistical and time series data produced by the analysis procedure:

- Verified the correct shaft rps, model forward speed, and heading angle;
- Reviewed yaw rate to ensure that enough data was acquired to analyze the run. If not enough data was acquired, the run was repeated;
- Reviewed the QUALISYS^{TM} X / Y linear displacement for any anomalies that could affect the integrity of the results. If there were large defects, the run was repeated;
- Reviewed the rudder angle integrity during the run. The rudder was found to be inconsistent during the manoeuvre, then the run was repeated; and
- Reviewed the telemetry and QUALISYS^{TM} signal integrity channels for evidence of significant signal loss during critical segments of the run. If significant signal loss was detected, the run was normally repeated.

4.5 Manoeuvring Offline Analysis

Igor Pro™ was again utilized to analyze the manoeuvring data. The only modification to the procedure files to analysis model scale data was to convert the data to full scale values before being processed and the output tables included information on the particulars of the file. A typical turning circle graph (nominal forward speed 8 knots with 15° rudder angle to starboard) can be seen in Figure 4-25, while the zigzag graph is shown in Figure 4-26 and a typical pullout graph is displayed in Figure 4-27. The turning circle and zigzag results are summarized in Table 4-14 and Table 4-15, respectively. As with the full scale analysis, the pullout manoeuvres were only analyzed for the 15° rudder angle.

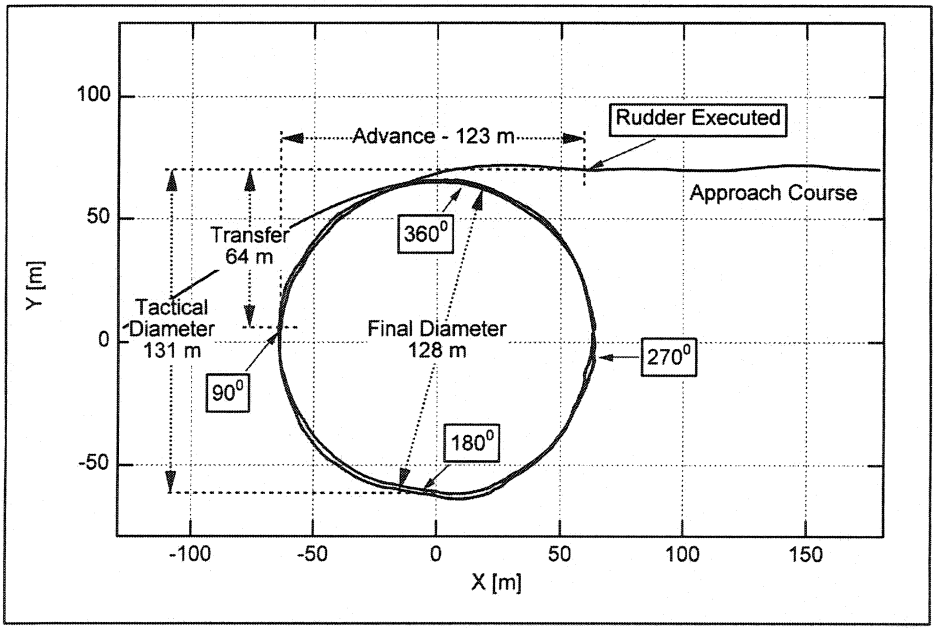

Figure 4-25: Offline Analysis – Typical Turning Circle Graph

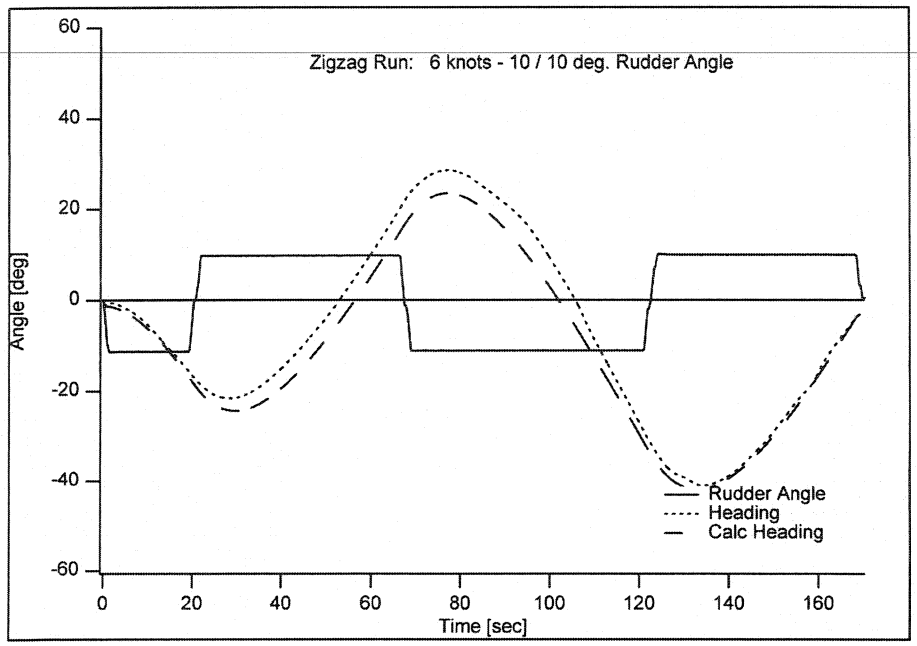

Figure 4-26: Offline Analysis – Zigzag Graph

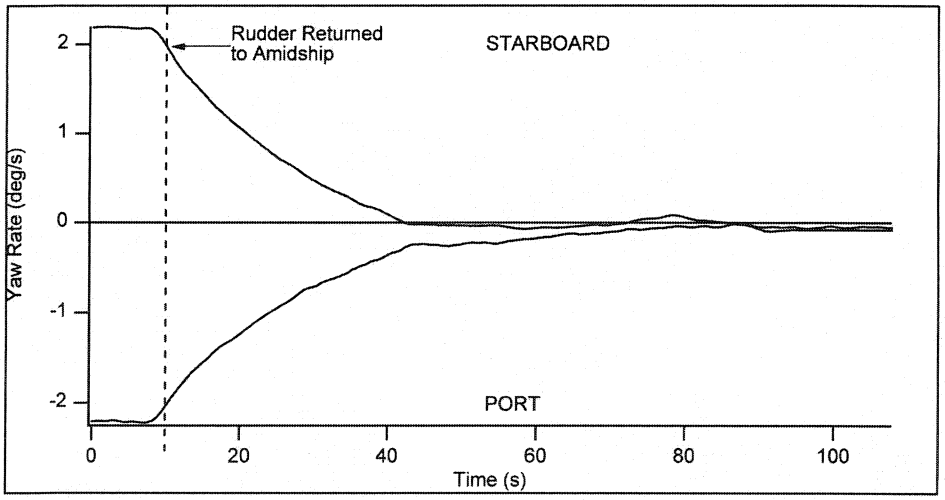

Figure 4-27: Offline Analysis – Typical Pullout Graph

Table 4-14: Offline Analysis – Summary of Turning Circle Data

'Lauzier' - Summary Table - Model Turning Circle Data

July 2003 — IMD Proj. # 01960

File Name	Time	Forward Speed (m/s)	Nominal Rudder Angle (deg. P/S)	Advance (m)	Transfer (m)	Tactical Diameter (m)	Final Diameter (m)	Yaw Rate in Turn (deg./s)	Rudder Angle in Turn (deg.)	Heel Angle in Turn (deg.)	Forward Speed in Turn (m/s)	Comments
MAN_002.DAC	10:23	0.891	15 P	116.60	57.90	129	123	-2.23	15.32	0.84	2.44	
MAN_004.DAC	10:45	0.891	15 S	120.09	58.55	133	128	2.20	-14.91	-0.59	2.49	
MAN_005.DAC	10:55	0.891	32 P	76.40	30.14	69	65	-2.95	32.58	0.58	1.68	
MAN_008.DAC	11:13	0.891	32 S	78.36	39.88	78	69	2.98	-34.72	-0.24	1.73	
MAN_011.DAC	11:44	1.188	15 P	114.60	66.60	133	123	-2.95	15.96	1.27	3.16	748 points removed from the start
MAN_013.DAC	15:36	1.188	15 S	123.08	64.11	131	128	2.86	-15.17	-1.02	3.20	1586 points removed from the start
MAN_014.DAC	15:44	1.188	32 P	78.41	29.34	68	63	-3.83	32.81	1.04	2.17	
MAN_015.DAC	15:48	1.188	32 S	83.13	31.39	73	68	3.74	-34.47	-0.71	2.27	

Table 4-15: Offline Analysis – Summary of Zigzag Data

M/V Louis M. Lauzier

Zigzag Manoeuvre Results

Model Summary Table

File Name		MAN_016
NF Time		15:58
Nominal		
Forward Speed	**MS (m/s)**	0.891
	FS (kts)	6
Zigzag		10 / 10
Run Heading		
Time to Reach Execute	**(s)**	15.38
Reach	**(s)**	52.86
Period	**(s)**	95.97
Nomoto Coefficients		
Delta R	**(deg)**	0.26
K(mean)	**(1/s)**	0.1701
T(mean)	**(s)**	15.071
Calculated Heading		
Time to Reach Execute	**(s)**	14.80
Reach	**(s)**	56.33
Period	**(s)**	94.25
Comments	Large Rudder lag.	

As seen in Figure 4-26, there was not a good Nomoto match between the heading and the calculated heading. The main reason for this mismatch was the large rudder lag at each rudder execute due to the display update time of the computer system controlling the model. The display would only update a change of heading every four or five degrees

resulting in a delay time for the operator to proceed to the next execute once the heading angle reaches or bypasses the rudder angle.

By viewing the pullout manoeuvre, it can be seen that the model was slightly unstable to the port side.

The Igor Pro™ generated table and graphs for the three manoeuvres can be seen in the IMD technical report of the model manoeuvring and seakeeping experiments [24].

4.6 Discussion

Since the seakeeping and manoeuvring tests were performed using the same model, all model issues will be discussed in the seakeeping section.

Observations:

As discussed in the above section, when operating the zigzag manoeuvre, the displayed heading angle had a small time lag compared to the real time value. This resulted in large rudder lag during the run sequence. There are a couple of possible solutions to this dilemma: have the update in real time or create an autopilot program that will alter the rudder angle. This would eliminate any errors due to human delay.

Because of tank time restraints, the full manoeuvring test program was not completed. In the future, enough tank time should be sought after to complete the entire program. Also, due to rps constraints on the motor, the 11.5 knot equivalent test speeds were not achievable. A slower design speed should be chosen instead. Furthermore, due to the small confines of the OEB and the necessity of having at least four executes to analyze to determine the Nomoto coefficients, the likelihood of completing the remaining

zigzags are unlikely. However, those runs should still be executed to obtain the normal zigzag parameters, such as TRE and Reach.

Analysis Comments:

Analyzing the manoeuvring data was, at times, a very tedious process. The manoeuvres were analyzed using the QUALISYS™ data, which in its current setup, produces dropouts or spikes in the data as the model changes orientation and distance from the infra-red cameras. Therefore, the data had to be smoothed and/or de-spiked before the Igor Pro™ could properly analyze the test runs. For the zigzag manoeuvre, the de-spiking process had to be carried out manually in order to maintain the integrity of the run.

In addition to the de-spiking process on the zigzag manoeuvre, the procedure file had to be modified to take the last heading point as the zero crossing point. This was required because the zigzag had the minimum of four executes required to analyze the run to obtain the Nomoto coefficients. Due to the model coming up close to the end of the OEB, the run was terminated prior to the heading angle reaching the original heading direction. The modification was made because the heading angle was only off by a couple of degrees from the original path.

5.0 Model Seakeeping Experiments

The following section describes the experimental setup and testing procedure as well as the data analysis for the set of seakeeping tests completed in the OEB located at the Institute for Marine Dynamics in April / May 2003. Experiments were performed

using the 1:12 scale 'Lauzier' model (IMD605). The model was instrumented to measure the rudder angle and the shaft rotation as well as the ship's motion. The motions were measured using an onboard MotionPak™ and the OEB QUALISYS™ system. A bow accelerometer was added solely as verification for the MotionPak™ analysis algorithm. In addition, four wave probes were placed in the OEB to measure the wave elevation to derive the model wave spectrum. For details on the instrumentation and calibration methodology refer to the IMD technical report of the model seakeeping and manoeuvring experiments [24].

5.1 Offshore Engineering Basin Configuration

The OEB was configured as follows for these experiments:

Water Depth: The water depth was set at 2.5 m; thus the model was assumed to be operating in deep water.

Blanking Walls: Blanking walls used to cover the beaches on the north side were removed for all experiments.

Segmented Wave Board Configuration: All boards were set in piston mode with the bottom of the wave makers adjusted to 1.3 m above the floor of the OEB.

Wave Generation: An irregular wave was generated at two different wave directions (25° and 65° relative to the west wall of the OEB), depending on the relative heading angle of the model. The irregular wave spectrum was a scaled match to the non-directional irregular wave spectrum experienced during the full-scale experiments. Although eleven spectra were measured on November 2001, the median spectrum for the day of testing was chosen as the target spectrum, see Table 3-9 for spectrum parameters

(time = 14:30). The matching process is done using wave probes following IMD standards [25]. The length of the irregular wave was 347 seconds (20 minutes full scale). Due to the length of the OEB, it was not possible for the model to experience the entire length of the irregular wave in one test run. To do so, the model was tested against segments of the wave history. After a run was completed, the time section of the wave that the model encountered was recorded. During the next run, the entire wave profile was run again, but the wavemakers in the OEB did not engage until the end of the time segment recorded in the previous run (minus a few seconds to account for the wave to reach the model).

Wave Probes: The four wave probes used to measure the wave elevation were placed in their allocated positions: three on the North side of the OEB and one on the South West corner.

Model Service Dock: A platform was set up adjacent to the north wall roughly 10 m west of test center so that the model could be launched/recovered using the overhead crane. This dock had to be moved to the South side of the tank for some of the wave heading angles to minimize interference with the QUALISYS^{TM} cameras mounted on the east end.

5.2 Model Preparation

For the seakeeping experiments, the 1:12 scale model was ballasted and trimmed to the displacement of 155 kg. The free running model was tethered to the shore as a part of the model acceleration system. To operate the model, the shaft speed and rudder angle were controlled and manipulated by software installed on an on-shore computer that

communicates with the model via a wireless modem. The computer operator controlled the model using either the levers on the software control panel or a commercial video game steering wheel and foot pedals set. During the seakeeping testing, the software was set to the autopilot mode. The autopilot was a prototype system designed and built by IMD. This autopilot kept the model on a set course during the test run by monitoring the heading angle supplied to the computer from the QUALISYS™ system and independently controlling the rudder angle. The autopilot gain coefficients for the shipboard autopilot were unknown so an assumption was required to select the model autopilot gain values. The following gain values were used:

Yaw angle gain coefficient = 1.0 Yaw rate gain coefficient = 0.0

Once the autopilot mode was set, the model operator set the shaft speed and required nominal direction before the run, and then takes manual control of model at the end of the run.

5.2.1 Autopilot Software

The prototype autopilot used to control model IMD605 in the IMD OEB in May 2003 was a software module that received model heading information from the QUALISYS™ optical tracking system and sent packetized commands over a spread spectrum radio link to control the rudder angle setting on the model. The autopilot had an option for course keeping. Course keeping was accomplished through a Kalman filter based Proportional-Integral-Differential (PID) algorithm to control the model rudder angle.

Data from the QUALISYS™ optical tracking system was transmitted to the autopilot via an RS422 communications link, in the form of ASCII sentences. The sentences were received at a rate of approximately 30 per second and contained the following data: x position, y position, z position, roll angle, pitch angle, yaw angle (heading in an OEB reference system), and RMS error. The autopilot software used the yaw angle and the RMS error.

The RMS error value indicated the integrity of the QUALISYS™ data. Since the autopilot required a good-quality yaw signal to operate properly, the RMS signal was used to 'filter' the information fed to the autopilot. When the RMS error value was negative, the QUALISYS™ system was not tracking the model. As well, when the RMS error value was too high (>10 in this instance), the QUALISYS™ data was considered unusable. When the RMS error value indicated good yaw data, the yaw was fed to the Kalman filter. When the RMS error indicated a bad yaw value, the predicted yaw from the previous iteration was fed back into the filter to effectively implement inertial navigation.

The Kalman filter incorporated a linear numerical steering model for the test vessel. The parameters for the model were determined through analysis of full scale 'Lauzier' zigzag manoeuvre test data prior to the test program. The Kalman filter predicted the model's yaw and the yaw rate in real time by minimizing the mean square error between the state of the numerical model and the observed (measured) yaw signal. The output can be thought of as an 'optimal' blend of the measured yaw and the ideal (numerically determined) yaw, while the yaw rate was numerically determined. Since the

filter continuously produced a prediction of the vessel's state, there was no phase lag in the resulting signal as there would be if a normal digital filter were applied. Using the Kalman filter computed yaw and yaw rate, the autopilot PID module computed error as the predicted yaw minus the actual yaw and then computed a rudder angle by proportional gain times error minus differential gain times predicted yaw rate. (The "Integral" component of PID control was not implemented.) The PID module also had a dead band setting to prevent the rudder from being over-commanded; the rudder is commanded to move when the resulting change in angle is greater than the dead band threshold.

When the operator engaged autopilot, the rudder angle computed by the PID module was used to command the rudder on the model. Otherwise, the rudder commands were determined through the operator interface, from the joystick or the rudder slider control on the screen. If the RMS error indicated that the QUALISYS™ system was not tracking the model, then the operator "armed" the autopilot so that it will automatically engaged when the model's attitude became known. In this instance, the rudder angle was held at zero degrees until the Kalman filter received a pre-determined number of good QUALISYS™ fixes (default = 5 samples). This usually occurred at the start of any given run as the model started from a QUALISYS™ dead zone where QUALISYS™ information was unavailable.

Once the autopilot became engaged, it remained engaged until the operator turned it off. The autopilot was tolerant of QUALISYS™ dropouts since the Kalman filter was able to "fill in" missing data for short dropouts. However, if the QUALISYS™ data

remained dropped for 100 consecutive samples, the autopilot automatically shut itself down and reverted the model to manual steering control.

5.3 Model Acceleration System

To obtain maximum test run length in nominally head and bow seas, a moveable static weight based model acceleration system was employed at the beginning run to propel the model forward from a stationary position. The acceleration system consisted of a 'U' shape aluminium frame containing a foam insert designed to conform to the test waterline of the model and 2 – 20 kg weights. The weights, which were suspended just underneath the surface of the water, were connected to the vertical post at the end of the launch system. A series of ropes and pulleys translate the dropping of the weights to a horizontal thrust of the system that acted on two pins bolted to the port and starboard of the model at its LCG. In the other heading angles, the launch system was used to stabilize the model. In these cases, the model was accelerated using its own onboard power and exploiting the wave force acting on the stern. The shore side equipment included a manually operated winch used to raise the weights into position.

As a safety feature, a lightweight safety line anchored onshore was attached to an eyebolt on the stern of the model. The line impeded the model at the end of a run to prevent it from accidentally ramming the sides of the OEB.

5.4 Seakeeping Test Program

The test program consisted of two forward speeds, each with five headings with respect to the dominant incident wave direction. In addition, the forward speed runs, a zero forward speed drift run was carried out in nominally beam seas. A head seas is defined as 180°. The seakeeping test matrix is provided in Table 4-16.

Table 4-16: Seakeeping Test Program

Forward Speed (m/s)	Heading Angle (deg)
0.965	165 / 125 / 80 / 35 / 15
1.560	155 / 115 / 75 / 35 / 15

The heading angle was based on the heading experienced by the full-scale 'Lauzier' during its seakeeping sea trials. Although the heading angles are supposed to represent the change of heading from head seas to following seas in 45° intervals, that was not what was experienced by the 'Lauzier' during the sea trials. Due to the multi-directional behaviour of the waves encountered, at times, the sea direction did not appear to conform to the expected direction either because the sea direction was changing or the original direction determined was incorrect. From analyzing the wave probe data, the headings displayed in Table 4-16 were deemed the most likely heading angles encountered by the 'Lauzier'.

To achieve the longest testable distance, the model acceleration system was moved to various locations around the tank. Also, the two dominant wave directions for the irregular wave added more flexibility in positioning the acceleration system. This can be seen in the table below.

Table 4-17: Position of the Model Acceleration System

Heading	Launch Position	Wave Direction
165°	NE corner	25°
125°	NE corner	65°
80°	SE corner	65°
35°	SW corner	65°
15°	SW corner	25°
155°	East side	25°
115°	East side	65°
75°	SE corner	65°

Whenever the launch system was moved, the model control center was also moved. The ideal position for the control center was behind the launching system so that the model controller had a view of the entire run, looking at the model from astern.

While working through the test program, it was noted that the launching system was in the wrong position during the heading angles of 75° and 80° seakeeping experiments. The actual heading angles were 105° and 100°. The error occurred when interpreting the sketches that illustrated the launching position with respect to the wave heading.

5.5 Seakeeping Online Analysis

The online analysis was carried out on a workstation in the OEB Control Room immediately after each run to verify the integrity of the acquired data. The online command procedure followed that outlined in the IMD technical report of the model manoeuvring and seakeeping experiments [24]. As part of the online analysis, all data was converted to full scale values. The following checks were carried out manually by reviewing the statistical and time series data produced by the analysis procedure:

- Verified the correct shaft rps, model forward speed, and heading angle;

- Compared the standard deviation of motion channels measured by QUALISYS™ and MotionPak™;
- Reviewed the telemetry and QUALISYS™ signal integrity channels for evidence of significant signal loss during critical segments of the run. If significant signal loss was detected, the run was normally repeated; and
- Plotted and compared the pitch and roll angle data from QUALISYS™ and MotionPak™ on the same time base.

5.6 Seakeeping Offline Analysis

To analyze the seakeeping data, each individual run was de-spiked to remove any QUALISYS™ signal dropouts. The MotionPak™ analysis software was run to compute the motions for the nominal CG of the model. Review was completed on the QUALISYS™ heading angle and forward speed channels in the time domain to identify an appropriate steady state time segment for further analysis. Since a long calm water delay interval was acquired on some runs, care was exercised to ensure no data was lost when the MotionPak™ analysis routine was used (roughly 5% of data was lost of the beginning and end of analyzed MotionPak™ data due to the nature of the Fast Fourier Transformation based analysis routine).

All the data was trimmed to the appropriate steady state time segments and merged together to obtain a final file/channel that spanned the entire twenty minute full scale wave spectrum. A fixed three second offset was used for each segment to provide overlap ensuring a relatively smooth transition in the time domain between segments. As many as 29 segments were required to cover the entire representative wave time history.

Each of the merged channels was reviewed in the time domain and edited manually to remove any remaining spikes through selecting the beginning and end of the glitch, then using linear interpolation to fill the gap. Any major motion anomalies, such as large transient motions at the beginning of a run, were identified and avoided during further analysis.

Once all the spikes and anomalies were removed, the basic statistics (minimum, maximum, mean, standard deviation) for all channels were calculated. The number of wave encounters was also determined by carrying out a zero crossing analysis on the heave acceleration channel and determining the significant wave height/spectral period of the north center wave probe data through execution of a variance spectral density analysis on this channel. This information was output in a tabular form.

Tables of basic statistics for each merged run are provided in the IMD technical report of the model manoeuvring and seakeeping experiments [24], while a summary of the seakeeping results is provided in Table 4-18. The relationship between the roll angle, pitch angle, and the accelerations versus the heading angle are provided in Figure 4-28 (6.5 knots) and Figure 4-29 (9.5 knots).

Table 4-18: Offline Analysis - Model Seakeeping Statistics

Summary of Model Seakeeping Statistics

M/V LOUIS M. LAUZIER — IMD Proj.# 01960

File Name	Roll Angle (deg.)	Pitch Angle (deg.)	Yaw Angle (deg.)	Sway Displ. (m)	Heave Displ. (m)	Surge Accel. (m/s^2)	Sway Accel. (m/s^2)	Heave Accel. (m/s^2)
Zero Speed Drift Runs in Beam Seas:								
SPD0_HDG90_R2	5.001	1.745	5.189	1.476	0.791	0.472	1.500	0.378
Speed = 6.5 knots:								
SPD6_HDG15	2.899	1.860	2.288	1.359	0.751	0.343	0.826	0.228
SPD6_HDG35	3.277	1.452	2.978	1.380	0.688	0.261	0.948	0.249
SPD6_HDG100	4.490	1.370	1.513	1.534	0.789	0.314	1.344	0.458
SPD6_HDG125	5.010	1.590	2.162	1.506	0.800	0.376	1.555	0.544
SPD6_HDG165	3.441	2.083	2.309	1.042	0.784	0.484	1.059	0.544
Speed = 9.5 knots:								
SPD10_HDG15	2.029	1.697	1.445	1.516	0.660	0.288	0.563	0.161
SPD10_HDG35	2.873	1.302	2.031	1.666	0.639	0.229	0.830	0.227
SPD10_HDG105	4.465	1.612	1.887	1.668	0.772	0.335	1.350	0.588
SPD10_HDG115	4.639	1.626	1.467	1.478	0.758	0.355	1.427	0.604
SPD10_HDG155	3.457	2.152	1.445	1.045	0.762	0.525	1.079	0.728

NOTE: 180 deg. is defined as a head sea.
The above values are Standard Deviation values of the particular motion.
The accelerations are measured the centre of gravity of the model.

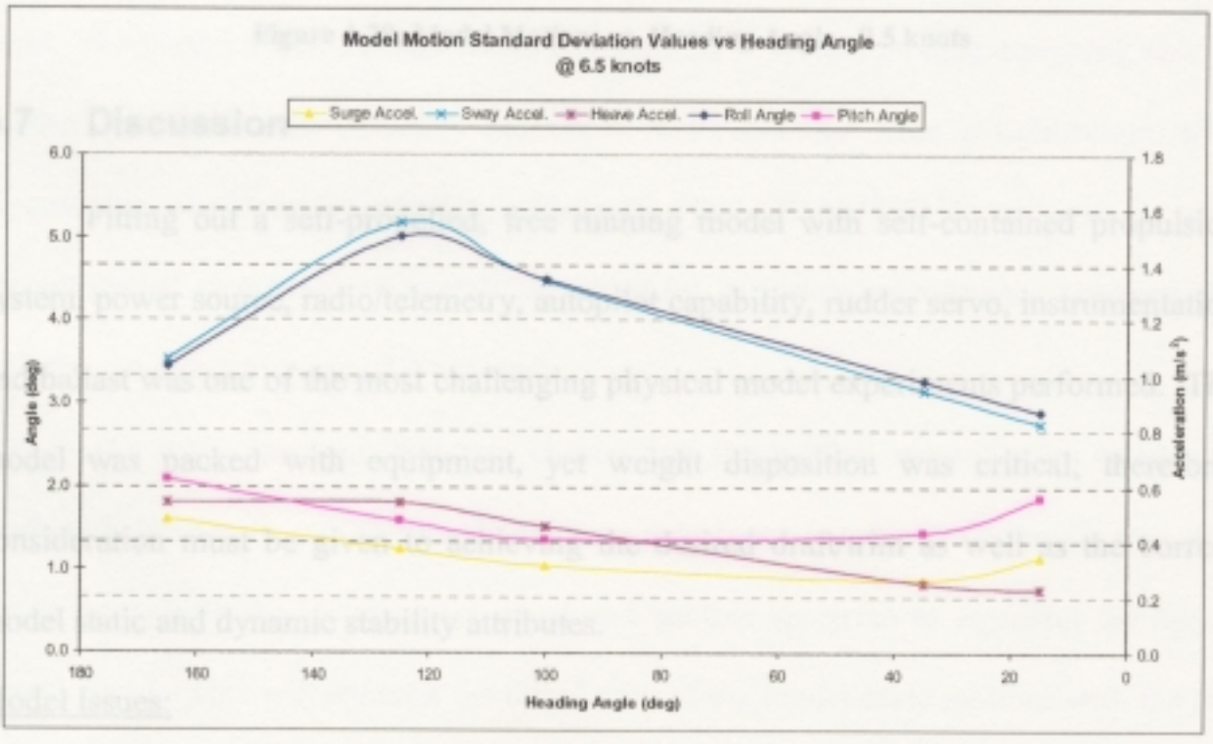

Figure 4-28: Model Motions vs. Heading Angle - 6.5 knots

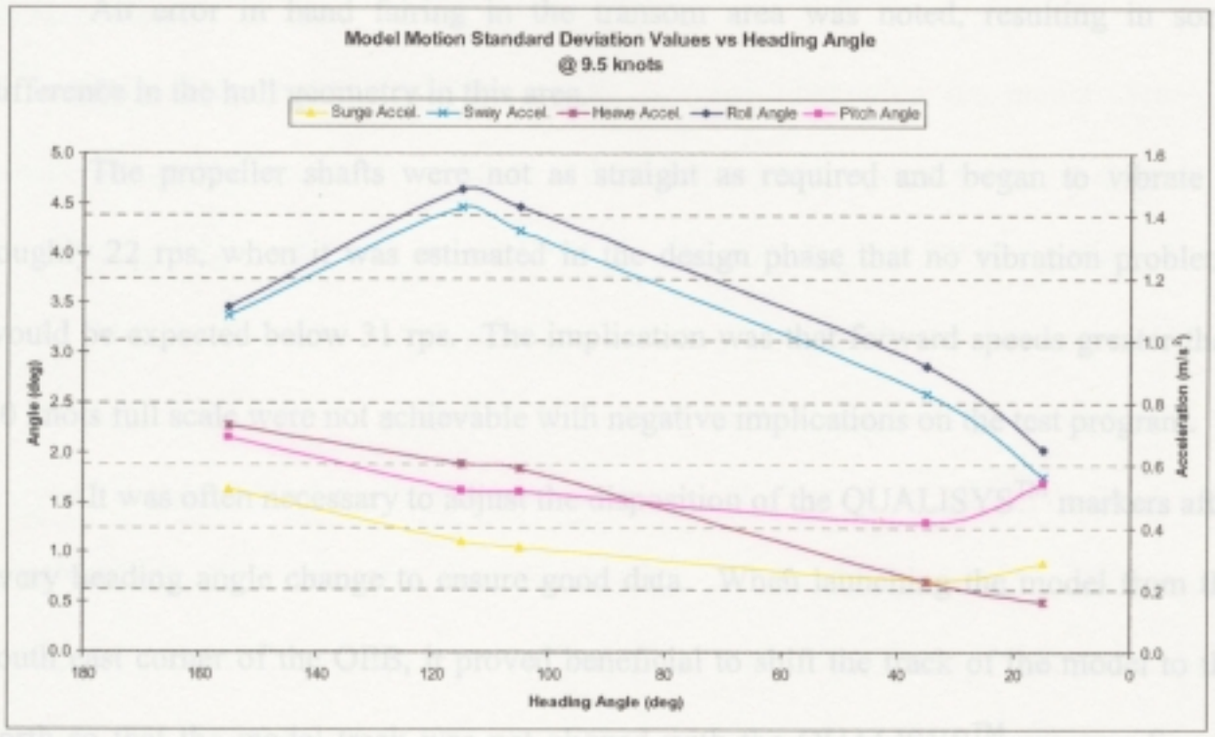

Figure 4-29: Model Motions vs. Heading Angle - 9.5 knots

5.7 Discussion

Fitting out a self-propelled, free running model with self-contained propulsion system, power source, radio/telemetry, autopilot capability, rudder servo, instrumentation and ballast was one of the most challenging physical model experiments performed. The model was packed with equipment, yet weight disposition was critical; therefore, consideration must be given to achieving the desired draft/trim as well as the correct model static and dynamic stability attributes.

Model Issues:

The required radius of gyration in roll target was a significant obstacle to overcome. Even with the large 24 V batteries extended outboard as far as feasible, an error between desirable and achievable radius of gyration in roll was in the order of 10%.

An error in hand fairing in the transom area was noted, resulting in some difference in the hull geometry in this area.

The propeller shafts were not as straight as required and began to vibrate at roughly 22 rps, when it was estimated in the design phase that no vibration problems would be expected below 31 rps. The implication was that forward speeds greater than 10 knots full scale were not achievable with negative implications on the test program.

It was often necessary to adjust the disposition of the QUALISYS™ markers after every heading angle change to ensure good data. When launching the model from the south east corner of the OEB, it proved beneficial to shift the track of the model to the north so that the model track was not aligned with the QUALISYS™ cameras line of sight. Suggested improvements in the QUALISYS™ system include designing new IR marker masts that are vertically adjustable and fabricated from a lightweight, non-electrically conductive material. Elevating the QUALISYS™ cameras is also recommended to provide an overall improvement in system performance although this will require a re-surveying of the system.

The wave spectrum that was chosen was the median spectrum for the day of testing. In the future, two spectra should be matched: one spectrum to represent the set of experiments with the lower vessel speed and another spectrum to represent the higher vessel speed. This will enhance the correlation of the model scale motions with the full scale motions by reducing the time differences between the wave spectrum experienced by the ship and the matched wave spectrum. Therefore, reducing the chances that the sea state changed by any significant amount in that time span.

Observations:

Due to an error in interpreting the sketches illustrating the model launching positions, experiments were carried out at the following two incorrect heading angles:

Heading Angle = 80° was actually 100° Heading Angle = 75° was actually 105°

Moving the model launch apparatus to a new location often required several hours as the launch mechanism as well as the model control computer etc. also had to be moved. Considerable progress has been made over the last six months in devising ways to reduce the time to move the launch mechanism. A future change could include using a laptop computer with wireless EtherNet card rather than a cumbersome desktop computer to control the model.

During the test program, a large amount of time was lost due to moving the model launch system, various QUALISYS™ problems, investigation of the shaft vibration issue, and other miscellaneous delays. This caused over half the test time to be unproductive. Some delays are unavoidable; however, techniques need to be developed to mitigate these overall problems encountered. In the future, it is recommended that all test programs include an increase of 25% in the tank time required due to unforeseen problems.

Analysis Comments:

As mentioned in the manoeuvring section, in its current setup, QUALISYS™ produces dropouts or spikes in the data when the model changes orientation and distance from the camera setup. This in turn created a large problem in de-spiking the data before the proper analysis of the results could take place.

6.0 Future Experiments

From December 2002 to January 2003, wake survey experiments were unsuccessfully attempted on the starboard propeller blade area. The purpose of these experiments was to provide proof that the sonar caisson disrupts the fluid flow entering the starboard propeller. This test is to back up the hypothesis that disturbed fluid flow is the reason for the difference in propeller torque between the port and starboard propeller seen in both the model and full scale experiments. To carry out this experiment, a wake survey needed to be performed with and without the caisson attached to the hull. For a wake survey, the propeller was removed and replaced with a group of five pressure probes with the centre of the propeller acting as the origin of the analysis. The middle wave probe was primarily used for depth measurements, while the differences in pressure between the top and bottom probes and the left and right probes was used to determine the fluid flow at a particular point. To carry out the wake survey, the model was towed down the tank while the wave probes measured the fluid flow at specific points around the propeller blade area. The number of points in the wake survey was sufficient enough to define four separate circles around the propeller blade area. The circles were defined by four radii: 22.2 mm, 58.3 mm, 84.8 mm, and 111.3 mm. Another method utilized during the experimentation was a sweep survey. A sweep survey is when the probes perform a continuous measurement around the specified circle.

During testing however, the analysis program produced large jumps in pressure between consecutive runs. For this reason, the pressure distribution for the propeller blade area was inconsistent and unreliable. Although the sweep method produced more

consistent results, it is a new method; therefore, unproven. Attempts to determine the pressure problem were unsuccessful during the allotted tank time; therefore, future experiments are required to correct this issue and to carry out the wake survey on the 'Lauzier'.

To complete the ship / model correlation study, a second set of powering experiments are scheduled to be carried out on the 1:12 scale model in the MUN Tow Tank. These results will further validate the powering prediction methodology as well as address any scaling issues when it comes to modeling vessels. Also, another set of manoeuvring experiments will be performed on the 1:6 scale model using the Planar Motions Mechanism (PMM) in the IMD Ice Tank.

Chapter 5 Ship / Model Correlations

1.0 Introduction

In this chapter, comparisons are analyzed between the model scale and full scale data obtained as a part of the ship / model correlation study performed on the M/V Louis M. Lauzier. The comparisons will include predictions based on numerical models of the 'Lauzier' carried out by Dr. D. Bass.

2.0 Powering Comparison

For the powering component of the correlation study, the calculated delivered power from the 'Lauzier' was compared against numerical and model scale predictions. The numerical prediction was based on the NavCAD^{TM} model as discussed in Chapter 4. It had a reliable prediction of power, within 10%, between the speeds of 6 and 8 knots. At higher speeds, the difference steadily increased to 35% at 11 knots.

The model scale predictions were based on both the ITTC '57 and ITTC '78 power prediction methods with modifications for added full scale fouling effects. Each method produced results with large differences when compared to the full scale results at slow speeds and increasing reliability at higher speeds. The ITTC '57 method decreased from a difference of 29% at 6 knots to 13% at 11 knots. The ITTC '78 method was more reliable with a difference of 19% at 6 knots to within a 10% between 8 and 11 knots, highlighted with only a 3% difference at 11 knots. It is believed that these methods under-predict the power at lower speeds due to the increase in wake resistance at these

speeds. Due to modifications to the stern, at lower speeds the propeller wake has a greater interaction with the hull; therefore, increasing the wake resistance. However, in model scaling, it is difficult to model this added wake resistance, consequently, under-predicting the resistance.

The powering comparison table and graph can be seen in Table 5-1 and Figure 5-1. Also included are comparison graphs using FLOW-3D®[4] and an extrapolation method, E2001 [26] based on results solely from loading varying self-propulsion tests. In Figure 5-2, the model scale resistance (appended and bare hull) is compared to resistance calculated from FLOW-3D®. From this figure, it showed that FLOW-3D® predicted hull resistance in between the measured appended and bare hull resistance curves. Figure 5-3 compares the E2001 method, which was developed by Sue Molloy, with the ITTC '78 power prediction.

Table 5-1: Powering Comparison Table

M/V Louis M. Lauzier
Ship Powering Comparison

Speed	(knots)	5.0	6.0	7.0	8.0	9.0	10.0	10.4	11.0
Full Scale	(kW)	30.5	73.4	111.2	158.8	233.8	351.8	414.5	528.5
NavCAD	(kW)	41.9	67.4	101.5	144.4	198.6	264.9	294.9	344.1
Diff.	%	*37.3%*	*8.2%*	*8.7%*	*9.1%*	*15.1%*	*24.7%*	*28.9%*	*34.9%*
ITTC '57	(kW)	30.3	51.9	85.3	126.8	190.6	292.3	350.6	459.5
Diff.	%	*0.8%*	*29.3%*	*23.2%*	*20.2%*	*18.5%*	*16.9%*	*15.4%*	*13.1%*
ITTC '78	(kW)	34.6	59.2	98.8	144.4	220.0	325.2	393.0	511.7
Diff.	%	*13.2%*	*19.3%*	*11.1%*	*9.1%*	*5.9%*	*7.6%*	*5.2%*	*3.2%*

[4] FLOW-3D is a registered trademark of Flow Science, Inc. of Santa Fe, NM, USA.

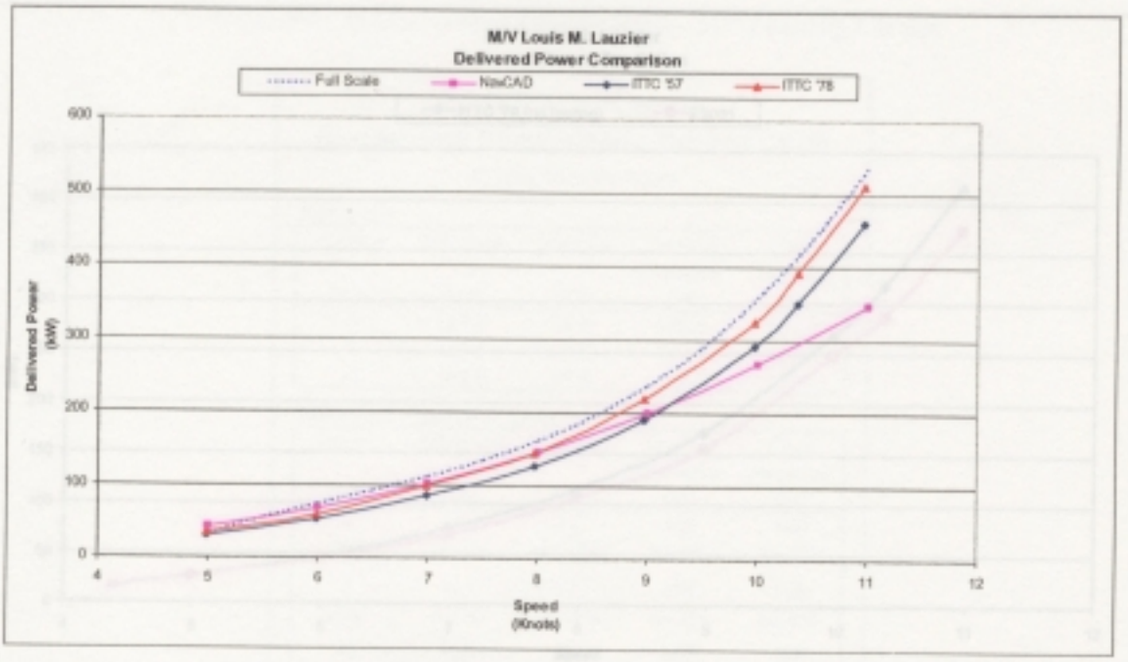

Figure 5-1: Power Comparison

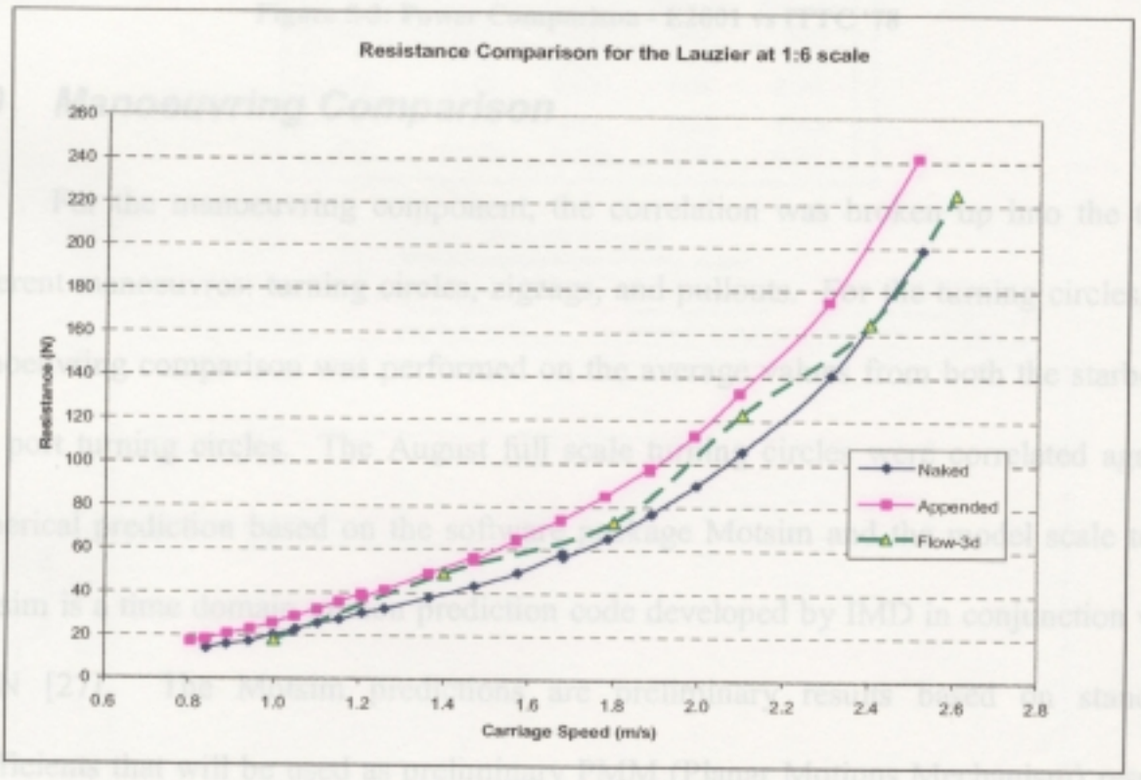

Figure 5-2: Resistance Comparison - Flow3D

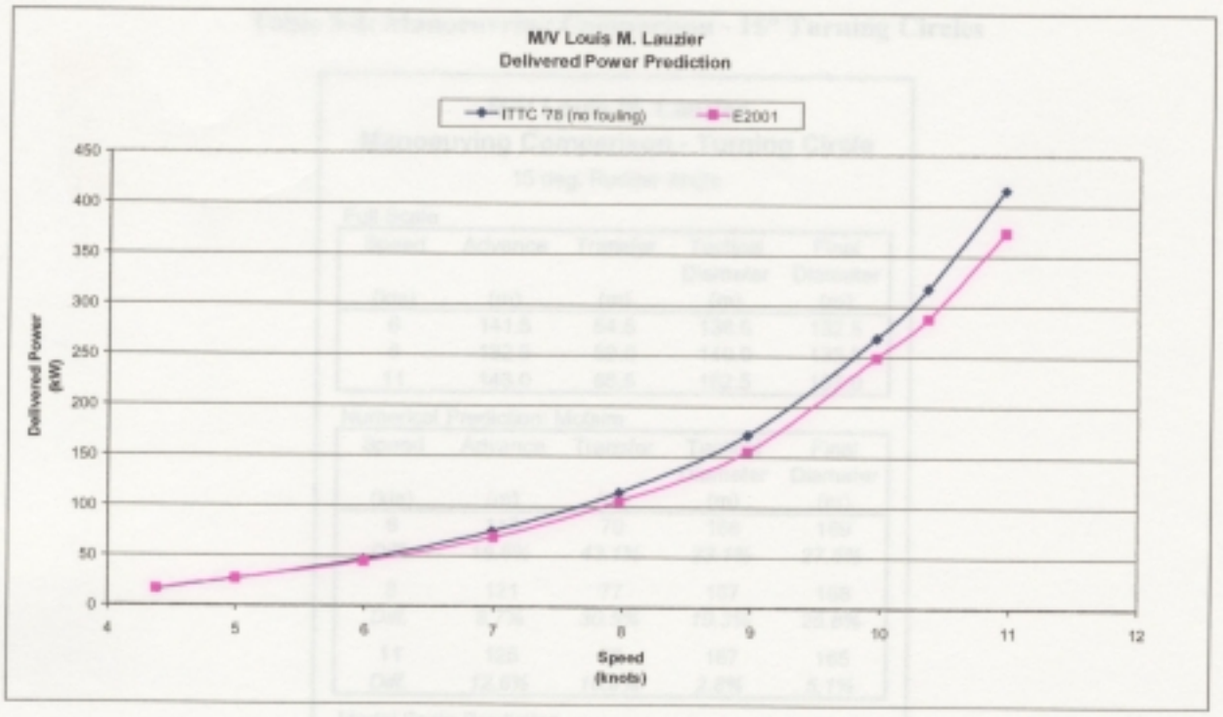

Figure 5-3: Power Comparison - E2001 vs ITTC '78

3.0 Manoeuvring Comparison

For the manoeuvring component, the correlation was broken up into the three different manoeuvres: turning circles, zigzags, and pullouts. For the turning circles, the manoeuvring comparison was performed on the average values from both the starboard and port turning circles. The August full scale turning circles were correlated against numerical prediction based on the software package Motsim and the model scale tests. Motsim is a time domain motion prediction code developed by IMD in conjunction with MUN [27]. The Motsim predictions are preliminary results based on standard coefficients that will be used as preliminary PMM (Planar Motions Mechanism) results. Manoeuvring comparison tables and graphs can be seen in Table 5-2 and Figure 5-4 for 15° rudder angle and Table 5-3 and Figure 5-5 for full rudder angle turning circles.

Table 5-2: Manoeuvring Comparison - 15° Turning Circles

M/V Louis M. Lauzier
Manoeuving Comparison - Turning Circle
15 deg. Rudder Angle

Full Scale

Speed (kts)	Advance (m)	Transfer (m)	Tactical Diameter (m)	Final Diameter (m)
6	141.5	54.5	136.5	132.5
8	132.5	59.0	140.0	133.5
11	143.0	68.5	162.5	157.0

Numerical Prediction: Motsim

Speed (kts)	Advance (m)	Transfer (m)	Tactical Diameter (m)	Final Diameter (m)
6	118	78	168	169
Diff.	*16.6%*	*43.1%*	*23.1%*	*27.5%*
8	121	77	167	168
Diff.	*8.7%*	*30.5%*	*19.3%*	*25.8%*
11	125	76	167	165
Diff.	*12.6%*	*10.9%*	*2.8%*	*5.1%*

Model Scale Prediction

Speed (kts)	Advance (m)	Transfer (m)	Tactical Diameter (m)	Final Diameter (m)
6	118.3	58.2	131.0	125.5
Diff.	*16.4%*	*6.8%*	*4.0%*	*5.3%*
8	118.8	65.4	132.0	125.5
Diff.	*10.3%*	*10.8%*	*5.7%*	*6.0%*

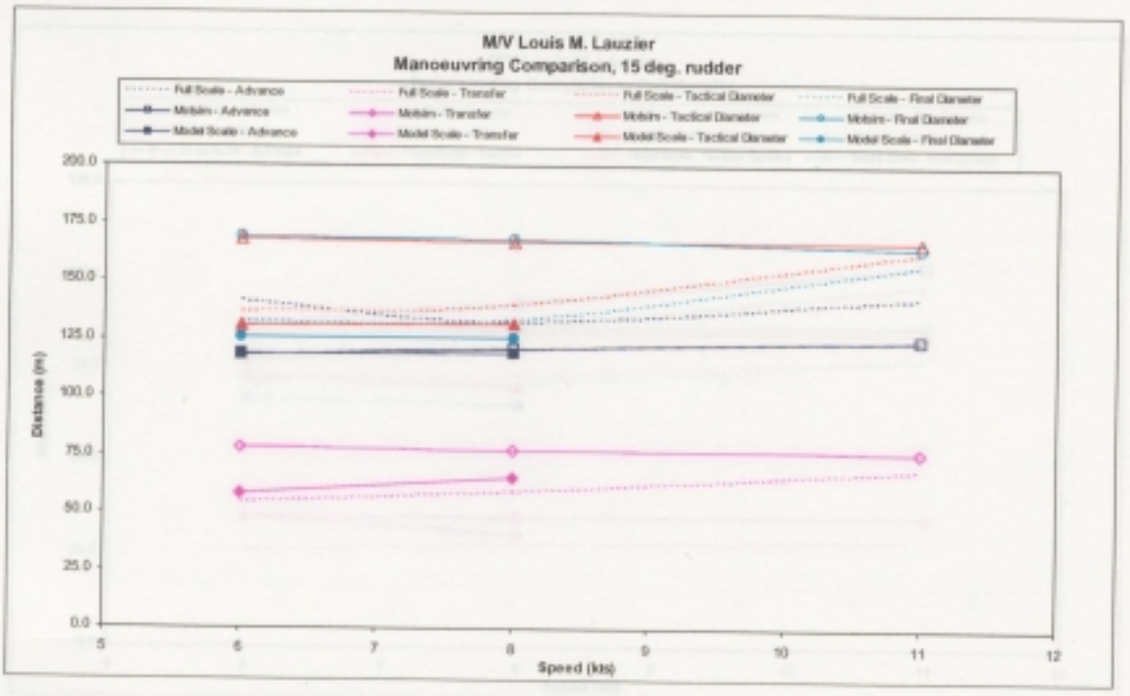

Figure 5-4: Manoeuvring Comparison - 15° Turning Circles

Table 5-3: Manoeuvring Comparison - Full Rudder Angle

M/V Louis M. Lauzier
Manoeuving Comparison - Turning Circle
Full Rudder Angle

Full Scale

Speed (kts)	Advance (m)	Transfer (m)	Tactical Diameter (m)	Final Diameter (m)
6	83.0	26.0	72.0	71.5
8	86.5	27.5	73.5	71.0
11	98.0	29.0	78.0	78.0

Numerical Prediction: Motsim

Speed (kts)	Advance (m)	Transfer (m)	Tactical Diameter (m)	Final Diameter (m)
6	87	35	85	86.7
Diff.	*4.8%*	*34.6%*	*18.1%*	*21.3%*
8	93	35.2	85	86.6
Diff.	*7.5%*	*28.0%*	*15.6%*	*22.0%*
11	103	35	85	87
Diff.	*5.1%*	*20.7%*	*9.0%*	*11.5%*

Model Scale Prediction

Speed (kts)	Advance (m)	Transfer (m)	Tactical Diameter (m)	Final Diameter (m)
6	77.4	35.0	73.5	67.0
Diff.	*6.8%*	*34.7%*	*2.1%*	*6.3%*
8	80.8	30.4	70.5	65.5
Diff.	*6.6%*	*10.4%*	*4.1%*	*7.7%*

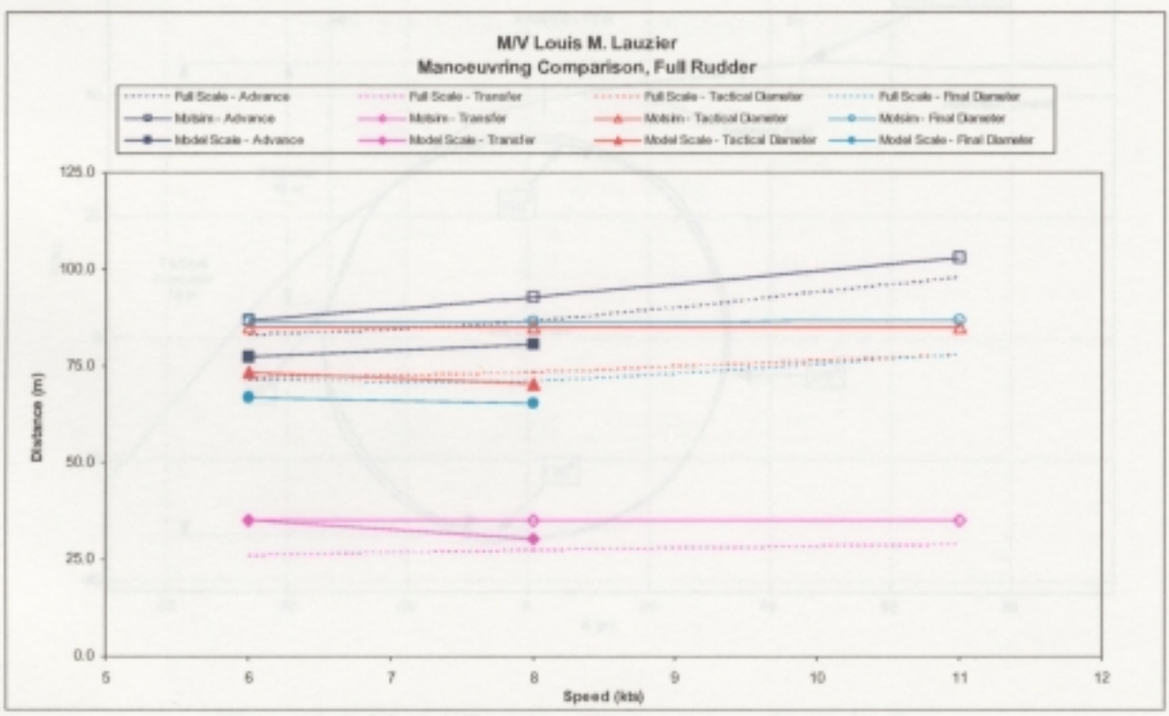

Figure 5-5: Manoeuvring Comparison - Full Rudder Angle

When dealing with a small scale of the original vessel, scaling issues do arise, particularly with fluid flow over the hull and rudders. Therefore, a correlation that produces less than a 20% difference between the two scales is deemed a success. This is the case for this study, where only two measured parameters are over 10.8%; the advance measurement for 15° rudder angle at 6 knots with a difference of 16.4%, the transfer measurement for full rudder at 6 knots with a difference of 34.7%. The large transfer error is influenced by the starboard turning circle, as seen in Figure 5-6, where a large transient area is identified. This area shows that the model traveled in a straight line after the rudder was initiated. I believe that if this run was repeated, it would not have the same deficiency because analysis of the other turning circles did not produce similar transient areas.

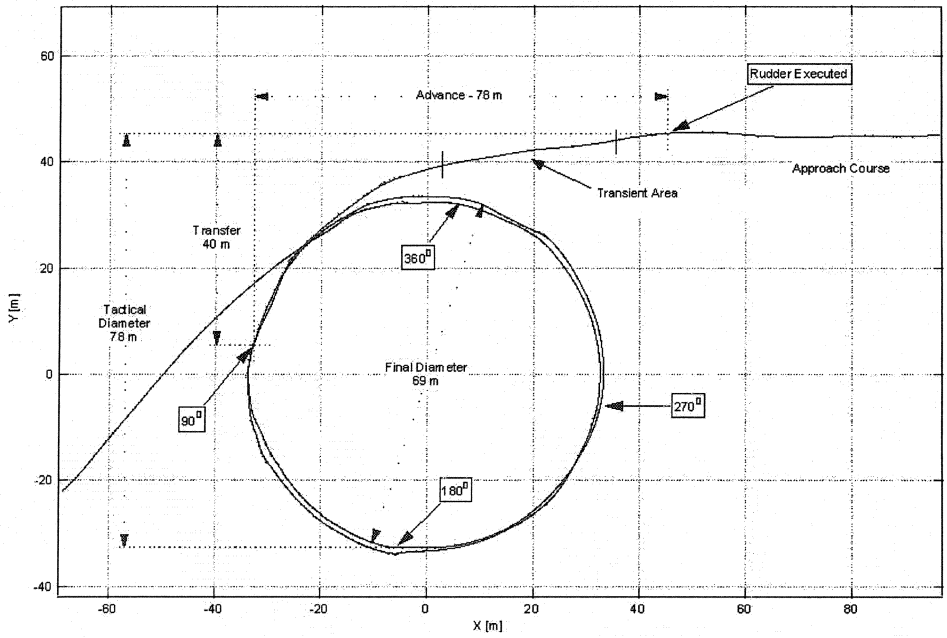

Figure 5-6: Model Turning Circle - Large Transfer Error

As for the numerical predictions, the only parameter that was influenced by speed was the advance for full rudder angle. All the other parameters had little variation with speed. Future work still needs to be performed for the higher model speeds to correlate with 11 knots, full scale.

The zigzag manoeuvres, model scale versus full scale, also produced a reliable prediction within 15% of the full scale data. To better correlate the two zigzags, the full scale zigzag that had comparable rudder lag was chosen. The zigzag comparison can be seen in Table 5-4. Using the Nomoto coefficients from the model scale analysis (K & T), a new heading was calculated based on the full scale rudder activity. This new calculated heading, in comparison to the actual heading and the heading calculated from the full scale Nomoto coefficients is depicted in Figure 5-7. No numerical prediction was carried out on the zigzag manoeuvre.

Table 5-4: Manoeuvring Comparison – Zigzag

M/V Louis M. Lauzier
Manoeuving Comparison - Zigzag
10/10 Rudder Angle

Speed (kts)	TRE (m)	Reach (m)	Period (m)
Full Scale			
6	14.86	59.25	109.54
Model Scale			
6	15.38	52.86	95.97
Diff.	*3.5%*	*10.8%*	*12.4%*

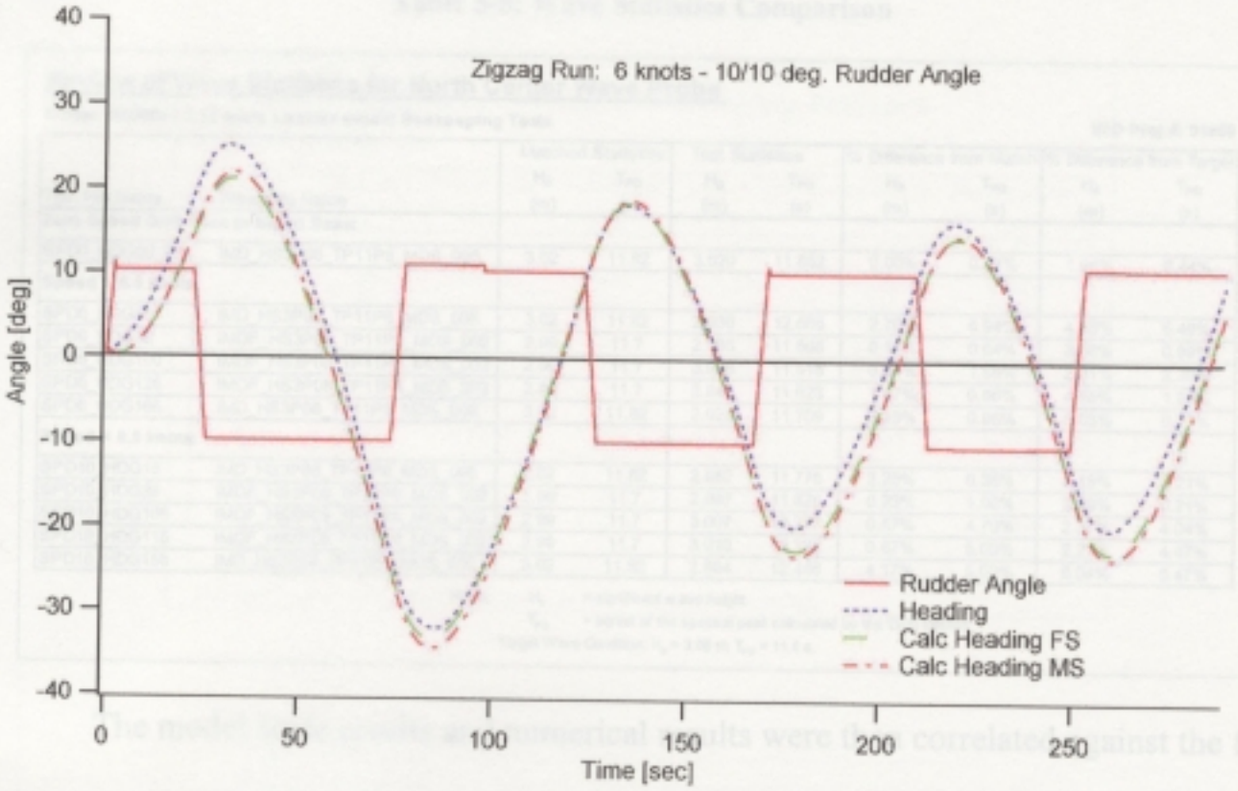

Figure 5-7: Manoeuvring Comparison – Heading Angle Plot

As noted in the previous two chapters, the pullouts manoeuvres for the full scale and model scale results both produced a slight instability to the port side. No numerical prediction was carried out on the pullout manoeuvre.

4.0 Seakeeping Comparison

Unlike the previous two components, to match the results of the full scale experiments with the model scale results, the wave conditions need to be identical. As a result, the model wave was matched to the full scale wave. The matching process [25] was done prior to model experimentation to achieve a wave resembling the target wave condition experienced throughout the 'Lauzier' sea trial. The test wave experienced by the model throughout the test run was also analyzed and compared against the matched wave and the target wave statistics, as noted in Table 5-5.

Table 5-5: Wave Statistics Comparison

Review of Wave Statistics for North Center Wave Probe

Model: IMD605 - 1:12 scale Lauzier model Seakeeping Tests **IMD Proj.#: 01960**

		Matched Statistics		Test Statistics		% Difference from Match		% Difference from Target	
		H_S	T_{PD}	H_S	T_{PD}	H_S	T_{PD}	H_S	T_{PD}
Test File Name	Wave File Name	(m)	(s)	(m)	(s)	(m)	(s)	(m)	(s)
Zero Speed Drift Runs in Beam Seas:									
SPD0_HDG90_R1	IMD_HS3P08_TP11P8_MDS_006	3.02	11.82	3.020	11.852	0.00%	0.27%	1.95%	0.44%
Speed = 6.5 knots:									
SPD6_HDG15	IMD_HS3P08_TP11P8_MDS_006	3.02	11.82	2.936	12.566	2.78%	5.94%	4.68%	6.49%
SPD6_HDG35	IMDF_HS3P08_TP11P8_MDS_002	2.99	11.7	2.985	11.695	0.17%	0.04%	3.08%	0.89%
SPD6_HDG100	IMDF_HS3P08_TP11P8_MDS_002	2.99	11.7	3.018	11.518	0.94%	1.58%	2.01%	2.39%
SPD6_HDG125	IMDF_HS3P08_TP11P8_MDS_002	2.99	11.7	2.940	11.623	1.67%	0.66%	4.55%	1.50%
SPD6_HDG165	IMD_HS3P08_TP11P8_MDS_006	3.02	11.82	2.925	11.709	3.15%	0.95%	5.03%	0.77%
Speed = 9.5 knots:									
SPD10_HDG15	IMD_HS3P08_TP11P8_MDS_006	3.02	11.82	2.952	11.775	2.25%	0.38%	4.16%	0.21%
SPD10_HDG35	IMDF_HS3P08_TP11P8_MDS_002	2.99	11.7	2.997	11.825	0.23%	1.06%	2.69%	0.21%
SPD10_HDG105	IMDF_HS3P08_TP11P8_MDS_002	2.99	11.7	3.007	12.277	0.57%	4.70%	2.37%	4.04%
SPD10_HDG115	IMDF_HS3P08_TP11P8_MDS_002	2.99	11.7	3.010	12.328	0.67%	5.09%	2.27%	4.47%
SPD10_HDG155	IMD_HS3P08_TP11P8_MDS_006	3.02	11.82	2.894	12.446	4.17%	5.03%	6.04%	5.47%

Notes: H_S = significant w ave height

T_{PD} = period of the spectral peak calculated by the 'Delft Method'

Target Wave Condition: H_S = 3.08 m, T_{PD} = 11.8 s.

The model scale results and numerical results were then correlated against the full scale results. The numerical predictions were achieved using the software program Motsim using the measured directional wave spectrum from the full scale sea trials. The Motsim program however, outputs the surge, sway, and surge displacement instead of their accelerations. Extra computation is needed to achieve those values. For this reason, the acceleration comparison will not include Motsim values. The displacement graph will display an example comparison of only the heave displacement for all three cases. It should be noted that the vessel speeds are slightly different at the higher speeds (9.5 knots for the model, compared to 10.5 knots full scale). The standard deviation of selected values produced by Motsim can be seen in Table 5-6. Comparison graphs for 6.5 knots can be seen in Figure 5-8, Figure 5-9, and Figure 5-10, for the roll and pitch angles, Yaw angle and heave displacement, and the accelerations, respectively. Figure 5-11, Figure 5-12, and Figure 5-13 are the comparison graphs for 10.5 knots.

Table 5-6: Motsim Seakeeping Predictions

Summary of Motsim Seakeeping Statistics

M/V Louis M. Lauzier **IMD Proj.#: 01960**

Speed (kts)	Heading	Roll Angle (deg)	Pitch Angle (deg)	Yaw Angle (deg)	Sway Displ. (m)	Heave Displ. (m)
6.5	-15	2.407	1.603	0.986	1.30	0.722
6.5	35	3.014	1.441	1.142	1.35	0.825
6.5	80	4.648	1.386	1.189	0.90	0.784
6.5	125	3.702	1.837	0.934	0.80	0.734
6.5	165	2.337	2.163	0.761	0.45	0.859
10.5	-25	2.660	1.480	1.869	1.48	0.780
10.5	32	2.831	1.422	2.432	1.75	0.731
10.5	76	3.966	1.185	1.775	1.10	0.763
10.5	115	4.080	1.479	1.002	0.98	0.797
10.5	155	2.353	1.679	0.659	0.60	0.711

The above values are Standard Deviation values of the particular motion.

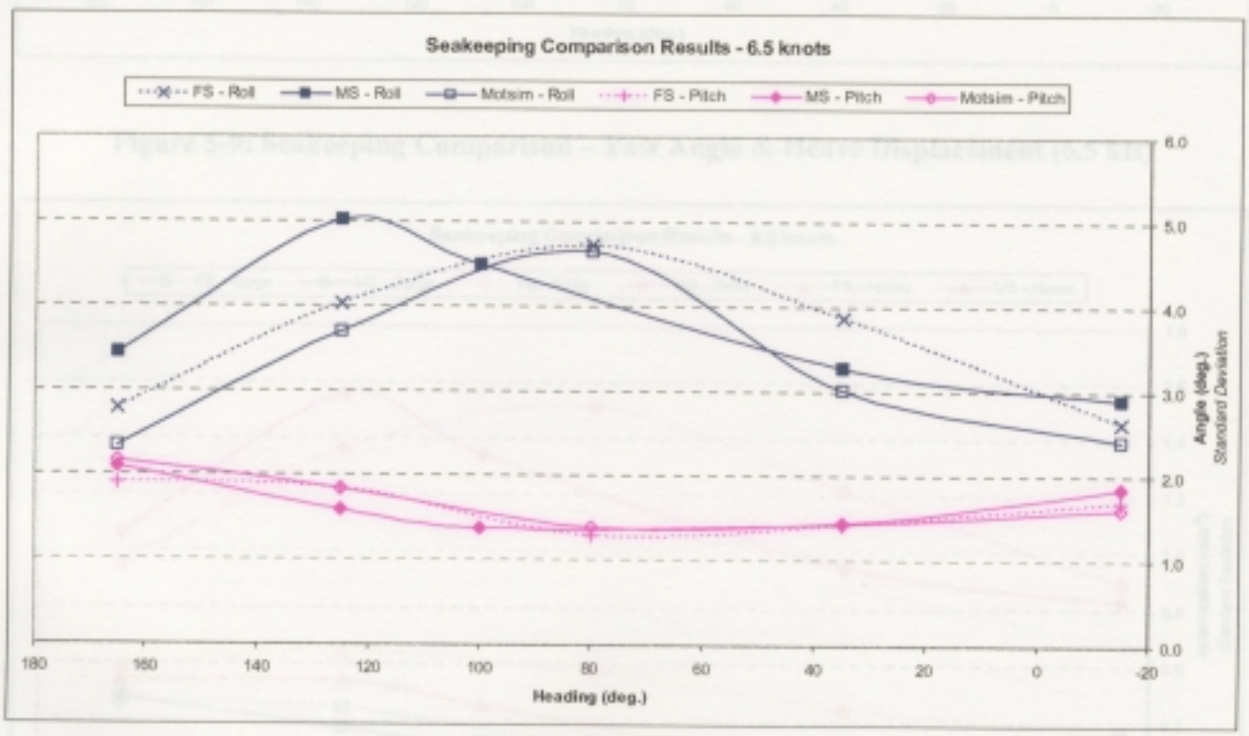

Figure 5-8: Seakeeping Comparison - Roll & Pitch Angle (6.5 kts)

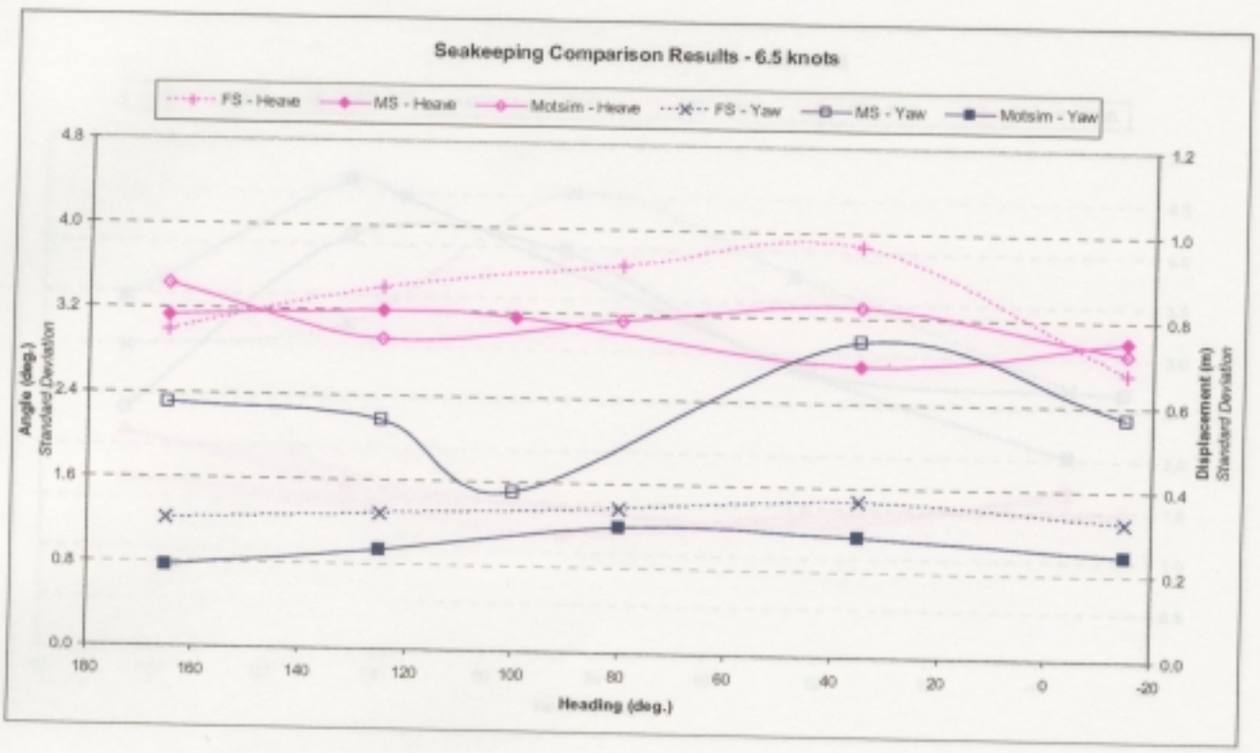

Figure 5-9: Seakeeping Comparison – Yaw Angle & Heave Displacement (6.5 kts)

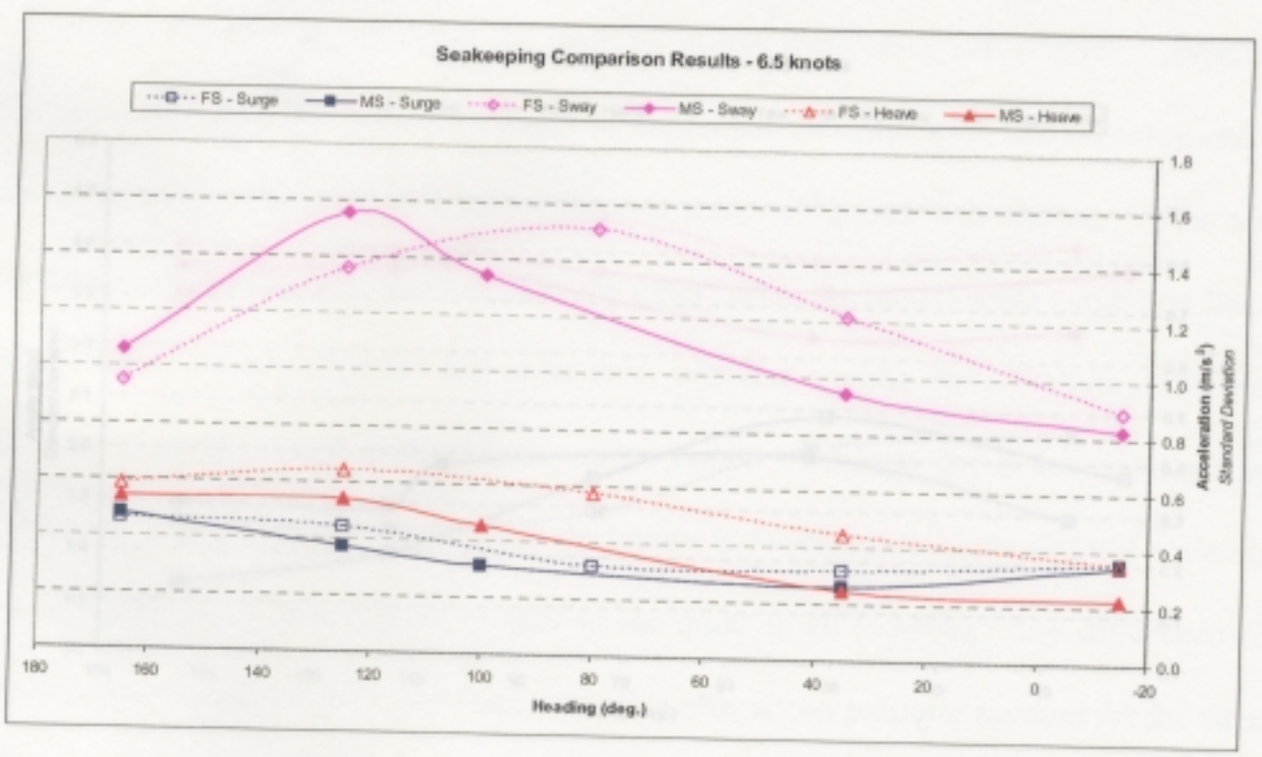

Figure 5-10: Seakeeping Comparison - Accelerations (6.5 kts)

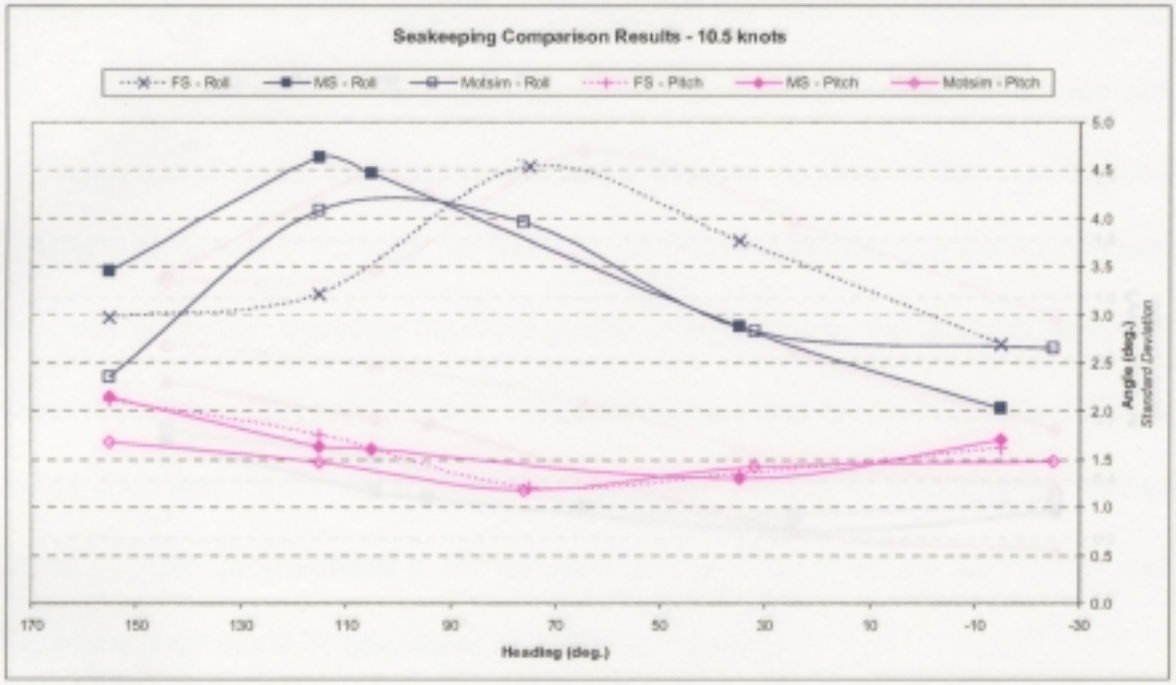

Figure 5-11: Seakeeping Comparison - Roll and Pitch Angle (10.5 kts)

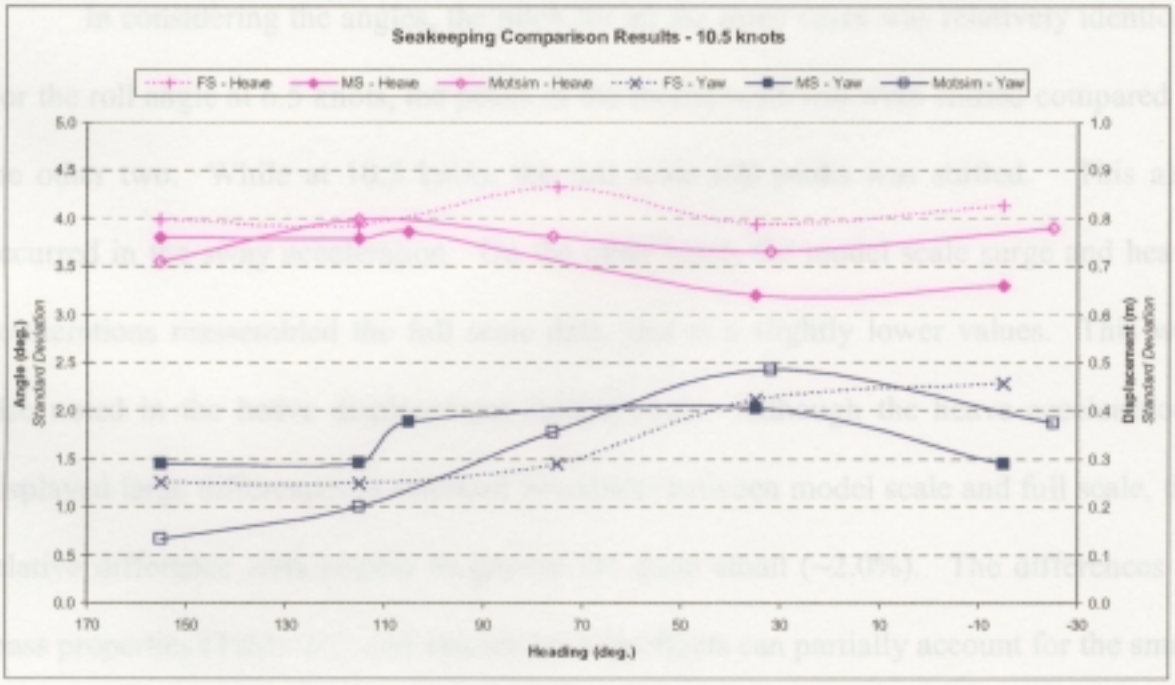

Figure 5-12: Seakeeping Comparison – Yaw Angle & Heave Displacement (10.5 kts)

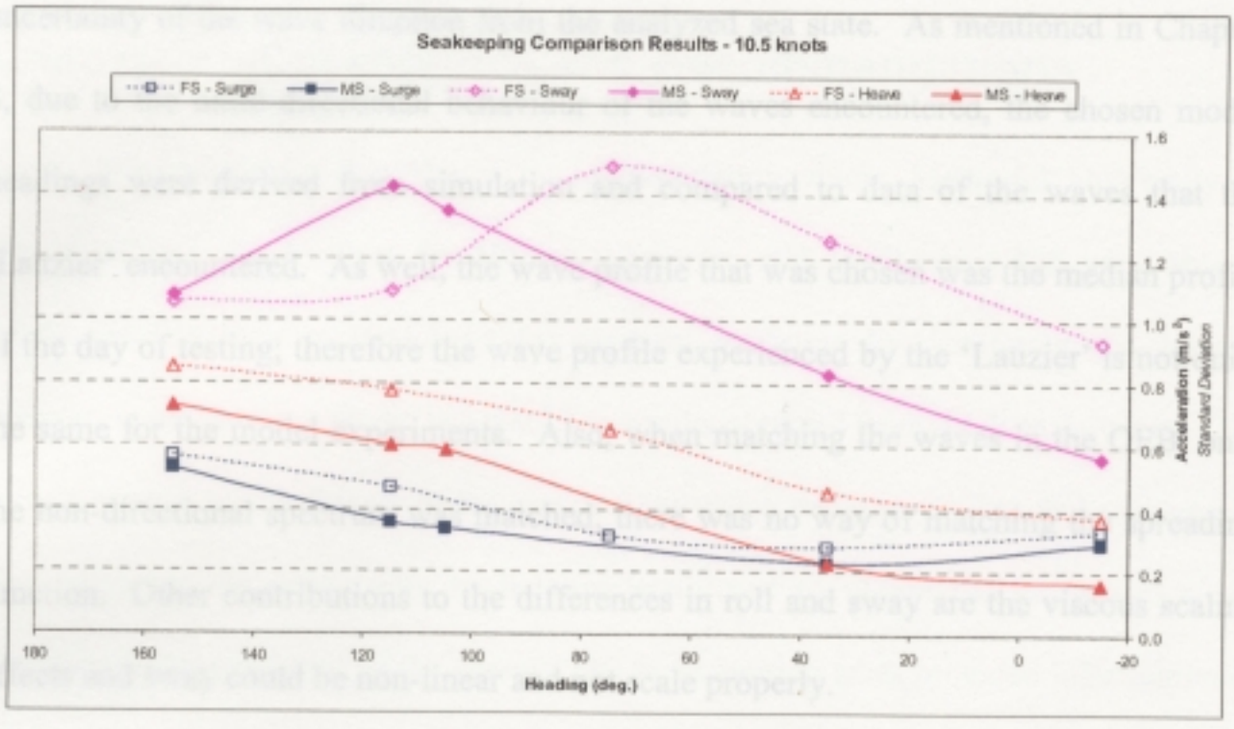

Figure 5-13: Seakeeping Comparison - Accelerations (10.5 kts)

In considering the angles, the pitch for all the three cases was relatively identical. For the roll angle at 6.5 knots, the peaks of the model scale roll were shifted compared to the other two. While at 10.5 knots, the full scale roll peaks was shifted. This also occurred in the sway acceleration. On the other hand, the model scale surge and heave accelerations reassembled the full scale data, just at a slightly lower values. This was also noted in the heave displacement comparisons. Although the heave accelerations displayed large differences in standard deviations between model scale and full scale, the relative difference with respect to gravity are quite small (~2.0%). The differences in mass properties (Table 4-1) and viscous scaling effects can partially account for the small differences between full scale and model scale values.

In the particular cases, where the model scale motions (roll and sway) were slightly shifted compared to the full scale motions, it can be partially attributed to the

uncertainty of the wave direction from the analyzed sea state. As mentioned in Chapter 4, due to the multi-directional behaviour of the waves encountered, the chosen model headings were derived from simulation and compared to data of the waves that the 'Lauzier' encountered. As well, the wave profile that was chosen was the median profile of the day of testing; therefore the wave profile experienced by the 'Lauzier' is not quite the same for the model experiments. Also, when matching the waves in the OEB, only the non-directional spectrum was matched, there was no way of matching the spreading function. Other contributions to the differences in roll and sway are the viscous scaling effects and sway could be non-linear and not scale properly.

The yaw angle comparison was added for completeness. At the present time, the poor correlation at 6.5 knots can not be explained due to lack of relevant data.

Chapter 6 Conclusions and Recommendations

By performing this ship / model correlation study, Memorial University of Newfoundland, the Institute for Marine Dynamics, and Marineering Ltd were able to partly validate their methodology for physical modeling by accurately and reliably correlating many of the model test results to results obtained from a full scale vessel. The testing procedures used were in the areas of powering, manoeuvrability and seakeeping. The powering, or propulsion, trials were performed to obtain the performance and propulsive characteristics of the vessel. The manoeuvring trials provided information on the handling characteristics of the ship, for operational purposes. Finally, the seakeeping trials were carried out to define the seaworthiness characteristics of the ship by assessing the relationship between the motions of the ship and the related environmental conditions in which the ship was tested.

Using the powering trials, I was able to correlate the model scale results to the full scale results to within 10% using the ITTC '78 power prediction. This was achieved by increasing the ship frictional resistance coefficient to account for hull fouling by 48.75%, based on a Royal Navy practice. In spite of this, further investigation should be carried out on the actual percentage that should be used on the 'Lauzier' or any other ship operating out of the St. John's harbour.

Although there is currently no full scale prediction method that will extrapolate the model scale results to full scale results, besides just scaling each parameter by the appropriate scaling factor, I was able to correlate certain parameters of each manoeuvre

within a reasonable level of accuracy: 11% for the turning circle manoeuvres and 15% for the zigzag manoeuvres. This is deemed a success in correlation with this size of a model due to the uncertainty of viscous scaling effects over the hull and rudder. The analysis also showed that the Nomoto coefficients for the vessel from the zigzag manoeuvre could be accurately calculated. The model scale manoeuvring test program should be expanded to include more speeds and rudder angles than that performed on the full scale vessel. This will further enhance the understanding of the effect of these parameters on each manoeuvre.

When dealing with the seakeeping correlation, much depends on how well IMD can accurately match a particular sea state, leaving little concern in future seakeeping trials about matching the observed sea state. With the correlation analysis, the model scale results compared relatively well to the full scale motions. In the particular cases where the peaks of the model scale motions were slightly shifted compared with the full scale motions, it can be attributed to the uncertainty of the wave direction from the analyzed sea state. In the future, full scale seakeeping trials should abide by the ITTC recommended test pattern along with performing the tests in a sea state where the wave spectrum is more unidirectional. The wave buoy analysis has difficulty in deciphering these sea conditions and calculating the actual wave direction. As well, the model test program should contain two matched wave profiles, one for each vessel speed. By following these recommendations, it should mitigate the problems I experienced in this study with respect to wave direction.

REFERENCES

[1] Muckle, W., "Naval Architecture for Marine Engineers", Newnes-Butterworths, Toronto, 1978.

[2] ITTC, "Eighth International Towing Tank Conference Proceedings", Canal de Experiencias Hidrodinamicas, Madrid, 1959.

[3] ITTC, "Fifteenth International Towing Tank Conference Proceedings", Nederlands Ship Model Basin, Wageningen, 1978.

[4] Hughes, G., "An Analysis of Ship Model Resistance into Viscous and Wave Components", *Transactions of the Royal Institute of Naval Architecture*, Vol. 108, p.289.

[5] SNAME, "Principles of Naval Architecture Volume II: Resistance, Propulsion and Vibration", 1989.

[6] SNAME, "Principles of Naval Architecture Volume III: Motions in Waves and Controllability", 1989.

[7] Nomoto, K., "Analysis of Kempf's Standard Manoeuvre Test and Proposed Steering Quality Indices", Symposium on Ship Manoeuvrability, Washington, D.C., 1960.

[8] Lloyd, A.R.J.M., "Seakeeping: Ship Behaviour in Rough Weather", Ellis Horwood Limited, Toronto, 1998.

[9] Institute for Marine Dynamics Laboratory Memorandum, "Measurement of Strain due to Torque and Thrust Loads on Full Scale Propeller Shafts", LM-1993-03, January 1993.

[10] Holtrop, J.,"A Statistical Re-Analysis of Resistance and Propulsion Data", *International Shipbuilding Progress*, Vol. 31, No. 363, November 1984.

[11] Institute for Marine Dynamics Quality System Work Instruction Manual, "Set Up of Shaft Torque/Thrust Measurement", V1.0, TRL-04, February 2002.

[12] Cumming, D., Hopkins, D., Williams, J., and Janes, G., "Description of Manoeuvring, Propulsion, and Seakeeping Trials Carried Out on the M/V Louis M. Lauzier July – November 2001", IMD Technical Report #TR-2003-13, July 2003.

[13] ITTC Procedures Book, 22nd ITTC, Seoul, Korea & Shanghai, China, September, 1999.

[14] Sentry Wave Buoy Operation Manual, Neptune Sciences, Inc., Slidell, Louisiana, USA.

[15] Institute for Marine Dynamics Standard Test Method, "Construction of Models of Ships, Offshore Structures, and Propellers", V5.0, 42-8595-S/GM-1, January 2001.

[16] Hopkins, D., Cumming, D., "Description of Propeller Open Water, Resistance and Propulsion Experiments Carried Out on M/V Louis M. Lauzier Model IMD597", IMD Technical Report #TR-2003-20, Fall 2003.

[17] Institute for Marine Dynamics Standard Test Method, "Resistance on Open Water", V4.0, 42-8595-S/TM-1, February 2001.

[18] Hopkins, D., "R-Class Icebreaker Propeller Open Water Experiments", IMD Lab Manual, LM-2002-25, November 2002.

[19] Institute for Marine Dynamics Standard Test Method, "Propeller Open Water Tests", V4.0, 42-8595-S/TM-2, February 2002.

[20] Institute for Marine Dynamics Standard Test Method, "Model Propulsion in Open Water", V4.0, 42-8595-S/TM-3, March 2002.

[21] ITTC, "23rd International Towing Tank Conference Proceeding" Scuola Navale Militare, Venice, 2002.

[22] Institute for Marine Dynamics Standard Test Method, "Prediction of Ship Powering", V4.0, 42-8595-S/TM-4 November 2002.

[23] Canadian National Defence Standard, "Hydrodynamic Model Tests and Sea Trials", D-03-002-009/SG-001, November 1992, p. 3-4-3.

[24] Cumming, D., Hopkins, D., Bass, D., "Description of Seakeeping and Manoeuvring Experiments Carried Out on M/V Louis M. Lauzier Model IMD605", Fall 2003, IMD Technical Report #TR-2003-15.

[25] Institute for Marine Dynamics Standard Test Method, "Environmental Modeling – Waves, Wind, and Current", V3.0, 42-8595-2/GM-3, February 2001.

[26] Molloy, S., "Ship Powering Prediction Using Load Varying Self-Propulsion Tests", MUN Masters Thesis, May 2001.

[27] Pawlowski, J.S., Bass, D.W., "Theoretical and Numerical Study of Ship Motions in Heavy Seas", Trans. SNAME, New York, October 1991.